What is the role of phosphorylation of the Ca^{2+}/calmodulin-dependent glutamate decarboxylase isozyme, AtGAD1, in response to phosphate nutrition of *Arabidopsis thaliana*?

Lee Marie Raytek

A thesis submitted to the Department of Biology
in conformity with the requirements for
the degree of Master of Science

Queen's University
Kingston, Ontario, Canada
June 2022

ABSTRACT

Orthophosphate ($H_2PO_4^-$; Pi) is an essential but limiting macronutrient required for many fundamental aspects of plant metabolism, particularly photosynthesis and respiration. Pi starved (-Pi) plants elicit a Pi starvation response that alters gene expression and metabolism to enhance their efficiency of Pi acquisition and use. We recently employed liquid chromatography-tandem mass spectrometry (LC-MS/MS) to assess the impact of Pi nutrition on the phosphoproteome of cell cultures of the model plant *Arabidopsis thaliana*. Forty-eight hours following Pi resupply to -Pi cells, the glutamate decarboxylase isozyme AtGAD1 (AT5G17330.1) became *in vivo* hyperphosphorylated at multiple seryl residues near its N-terminus. AtGAD1 is a root-specific, Ca^{2+}/calmodulin-activated cytosolic isozyme that catalyzes the first committed step of the γ-aminobutyrate (GABA) shunt by decarboxylating glutamate into GABA. Although phosphoproteomic studies have documented widespread plant GAD phosphorylation, there have been no reports on the functions nor mechanisms of plant GAD phosphorylation. Here, I developed and validated a spectrophotometric GAD activity assay, as well as an anti-(pSer8 phosphosite-specific) antibody (α-pSer8) to corroborate our LC-MS/MS detection of AtGAD1 phosphorylation. I fully purified AtGAD1 from Pi-sufficient (+Pi) and -Pi cells (+P:GAD1 and -P:GAD1, respectively) to final specific activities of 20 and 32 (μmol GABA produced/min)mg^{-1}, respectively. LC-MS/MS, SDS-PAGE, immunoblotting, and analytical gel-filtration indicated that both final preparations exist as a homohexamer composed of identical 57 kDa AtGAD1 subunits. The 60% higher specific activity of purified -P:GAD1 relative to +P:GAD1 correlated with their differential phosphorylation as detected by LC-MS/MS and α-pSer8 immunoblotting, wherein -P:GAD1 was more highly phosphorylated at Ser4, Ser10, and Ser13, but was hypophosphorylated at Ser8 compared to +P:GAD1. Imaging fluorescent-protein tagged

AtGAD1 in *Arabidopsis* suspension cells, as well as microsomal fractionation and immunoblotting, indicated that GAD's cytosolic localization was unaffected by changes in nutritional Pi status. Collectively, my data suggest that Pi starvation increases the specific activity of GAD through differential phosphorylation. This change is expected to lead to greater GABA accumulation and/or flux through the GABA shunt in -Pi plants. This work adds to the literature showing that the GABA shunt is important during abiotic stress responses and expands the knowledge base for future engineering of improved Pi-use efficiency in crops.

CO-AUTHORSHIP

Bioinformatic analyses were conducted by MVG and LMR. LMR maintained WT *Arabidopsis* cell cultures for all experiments and purified native AtGAD1 from +Pi and -Pi cells. Phosphosite-specific antibodies were generated and tested by LMR, and all SDS-PAGE gels and subsequent staining or immunoblotting was conducted by LMR. LC-MS/MS analysis was performed by MRG in RGU's lab at the Univ. of Alberta. GAD-GABase assays and microsomal fractionation experiments were performed by LMR. *pRTL2:mCherry-AtGAD1* and *pRTL2:AtGAD1-mCherry* constructs were cloned by LMR, and ND biolistically transformed these with *mito-GFP* into *Arabidopsis* cells. ND maintained transformed *Arabidopsis* cells and carried out fluorescence microscopy. LMR, WCP, and WS prepared the manuscript with input from all co-authors.

ACKNOWLEDGEMENTS

First and foremost, I would like to thank Profs. Bill Plaxton and Wayne Snedden for their unending support and guidance over the last three years. They took a chance on me as a summer student with no real prior lab experience and gave me the opportunity to fall in love with research. I'd also like to extend thanks to our instrumental collaborators in Profs. Barry Shelp and Rob Mullen's labs, who made much of my thesis work possible, as well as to my committee members Profs. Kenton Ko and Jacqueline Monaghan for all their advice and constructive criticisms throughout my project. I also owe a massive thank you to (Dr.!!) Ryan Kilburn of the Plaxton/Snedden Labs, who mentored me from the very beginning and was always willing to help troubleshoot experiments. To everyone else in the Plaxton and Snedden labs who I was fortunate enough to have crossed paths with: I would be so lucky to have a team of lab mates who are half as supportive as all of you in the future. You made my time in Kingston enjoyable despite working through the Covid-19 pandemic – and you all inspire me to be a better scientist! Lastly, I'm grateful to NSERC for funding this work.

Table of Contents

List of Tables

List of Figures

List of Abbreviations

2-OG	2-Oxoglutarate
2-OGDH	2-OG dehydrogenase
ACN	Acetonitrile
ALMT	Aluminum-activated malate transporter
CaM	Calmodulin
CIP	Calf intestinal alkaline phosphatase
DTT	Dithiothreitol
EGTA	Ethylene glycol-bis(β-aminoethyl ether)-N,N,N',N'-tetraacetic acid
EPSD	Eukaryotic Phosphorylation Site Database
FA	Formic acid
FPLC	Fast protein liquid chromatography
GABA	γ-aminobutyric acid
GABase	GABA-T and succinic semialdehyde dehydrogenase
GABA-T	GABA transaminase
GAD	Glutamate decarboxylase
GDH	Glutamate dehydrogenase
GORK	Guard cell outward rectifying potassium channel
JA	Jasmonic acid
KLH	Keyhole limpt hemocyanin
KO	Knockout
K_m	Michaelis-Menten constant
λ P'tase	λ phosphatase
LC-MS/MS	Liquid chromatography tandem-mass spectrometry
MAPK	Mitogen-activated protein kinase
MC-LR	Microcystin-LR
Mito-GFP	Mitochondrial-green fluorescent protein marker
M_r	Molecular mass
PBS	Phosphate-buffered saline
Pi	Inorganic phosphate
+Pi	Pi-sufficient

+P:GAD1	AtGAD1 purified from +Pi cells
-Pi	Pi-deprived
-P:GAD1	AtGAD1 purified from -Pi cells
PLP	Pyridoxal-5’-phosphate
PMSF	Phenylmethylsulfonyl fluoride
PTM	Post-translational modification
PSR	Phosphate starvation response
rAtGAD1	Recombinant AtGAD1
SSA	Succinic semialdehyde
SUBA	Subcellular Localizatio Database for Arabidopsis Proteins
TCA	Tricarboxylic acid
TPC1	Two pore channel 1
TPP	Thiamine diphosphate
Unit	µmol/min
V_{max}	Maximum velocity
WT	Wild type

Chapter 1: General Introduction

Inorganic phosphate (Pi; HPO_4^{-2}) is a critical macronutrient with essential roles in: (i) structural biology such as generating phospholipid bilayers and DNA backbones, (ii) regulating proteins and signal transduction pathways either allosterically or via phosphorylation, and (iii) bioenergetics as a pivotal substrate needed by ATP synthases during photosynthesis and respiration. In essence, Pi is necessary for life as we know it. While animals acquire Pi by consuming food, sessile plants can only take up soluble forms of Pi from the soil through low-affinity or Pi-starvation (-Pi) inducible high affinity Pi transporters of root cell plasma membranes (Dissanayaka *et al.*, 2021). Although Pi naturally occurs in soil, its levels in the soil solution are highly suboptimal for growth of most crop varieties, necessitating the use of >100,000,000 metric tonnes of Pi fertilizers around the globe annually (Lambers *et al.*, 2015). However, modern farming practices of applying chemical fertilizers as well as ploughing fields have led to the selection of high yielding, but 'lazy' crops that have become less efficient at taking up and using Pi. Although our current 'solution' of overusing Pi-fertilizers has yielded short-term benefits in crop productivity, Pi runoff from agricultural fields contributes to intense eutrophication of nearby aquatic and marine ecosystems, and formation of harmful and toxic algal blooms. Fertilizer application also has damaging effects on symbiotic mycorrhizal fungi in the soil that otherwise colonize roots of most land plants to deliver nutrients, including Pi, to the host plant (in exchange for sucrose) in a far less destructive way (Ezawa and Saito, 2018; Lambers *et al.*, 2015). Add to this the rapid depletion of precious, non-renewable rock-Pi reserves needed to manufacture Pi fertilizers, we are said to be entering a 'Pi crisis', and projections estimate that the world's rock-Pi resources will be mostly depleted by the end of this century (Lambers and Plaxton, 2015). This will severely limit our capacity to produce high

yielding crops at a time when food security will be of the utmost importance amidst climate change and a rapidly growing global population. For these reasons, there is an urgent need for development of crops engineered to enhance their Pi acquisition and usage efficiencies as strategies for both global food security and environmental protection.

-Pi plants acclimate to Pi deficiency by inducing a Pi starvation response (PSR) that improves their Pi acquisition and use efficiency (Fig. 2-1). The PSR includes post-translational modifications (PTMs) of many proteins involved in signaling, Pi acquisition and transport, and cellular metabolism (Dissanayaka *et al.*, 2021). Enzymes and metabolic pathways of –Pi plants are often altered to trigger stress responses and/or recycle Pi from non-essential phosphorylated metabolites. We recently evaluated changes in the soluble phosphoproteome 48 h following Pi-resupply to –Pi suspension cells of the model plant *Arabidopsis thaliana* (Mehta *et al.*, 2021). The impact of protein phosphorylation can be far-reaching, ranging from kinetic impacts on key enzymes, altered protein-protein interactions, as well as changes in subcellular protein localization and/or their susceptibility to proteolysis (Plaxton and Shane, 2015). Assessing how Pi nutrition influences the phospho-status of key proteins can provide important insights into how plants carry out various aspects of the PSR.

An interesting observation noted by Mehta and colleagues (2021) was that one of the most differentially phosphorylated proteins following Pi-resupply to the –Pi *Arabidopsis* cells was the glutamate (Glu) decarboxylase (GAD) isozyme AtGAD1. This finding is of interest because: (i) plant GADs are Ca^{2+}/calmodulin (CaM) activated enzymes that produce γ-aminobutyric acid (GABA), an enigmatic stress and signaling metabolite, while representing the first committed step of a tricarboxylic acid (TCA) cycle bypass known as the 'GABA shunt'

(Fig. 2-2A), and (ii) neither the functions nor mechanisms of plant GAD phosphorylation have been explored.

Elevated GABA levels have been implicated in a broad range of plant abiotic and biotic stresses including salinity, heat and cold stress, herbivory, and pathogen infection (Shelp *et al.*, 2021; Shelp *et al.*, 2012a). More recently, a potential signal transduction role for GABA was uncovered through the identification of GABA receptors and potential downstream effects of binding (Ramesh *et al.*, 2015; Xu *et al.*, 2021). Nevertheless, many questions remain unanswered regarding the role and regulation of GAD, GABA, and the GABA shunt in plant stress responses. Additionally, unraveling how PTMs such as reversible phosphorylation contribute to GAD control may provide insight into how plant GADs are regulated under a range of stresses. A better understanding of how GAD, GABA, and the GABA shunt help plants to acclimate to Pi deprivation may contribute to the development of crop varieties that require far less environmentally damaging, non-renewable, and costly Pi fertilizers, and that are potentially more tolerant to other stresses that also trigger changes in GAD phosphorylation.

Chapter 2: Literature Review

2.1 γ-Aminobutyric Acid (GABA)

GABA (also known as 4-aminobutyrate) is a ubiquitous, four-carbon, non-proteinogenic amino acid produced in bacteria, archaea, and eukaryota kingdoms (Fig. 2-2B). However, it remains unclear whether GABA's functions across taxa are conserved or if it has evolved to take on divergent roles. Although GABA was first discovered in potato tubers in 1949 (Steward, 1949), it was following the detection of GABA in mammals that research into its function and metabolism ensued (Narayan and Nair, 1990). The GABA metabolism pathway, termed the GABA shunt (Fig. 2-2), is highly conserved across kingdoms, and although the role of GABA is well-understood in the context of animal systems, many questions regarding GABA and the GABA shunt in plants remain unanswered.

2.1.1 The highly conserved GABA shunt

The major, conserved GABA biosynthetic pathway interfacing C and N metabolism across prokaryotes and eukaryotes is known as the GABA shunt. The pathway is aptly named as it serves as a shunt, or bypass, around two steps of the TCA cycle catalyzed by 2-oxoglutarate (2-OG) dehydrogenase (2-OGDH) and succinyl-CoA synthetase (Fig. 2-2A). The shunt diverts 2-OG away from the mitochondrial TCA cycle, shuttling it through a partially cytosolic pathway. Glu dehydrogenase (GDH) converts 2-OG and NH_4^+ into Glu in a reversible manner. Following Glu export to the cytosol, GAD catalyzes the first committed step of the GABA shunt while consuming a proton to convert Glu into GABA and CO_2 (Michaeli *et al.*, 2011). Plastid-derived Glu occurring as a product of Glu synthase may also be transported into the cytosol to supplement the GAD reaction (Shelp *et al.*, 2021). The cytosolic and mitochondrial

compartmentation of the shunt are connected by the presence of GABA permease transporters embedded within the mitochondrial inner membrane (Michaeli *et al.*, 2011). Following GABA import into the mitochondria, it undergoes deamination by GABA-transaminase (GABA-T) into succinic semialdehyde (SSA) (Fig. 2-2). In the process, GABA's amine group is transferred to a ketoacid such as 2-OG, pyruvate, or glyoxylate to respectively yield the amino acids Glu, alanine, or glycine (Trobacher *et al.*, 2013). SSA can then be oxidized into succinate by SSA dehydrogenase coupled to $NADP^+$ reduction into NADPH (Fig. 2-2). This step is subject to feedback inhibition by NADPH and ATP (Shelp *et al.*, 2021). Finally, succinate can re-enter the TCA cycle, which may suggest that cells are able to continue cellular respiration during times when 2-OGDH and/or succinyl-CoA synthetase may otherwise be inhibited. Alternatively, SSA can be diverted from the GABA shunt into γ-hydroxybutyrate by glyoxylate/SSA reductase coupled to NADPH oxidation (Fait *et al.*, 2008). Despite the significance of the evolutionarily-conserved GABA shunt in central plant metabolism, relatively little is known about its physiological roles, making the study of its components so intriguing.

GABA can also be synthesized through an alternative route via peroxisomal catabolism of polyamines, although this pathway is not the major route for GABA production. GAD is the primary producer of the metabolite, as evidenced by the stark 8-fold reduction in root GABA levels of root-specific *atgad1* knockout (KO) mutants during heat stress (Bouché *et al.*, 2004). Meanwhile, shoot-specific *atgad2* mutants exhibited a similar trend of ~13-fold reduction of GABA in the shoots (Mekonnen *et al.*, 2016).

2.1.2 Functional Roles of GABA Across Kingdoms

Mammalian GABA was first identified in extracts of mouse brain tissue in the 1950s, and subsequently characterized as the chief inhibitory neurotransmitter in neurons (Kuffler and Edwards, 1958; Obata, 1972; Roberts and Frankel, 1950). High affinity GABA receptors were soon identified in these GABAergic neurons, which in conjunction with normal GABA levels, perception, and signal transduction is critical for proper central nervous system development (Li and Xu, 2008; Palacios *et al.*, 1981). GABA analogue medications, like Gabapentin, have been developed for their ability to bind GABA receptors and either reduce or mimic GABA signaling in the brain (Greenblatt and Greenblatt, 2018). Even over-the-counter GABA dietary supplements are marketed as having anxiety-relieving and mood-boosting effects. For this reason, there has been some biotechnology research into how to increase GABA levels in plants and microbes either for food or large-scale purification and oral consumption, such as the recent CRISPR-edited tomato (*Solanum lycopersicum*) in Japan (Waltz, 2021).

In some bacteria, GABA and the GABA shunt are critical for conferring resistance against acidosis. Because GAD consumes protons as it decarboxylates Glu, this system can be used to scavenge excess protons to regulate intracellular pH. For instance, gut microbes like *Escherichia coli* rely on the GABA shunt to survive the acidic pH of digestive tracts of animals (Castanie-Cornet *et al.*, 1999). As a result, GABA spikes can confer rapid resistance to acidosis in bacteria and the metabolite can then be transported out the cell.

2.1.3 GABA and Plant Abiotic Stress

Although GABA has the reputation of being an enigmatic metabolite in plants, it has always been viewed as a reliable stress marker due to its rapid accumulation in response to a

multitude of stresses. Levels of GABA vary depending on tissue type, growth conditions, and oscillations influenced by circadian rhythms, but it has been documented to reach the mM range, such as in tomato, where GABA (up to ~20 μmol/g FW) is the predominant amino acid in developing fruit and can be further accumulated under mild salt stress (Akihiro *et al.*, 2008; Yin *et al.*, 2010). Before the turn of the 21st-century, GABA was largely thought of as a cytosolic pH buffer, a contributor to C:N balance, and an osmoprotectant. Plant GAD activation under acidic pH, and subsequent H^+ consumption and GABA accumulation parallels the acid-activation and pH regulating function of GABA in bacteria (Bown and Shelp, 1997). In fact, asparagus cells exposed to acidosis for just 15 s exhibited a rapid 3-fold increase in GABA content (Crawford *et al.*, 1994). GABA may also be effective for maintaining C:N flux because its biosynthetic pathway interfaces C and N metabolism by assimilating carbons from Glu into the TCA cycle. Normal growth of wild-type (WT) *Arabidopsis* and inhibited growth of GABA-T mutants (i.e. *pop2*) on medium containing GABA as the only N source further supports the notion that GABA can serve as a N store and is involved in both N and C metabolism (Breitkreuz *et al.*, 1999).

Apart from maintaining C/N homeostasis, GABA was also characterized as a biocompatible solute much like proline, due to its accumulation during salt stress. Tomato roots exposed to salinity stress for 4 d exhibited a 2-fold increase in GABA levels, whereas GABA levels spiked up to 4-fold in developing fruit of tomato plants grown under mild salt stress (Kinnersley and Turano, 2000; Yin *et al.*, 2010). Exogenous GABA can indeed enhance salt tolerance of maize seedlings grown with up to 300 mM NaCl, by improving seedling growth, reducing water loss, and mitigating oxidative damage (Wang *et al.*, 2017).

There is mounting evidence that enhanced GABA shunt flux is necessary under salinity. In *Arabidopsis*, the *POP2* gene encoding GABA-T is strongly induced in roots during salt stress,

whereas salinity caused root swelling and wall degradation in *pop2* KO mutants (Renault *et al.*, 2013; Renault *et al.*, 2010). Metabolomic analysis of salt-stressed *pop2* plants revealed increased Glu (+40%) and reduced succinate levels (-40%) compared to WT, which the authors interpreted as evidence that the shunt is critical for a significant proportion of succinate production under salt stress. Moreover, it was reported that the GABA shunt mediates about 20% of total cellular respiration in excised wheat leaves during salt stress, but not under normal conditions (Che-Othman *et al.*, 2020). These studies support the hypothesis that besides GABA itself, the GABA shunt is essential during salt stress to support mitochondrial respiration.

Other abiotic stresses such as drought or heat stress similarly elicit GABA spikes and may also require activation of the GABA shunt to improve stress tolerance. A *gad1/2* double KO *Arabidopsis* mutant with low endogenous GABA levels exhibited defective stomatal closure on both the abaxial and adaxial leaf sides, and therefore, was hypersensitive to drought stress (Mekonnen *et al.*, 2016). Interestingly, a triple *gad1/2 x pop2* mutant reverted the sensitive phenotype back to WT, demonstrating the fine balance of GABA shunt metabolite levels during drought stress. Furthermore, freeze tolerance in the perennial grass *Brachypodium sylvaticum* was assessed, revealing that while both freeze-tolerant and -sensitive strains displayed similar increases in GABA upon freezing, they regulate the GABA shunt differently (Toubiana *et al.*, 2020). GABA has also been implicated in heat stress; application of exogenous GABA improves long-term heat tolerance (35 d) in creeping bentgrass (*Agrostis stoloniferai*) (Li *et al.*, 2016). Plants pretreated with GABA accumulated higher levels of metabolites associated with the GABA shunt, the TCA cycle, amino acid biosynthesis, and carbohydrate metabolism compared to those pretreated with water.

GABA has also been studied in the context of anoxia and hypoxia, revealing potentially different biochemical responses to these stresses. An early study conducted by Streeter and Thompson (1972) revealed that radish leaves exposed to anoxia for 4 h exhibited an impressive 100-fold increase in GABA content compared to control leaves. However, hypoxic stress did not elicit any change in root or shoot GABA levels in *Arabidopsis*, and transcript analysis of roots exposed to hypoxia over 24 h showed unchanged levels of both *GAD1* and *POP2* expression (Miyashita and Good, 2008). Furthermore, *pop2* mutants exhibit repressed accumulation of alanine compared to WT plants under hypoxia in the roots (Miyashita and Good, 2008). Given that alanine can be produced by pyruvate-dependent GABA-T activity, it is feasible that increased flux through the shunt occurs under hypoxic stress, resulting in GABA-dependent alanine accumulation. By contrast, GABA accumulation during anoxia may be more important because respiration (i.e. mitochondrial electron transport chain and TCA cycle activity) is oxygen-dependent, even with the support of the GABA shunt.

2.1.4 GABA and Plant Biotic Stress

GABA may also help plants acclimate to herbivory and pathogen infection. Insect footsteps stimulated rapid GABA accumulation (up to 5-fold) in tobacco and soybean leaves, along with superoxide (Bown *et al.*, 2002). Feeding on a diet supplemented with 1.6 to 2.6 μmol/g fresh weight GABA impeded the growth, development, and overall survival of leafroller (*Choristoneura rosaceana* cv Harris) larvae (Ramputh and Bown, 1996). Thus, the GABA spike in response to insect footsteps and leaf feeding may be effective for deterring herbivory due to the depressing effects of GABA on animal nervous systems when ingested. Indeed, transgenic plants producing enhanced GABA levels exhibited heightened resistance against insect pests.

Tobacco budworm larvae preferentially fed on WT leaf tissue over GABA accumulating leaves of transgenic tobacco (*Nicotiana tabacum* L.) plants overexpressing GAD (MacGregor *et al.*, 2003). Moreover, northern root nematodes infecting these GAD overexpressing plants exhibited a ~60% decrease in egg mass compared to WT tobacco plants (McLean *et al.*, 2003). GABA is similarly accumulated in *pop2* mutants which have a non-functional GABA-T. *Spodoptera littoralis* leafworms feeding on *pop2* leaves had significantly reduced larval weight compared to those feeding on leaves of WT *Arabidopsis* (Scholz *et al.*, 2017). The resistance mechanism in response to and in anticipation of insect herbivory seems to involve GAD and GABA, although the precise process has not yet been elucidated.

Recently, Scholz and co-workers reported that the role of GABA in herbivory is both jasmonate (JA)- and Ca^{2+}-independent (Scholz *et al.*, 2017; Scholz *et al.*, 2015). The two signaling pathways are induced in response to herbivory, where JA is translocated from local to distal leaves and Ca^{2+} waves are triggered via an electrical signal upon mechanical wounding. In *Arabidopsis*, JA translocation via AtJAT3/4 transporters embedded in plasma membranes of phloem cells are partially responsible for wound-induced JA accumulation in distal leaves. Mutant *atjat3/4* plants exhibited reduced systemic JA accumulation, whereas the opposite occurred with AtJAT3/4 overexpressors (Li *et al.*, 2020). Although at*gad1/2* and at*gad1/2 x pop2* mutants contained significantly reduced and increased levels of GABA, respectively, compared to WT in response to insect herbivory, levels of JA and JA-Ile were unaffected (Scholz *et al.*, 2015). Furthermore, treatment of WT leaves with a synthetic JA-Ile mimic triggered the expected upregulation of *JA-biosynthetic* and *JA-responsive* genes, but had no impact on GABA levels, indicating that the two pathways function autonomously. Meanwhile, systemic elevations in cytosolic Ca^{2+} levels in response to insect herbivory are the result of Ca^{2+} transport into the

cytosol of adjacent leaves via the Ca^{2+}-permeable tonoplast channel, TWO PORE CHANNEL 1 (TPC1-2) (Kiep *et al.*, 2015). Moreover, Ca^{2+} activates GAD (when complexed with CaM), the enzyme responsible for synthesising GABA (Snedden *et al.*, 1996). However, *tcp1-2* mutant plants still exhibited systemic GABA elevations, despite being incapable of transporting Ca^{2+} into the cytosol from vacuoles, the major storage compartment within adjacent leaves (Scholz *et al.*, 2017). D_2-labeled GABA is not translocated to these vascularly connected leaves, but rather endogenous GABA biosynthesis is stimulated upon wounding and application of exogenous labeled GABA. If neither JA/Ca^{2+}-signaling nor GABA translocation are responsible for accumulating the metabolite in systemic tissues, there must be some as yet undetermined mechanism that initiates this under herbivory attack.

Similar to the response during herbivory, GABA accumulation has often been associated with enhanced plant resistance against pathogenic infection. GABA is the major amino acid in the apoplast of tomato (*Lycopersicon esculentum*) leaves infected with the fungal pathogen *Cladosporium fulvum*, reaching up to 2.5 mM there (Solomon and Oliver, 2001, 2002). In addition, GABA was the most abundant amino acid (close to 1 mM) in the apoplast of common bean (*Phaseolus vulgaris*) plants following inoculation with an effector-triggered immunity-eliciting strain of the pathogenic microbe *Pseudomonas syringae* (O'Leary *et al.*, 2016). Metabolic footprinting analyzed a wide range of nutrient sources, and although GABA was taken up by *P. syringae*, it was not the preferred nutrient as uptake was slower compared to malate, maleate, and Glu, amongst others, suggesting it may be able to use some of the enriched apoplastic GABA levels as a nutrient source. In fact, *C. fulvum* has a functional GABA-T that was induced during growth on GABA and Glu during infection (Solomon and Oliver, 2002). However, other evidence indicates that GABA accumulation decreased susceptibility to

infection, suggesting a role for GABA as a defense compound. While *P. syringae Pto* DC3000 was able to grow on GABA supplemented media, high GABA levels of *pop2* mutant plants as well as *gabt Pto* DC3000 mutants – both impaired in their abilities to degrade GABA – inhibited bacterial growth and expression of *hypersensitive reaction and pathogenicity* genes (Park *et al.*, 2010). GABA may serve as a nutrient source for pathogens; however, conditions that promote high accumulation of the metabolite confer greater resistance to host plants, indicating a protective role of GABA against infection in some pathosystems.

In other cases, evidence suggests that perhaps GABA levels themselves are not critical but rather it is the tight control of flux through the GABA shunt that imparts greater resistance to infection. An ABA-deficient tomato mutant, *sitiens*, is less susceptible to infection by the necrotrophic fungus, *B. cinerea*, through a mechanism related to GABA metabolism (Seifi *et al.*, 2013). This mutant exhibits upregulated transcript expression of *GAD1/2* and *GABA-T* following inoculation, whereas this upregulation does not occur in WT tomato. Furthermore, although endogenous GABA levels were overall higher in WT compared to *sitiens*, GABA concentrations in the mutant leaves oscillated rather than staying relatively constant as in WT leaves. Taken together, the evidence provides a basis for temporal increases in GABA shunt flux being responsible for resistance against *B. cinerea*. The authors further postulated that this may be due to suppression of cell death, a favourable outcome when infected by a necrotrophic pathogen. In contrast, infection of tomato with a highly aggressive strain of the pathogenic bacterium *Ralstonia solanacearum*, RsH, led to downregulation of the shoot-specific GAD2 isoform and upregulation of enzymes involved in GABA metabolism, GABA-T and SSA dehydrogenase, at both transcriptional and translational levels (Wang *et al.*, 2019). However, this difference is likely due to a pathogen strategy of the highly virulent strain to compromise host defenses, which

may target GABA biosynthesis and/or GABA shunt flux. This was further supported by the virus-induced gene silencing of *GAD2*, which led to a more susceptible host against RsH.

GABA fulfils its protective role against various pathogens via different mechanism, most of which are not well understood; however, during bacterial infection the metabolite has been known to serve as an interspecies signal to interrupt quorum-sensing, and therefore virulence. Supplementing *Agrobacterium tumefaciens* with 0.5 and 1 mM GABA or wounded tomato stems (high [GABA]) inactivated a quorum-sensing mechanism (Chevrot *et al.*, 2006). Furthermore, selective GABA sensors in some bacteria are targeted by host-derived GABA, attenuating quorum-sensing (Planamente *et al.*, 2012). Here, we find evidence that not only can GABA act *in planta*, but it may also serve as an interspecies signal in host plant-microbe interactions to stave off infection.

Broadly speaking, the triggers and physiological effects of GABA are highly diverse, leaving many questions as to its role and evolutionary significance in plants unanswered. The mechanism of action against different pest and pathogen species (and abiotic stresses) are variable, making it difficult to pinpoint if and how GABA provides protection from such stressors.

2.1.5 Plant GABA Signaling

To add to its complexity, GABA has been suggested to serve as a signal molecule in plants, with evidence for the requirement of a GABA gradient cueing normal pollen tube growth and development. In *Arabidopsis*, the gradient ranges from 20 μM in the stigma up to 160 μM in the ovaries – an 8-fold increase from one end to the other (Palanivelu *et al.*, 2003). Similarly, tobacco pollen tubes displayed a ~5.6-fold increase in GABA levels from stigma to ovaries (Yu

et al., 2014). Unsurprisingly, *pop2* mutants exhibit defective pollen tube elongation and application of exogenous GABA exacerbates other elongation defects, such as impaired primary root growth (Renault *et al.*, 2011). Further transcriptome and microarray analysis of vegetative tissue from *pop2* mutants exposed to exogenous GABA revealed decreased gene expression of cell wall-related and secreted-protein genes. The need for normal GABA levels and gradients to cue cell elongation and development points to a role in signaling; a parallel to the GABA gradient-dependent development of nervous systems observed in animals (Li and Xu, 2008).

In the past, the fact that GABA can spike to such high concentrations (mM range) in plant tissues was used as a counterargument against GABA acting as a signaling molecule; however, such was the sentiment around the role of GABA in animals (which can also reach up to the mM range), until mammalian GABAergic receptors were discovered. Recently, GABA was discovered to bind and inhibit aluminum-activated malate transporter-1 (ALMT1) on wheat cell plasma membranes (Ramesh *et al.*, 2015). This provided the first evidence that even in plants, GABA can regulate another protein to transduce a signal. For years it was unclear whether intracellular or extracellular GABA was responsible for this inhibition (Long *et al.*, 2020; Ramesh *et al.*, 2018; Ramesh *et al.*, 2015; Sharma *et al.*, 2016). However, very recently the structure of *Arabidopsis* ALMT1 was established by cryo-electron microscopy, revealing that GABA binding occurs via the cytosolic face, supporting a role for intracellular regulation (Wang *et al.*, 2021). Like the mammalian $GABA_A$ receptor, ALMTs are anion channels, and GABA-binding prevents malate efflux from the cell and subsequent hyperpolarization of membrane potentials (Gilliham and Tyerman, 2016; Ramesh *et al.*, 2017). Besides the 12-amino acid domain to which GABA binds, ALMTs and $GABA_A$ receptors do not share sequence homology. Moreover, µM levels of GABA inhibit ALMTs, but activate $GABA_A$ receptors (Ramesh *et al.*,

2015). We are certainly in an exciting phase of GABA research, as discovery of the first GABA receptor is expected to help uncover downstream signaling pathways and physiological effects.

Plant ALMT families are relatively large (e.g., *Arabidopsis* contains 14 members that exhibit tissue-specific expression) and are involved in a range of functions not described by their namesake (Al^{3+}-activated). ALMT1 is expressed in the root apex and is not only activated by high Al^{3+}, but also high Fe^{3+} or low Pi. The exudation of carboxylates, such as malate, at the roots is especially important for chelating Al^{3+} and Fe^{3+} from soil-located, insoluble metal cation-Pi complexes, thereby solubilizing Pi for root uptake by –Pi plants (Dissanayaka *et al.*, 2021). Indeed, low Pi, high Fe^{3+}, and/or high Al^{3+} activates the STOP1 transcription factor, which upregulates root *ALMT1* expression (Balzergue *et al.*, 2017; Sawaki *et al.*, 2009). Malate exudation via ALMT1 was identified as being a component responsible for the of inhibition of root cell elongation during low Pi or high Fe^{3+} soil stress. In contrast, AtALMT12 is a guard cell quick anion channel involved in stomatal closure, but not opening (Sasaki *et al.*, 2010). This transporter does not respond to Al^{3+}, and loss-of-function mutants display a larger stomatal aperture width and more rapid water loss compared to WT. In conjunction with ALMT12, tonoplast-localized AtALMT6 and AtALMT9 also contribute to regulating guard cell volume for mediating stomatal opening and closure (Sharma *et al.*, 2016). GABA is known to be involved in regulation of stomatal conductance and aperture (Abdel Razik *et al.*, 2021; Mekonnen *et al.*, 2016; Xu *et al.*, 2021), which necessitates studies to investigate whether ALMTs are a target protein for mediating this phenomenon.

GABA regulation of ALMTs may be transducing signals as part of several physiological and biochemical pathways. Ramesh *et al.* (2015) assessed malate exudation from wheat roots via TaALMT1 in relation to pH and Al^{3+} stress and found reciprocal responses. During acid stress

alone, GABA accumulated to a high concentration, whereas root malate efflux was very low. In contrast, during Al^{3+}stress (100 μM Al^{3+} at acidic pH), GABA levels remained low while malate efflux was greatly enhanced. As well, *in vitro Arabidopsis* and grapevine pollen tube growth assays further demonstrated that GABA-regulated ALMT activity is involved in normal pollen tube growth, providing a mechanism for GABA signaling not only during stress responses but also in growth and development (Ramesh *et al.*, 2015). The authors concluded that similar GABA regulation likely exists for other ALMTs, given that their GABA-binding motif is highly conserved.

In the case of guard cell localized ALMTs, GABA accumulation during drought stress likely plays a role in regulating this transporter, and therefore stomatal aperture. Genetic studies have revealed that GABA regulation of tonoplast-localized AtALMT9 does indeed contribute to the drought response (Xu *et al.*, 2021). This transporter is specifically involved in malate and chloride uptake into vacuoles. Under non-stressed conditions *atgad2* mutants exhibit impaired stomatal closure and enhanced stomatal opening, compared to *atgad2/almt9* double mutants in which stomatal aperture and conductance revert back to WT phenotypes. It has been proposed that as GABA levels rise during drought stress, the consequent inhibition of malate transport into vacuoles reduces stomatal width to conserve water loss, subsequently improving water use efficiency (Xu *et al.*, 2021). By contrast, GABA accumulates during hypoxia (i.e. waterlogging), and exogenous GABA application improved the growth of hypoxic maize seedlings (Kreuzwieser *et al.*, 2009; Salah *et al.*, 2019). However, we cannot discount the possibility that GABA-induced stress responses to drought versus waterlogging are mediated by different pathways. ALMTs have additional functions in various cell membrane signaling pathways involved in gas exchange modulation, and response to pathogens, salinity, and acidosis (Gilliham

and Tyerman, 2016; Ramesh *et al.*, 2017), most of which are physiological responses that GABA plays a role in as well. Therefore, the involvement of GABA in regulating ALMT and the downstream physiological effects seem to indicate that the molecule is a player in cell membrane potential regulation and signal transduction.

Aside from ALMTs, a recent study identified guard cell outward-rectifying potassium (GORK) channels as an alternative GABA sensor and signal transducer. GORKs contain the same GABA-binding motif as found in ALMTs (Adem *et al.*, 2020). These channels are involved in K^+ transport and are expressed not only in guard cells as their name suggests, but also in other tissues such as the root epidermis. Wounding triggers Ca^{2+}-signaling, which in turn promotes CBL1-CIPK5 interaction, which phosphorylates guard cell GORK channel to enhance K^+ efflux (Förster *et al.*, 2019). Rapid K^+ depletion occurs in response to a range of other stresses, and there is emerging evidence that K^+ may be involved in some signaling pathways in plants (Shabala, 2017). Interestingly, 10 mM exogenous GABA appears to exert some control over GORK channels as K^+ efflux was transiently induced in root epidermal cells of WT but not *gork1 Arabidopsis* mutants (Adem *et al.*, 2020). Previously, greater water transpiration was measured from excised *gork1* rosette leaves compared to WT (Hosy *et al.*, 2003).

Given this, there is a great amount of interest to validate this GABA-GORK connection using biochemical and genetic approaches. It could be that GORKs serve an important role, particularly during stress responses by transducing GABA signals into K^+ efflux changes, although the mechanisms by which K^+ flux signatures are decoded are not yet known.

Owing to the past couple decades of research, researchers have amassed data identifying: GABA gradients in plant tissues essential for growth and development (Palanivelu *et al.*, 2003), (ii) wound-induced systemic GABA accumulation which is independent of GABA translocation

and elevations in Ca^{2+} concentration (Scholz *et al.*, 2017), (iii) interspecies GABA signaling to disrupt bacterial quorum-sensing (Chevrot *et al.*, 2006; Planamente *et al.*, 2012), and (iv) GABA receptors of plant cell membranes (Adem *et al.*, 2020; Ramesh *et al.*, 2017). Taken together, this evidence is strongly suggestive of a role for GABA in signal transduction pathways.

2.2 The Predominant GABA-producing enzyme: GAD

To better understand the functions and significance of GABA, we can study the activity and regulation of GAD, the well-characterized Ca^{2+}-CaM activated cytosolic enzyme responsible for irreversibly producing GABA as the first committed step of the GABA shunt (Fig. 2-2).

2.2.1 Tissue-Specific AtGAD Transcript Expression

The five *Arabidopsis* GAD (AtGAD) isozymes differ in their tissue-specific transcript expression levels. *AtGAD1* is highly expressed in roots, and stresses appear to have no effect on its constitutive transcriptional expression there, although abiotic stress (i.e. salinity) can induce its expression in shoots (Miyashita and Good, 2008; Scholz *et al.*, 2015). *AtGAD2* is expressed throughout most other tissues including shoots and flowers, although it has been detected in roots in some studies (Miyashita and Good, 2008; Scholz *et al.*, 2015). *AtGAD3/4* transcripts are expressed at low levels, although they have been detected in flowers and siliques, whereas abiotic stresses (e.g., hypoxia or salinity) transiently induce their expression in roots and vascular tissue (Miyashita and Good, 2008; Zarei *et al.*, 2017). *AtGAD5* is expressed in flowers, mature pollen and stamens (Miyashita and Good, 2008). AtGAD1 (AT5G17330) is one of the best-studied AtGAD isozymes due to its high basal expression in roots. An *atgad1* T-DNA insertional KO mutant exhibited no obvious phenotype compared to WT under normal conditions, although

root GABA levels were reduced seven-fold (Bouché *et al.*, 2004). Furthermore, *atgad1* mutants do not exhibit the typical spike in root GABA levels that follows heat stress, demonstrating the influence AtGAD1 holds in maintaining appropriate GABA levels under both normal and stressed conditions. Given that AtGAD1/2 together are responsible for producing the majority of GABA throughout the plant, many phenotypic studies used a double *atgad1/2* mutant to assess the impact of GABA and GABA shunt deficiency, as reported in previous sections.

2.2.2 Biochemical Properties of Plant GADs

GADs belong to the largest family of pyridoxal-5'-phosphate (PLP) dependent enzymes: fold I, possessing PLP-binding Lys residue (Fig. 2-3) (Astegno *et al.*, 2015). The 57-kDa AtGAD1 subunits exist in equilibrium as homodimers and trimers of dimers but exhibit enhanced activity in the hexameric form (Astegno *et al.*, 2015). GAD activity is regulated by a pH-dependent mechanism across all organisms, whereby acidification of the cytosol leads to upregulation of activity presumably upon mechanical stress causing vacuolar lysis and subsequent release of H^+ (Bouché *et al.*, 2004; Gut *et al.*, 2009). Acidic pH (< 6.5) provides a conducive environment for electrostatic interactions to form between N-terminal regions at subunit interfaces, promoting hexamerization, and therefore enhanced GAD activity. Plant GADs are unique in that they can also be activated by Ca^{2+}/CaM-binding at physiological pH (~7.2), which was first discovered in soybean (Snedden *et al.*, 1995). Ca^{2+}/CaM binding removes the autoinhibitory domains of two adjacent subunits in 3:1 Ca^{2+}/CaM:hexameric GAD stoichiometry, bringing together three homodimers to form the larger complex (Astegno *et al.*, 2015). For this reason, this mechanism of Ca^{2+}/CaM-activation is apparent at physiological pH where GAD would otherwise be in its dimeric state, but GAD becomes increasingly de-

sensitized to this as the pH drops, which also drives GAD hexamerization and maximizes GAD activity. In *Arabidopsis*, three out of five GAD isozymes (AtGAD1/2/4) possess a CaM-binding domain containing a key tryptophan residue at their C-terminus (Fig. 2-3) (Shelp *et al.*, 2012a). GAD is the only enzyme of central plant metabolism known to be regulated by Ca^{2+}/CaM binding, making it unique and a fascinating protein.

As evidence for CaM-binding of plant GADs mounted, studies reported that GAD activation at physiological pH was only stimulated with the addition of Ca^{2+} with CaM, which alters GAD conformation to displace the C-terminal autoinhibitory domain (Snedden *et al.*, 1995; Snedden *et al.*, 1996). Recombinant AtGAD1 (rAtGAD1) activity was stimulated 35-fold under these conditions, while recombinant (rAtGAD2) was stimulated 14-fold (Table 2-1) (Turano and Fang, 1998). Similar experiments using recombinant tobacco GADs reported 57-133-fold increase in GAD activity upon Ca^{2+}/CaM addition (Yevtushenko *et al.*, 2003; Yun and Oh, 1998). More recently, the autoinhibitory C-terminal domain was removed to drive GABA accumulation in tomato fruit (Takayama *et al.*, 2017). However, not all plant GADs are stimulated by this Ca^{2+}-dependent manner as some isozymes completely lack the CaM binding domain.

Various analyses of the kinetic properties of some native and recombinant plant GADs have been reported. The V_{max} of native GAD from rice germ is 7.6 μmol/min/mg (units/mg), whereas recombinant GADs typically exhibit higher V_{max} values. For instance, recombinant petunia GAD has a V_{max} of 30.6 units/mg at optimal pH, while recombinant AtGADs (rAtGADs) have V_{max} values ranging from ~30-70 units/mg depending on pH and presence/absence of Ca^{2+}/CaM (Table 2-1) (Astegno *et al.*, 2015; Snedden *et al.*, 1996; Turano and Fang, 1998; Wang *et al.*, 2010; Zhang *et al.*, 2007). GAD's K_m(Glu) has been measured to be as low as ~3

mM in cowpea and barley root, and as high as ~30 mM in rice (Table 2-1) (Inatomi and Slaughter, 1975; Wang *et al.*, 2010; Zhang *et al.*, 2007). In extracts of barley root, GAD activity was discovered to be enhanced 10% by the co-factor PLP (Inatomi and Slaughter, 1975). Further studies determined GAD's K_m(PLP) to range from ~1-2 μM in both potato and rice (Narayan and Nair, 1986; Wang *et al.*, 2010; Zhang *et al.*, 2007). Many facets of plant GAD kinetics have been explored and characterized, but rarely using native enzymes, with no studies reported on native AtGAD1. Thus, the impact of various GAD PTMs that occur *in planta* on its kinetic properties, but are absent in recombinant GADs, merit further exploration.

2.2.3 AtGAD1 Phosphorylation

An additional mechanism of GAD regulation may exist, as various high-throughput plant phosphoproteomic studies have identified *in vivo* phosphorylated forms of GAD, including AtGAD1 from both *Arabidopsis* suspension cells and seedlings (Lin *et al.*, 2015; Mehta *et al.*, 2021; Rayapuram *et al.*, 2018; Wu *et al.*, 2013). With at least 70% of eukaryotic proteins thought to undergo phosphorylation at some point in their lifetime (with many having multiple phosphosites), it is arguably the most important PTM (Plaxton and Shane, 2015). Enzyme phosphorylation can trigger diverse effects that may impact its activity and/or susceptibility to allosteric effectors, subcellular location, interaction with other proteins, or turnover via proteolysis.

Our recent collaborative phosphoproteomics study identified 587 phosphoproteins whose phosphorylation status significantly changed 48 h following Pi resupply to -Pi Arabidopsis suspension cells (Mehta *et al.*, 2021). Interestingly, one of the most hyperphosphorylated proteins in the entire dataset was AtGAD1, with multiple N-terminal seryl phosphorylation sites

(i.e. Ser4, Ser8, Ser10, Ser13, and Ser16) increasing in response to Pi refeeding. Importantly, there was no significant change in the abundance of AtGAD1 polypeptides, so N-terminal AtGAD1 dephosphorylation appears to be involved in some aspect of the PSR. However, this was not the first study to detect AtGAD1 phosphorylation *in planta*. Rayapuram *et al.* (2018) reported AtGAD1 phosphorylation at Ser13 and Ser16 in seedlings following microbe-associated molecular pattern treatment, while Lin *et al.* (2015) noted that AtGAD1 became more phosphorylated at Ser8, Ser10, and Ser13 upon brassinosteroid treatment of *Arabidiopsis* suspension cells. Interestingly, a phosphoproteomic study examining the impact of salinity stress on maize seedlings reported that the AtGAD1 ortholog ZmGAD1 (protein ID B4F972) became significantly dephosphorylated at analogous N-terminal seryl residues 0.5 h following application of 100 mM NaCl (Zhao *et al.*, 2019). This seems consistent with our observation that GAD is hypophosphorylated in –Pi, relative to Pi-resupplied *Arabidopsis* (Mehta *et al.*, 2021). However, dephosphorylated ZmGAD1 coincided with Glu accumulation in salt-stressed maize (GABA concentration was not measured) (Zhao *et al.*, 2019). The authors suggested this might be occurring so that Glu can be used preferentially as a substrate for proline rather than GABA synthesis during salt stress. Dephosphorylation of ZmGAD1's N-terminus was hypothesized to inhibit ZmGAD1activity, making the functions and mechanisms of plant GAD phosphorylation an unresolved and interesting question. Despite the recent identification of numerous phosphosites in plant GADs, to the best of my knowledge the function of this multisite phosphorylation has not been investigated. Likewise, nothing is known about the protein kinase(s) responsible nor upstream signaling pathways that mediate *in vivo* phosphorylation of plant GADs.

2.2.4 Functional Role of GAD Phosphorylation

The dramatic rise of GABA levels under a variety of stresses has been well-documented in plants, making GAD, the enzyme producing GABA, an integral component of stress response. AtGAD1 dephosphorylation in -Pi *Arabidopsis* cells (Mehta *et al.*, 2021) may be involved in enhancing enzyme activity to increase GABA levels and/or flux through the GABA shunt as part of the PSR. In this scenario, refeeding Pi to -Pi cells triggers AtGAD1 hyperphosphorylation at multiple N-terminal seryl residues, which in turn may inhibit its activity at a time when stress responses are no longer needed. Various metabolomic studies have documented increased GABA levels in either shoots and/or roots in response to Pi deprivation, and one study encountered a drastic 4-fold increase in the rate of GABA exudation from roots of -Pi corn plants compared to control conditions as well as other nutrient deficiencies (i.e. iron, potassium, nitrogen) (Carvalhais *et al.*, 2011; Hernández *et al.*, 2007; Huang *et al.*, 2008; Pant *et al.*, 2015; Sung *et al.*, 2015). Less commonly, other studies reported reduced GABA levels during plant Pi deprivation (Huang *et al.*, 2008; Valentinuzzi *et al.*, 2015). Despite this, the majority of metabolomic evidence suggests GABA spikes are innate to the plant PSR, similar to those observed in response to other abiotic stresses.

It was recently hypothesized that the GABA shunt functions as an important TCA cycle bypass during periods of stress that result in depletion of cellular levels of the enzyme co-factor thiamine diphosphate (TPP), thereby inhibiting 2-OGDH, a TPP-dependent enzyme of the TCA cycle (Joshi *et al.*, 2019). By upregulating the GABA shunt this blockage in the TCA cycle would be circumvented, allowing 2-OG to be converted into succinate via this alternative 'bypass' pathway (Fig. 2-2A). As is the case for most Pi-containing compounds (Dissanayaka *et al.*, 2021), severe Pi deprivation is expected to deplete TPP levels in -Pi plant cells. If indeed

TPP levels drop in response to Pi deprivation, upregulating GAD activity to divert 2-OG to the GABA shunt would compensate for impaired 2-OGDH activity thereby ensuring that the TCA cycle and hence mitochondrial respiration can continue. This suggests that the GABA shunt might serve as a critical bypass of TPP-limited 2-OGDH during Pi starvation. This hypothesis is reminiscent of several Pi- and adenylate-independent 'bypass' pathways of cytosolic glycolysis and mitochondrial electron transport that are upregulated in -Pi plants (see Fig. 2-1) (Dissanayaka *et al.,* 2021).

Apart from potential kinetic effects of AtGAD1 (de)phosphorylation, it is possible that its phosphorylation status either has an impact on, or is the result of, a change in subcellular localization. Interestingly, similar N-terminal phosphorylation at Ser3, Ser6, Ser10 and Ser13 was detected in human GAD2 (HsGAD2) when associated with the membranes of GABA-releasing vesicles at nerve synapses (Namchuk *et al.*, 1997). Phosphoablative HsGAD2 can still associate with neuronal membranes, indicating that phosphorylation is not required for binding; rather the N-terminus becomes phosphorylated after binding. If the function of N-terminal GAD phosphorylation is indeed evolutionarily conserved, previous studies on HsGAD2 may serve as a model for research into whether plant GAD phosphorylation also distinguishes membrane-associated from cytosolic GAD. To date, plant GADs have been frequently identified in soluble fractions of plant tissue extracts and are routinely characterized as cytosolic, although this is not particularly strong evidence for cytosolic localization. However, if phosphorylation is mediating membrane-association, extraction and fractionation in the absence of appropriate phosphatase inhibitors could lead to rapid *in vitro* GAD dephosphorylation by endogenous phosphatases leaving the enzyme largely in the soluble fraction. Even if GAD phosphorylation occurs after association to membranes, the extraction step may be harsh enough to break up weaker

associations. No plant GAD has been imaged *in vivo*, which would provide meaningful data to either corroborate its cytosolic location as suggested in the literature, or to reveal novel localization of GADs.

2.3 Research Objectives

As noted above, results of our recent phosphoproteomics study indicated that the nutritional Pi status of *Arabidopsis* suspension cells markedly influences AtGAD1's phosphorylation status (Mehta *et al.*, 2021). Specifically, AtGAD1 became hypophosphorylated as part of the PSR, whereas 48 h of Pi-resupply induced hyperphosphorylation at five conserved seryl residues located near its N-terminus. These observations raise the main research question of my thesis: **what is the role(s) of these PTMs on AtGAD1 function?** The overarching goal of my MSc thesis research is to test the hypothesis that this phosphorylation event regulates the enzyme by: i) inhibiting AtGAD1 activity (e.g. its Ca^{2+}/CaM-sensitivity), and/or ii) altering its subcellular localization by mediating membrane association. Enhanced AtGAD1 activity during Pi deprivation would be in line with biochemical phenomena observed under a variety of other stresses, for example, GABA accumulation and/or increased flux through the GABA shunt – two scenarios that are not mutually exclusive. An effect of phosphorylation on GAD kinetics and/or membrane association are also not mutually exclusive hypotheses. While plant GABA is not packaged into vesicles for downstream secretion to transduce neurotransmitter signals as in animals, potential binding of AtGAD1 in -Pi cells (-P:GAD1) to the mitochondrial envelope may not be out of the question. If AtGAD1's function in -Pi cells is to mediate Glu partitioning into the GABA shunt, it would be useful for the enzyme to associate with GABA transporters of the mitochondrial membrane, as subsequent steps of the GABA shunt are located within the matrix

of this organelle (Fig. 2-2A). If this is the case, it may point to evolutionarily conserved N-terminal multisite phosphorylation and function across kingdoms.

At the onset of my study into GAD and the GABA shunt, my efforts were aimed at developing and validating the necessary tools to test the different hypotheses aimed at elucidating the role of AtGAD1 phosphorylation. A microtitre-plate based, spectrophotometric GAD activity assay was developed and validated, along with phosphosite-specific anti-AtGAD1 antiserum (α-pSer8) to monitor AtGAD1's phospho-status via immunoblotting. To obtain differentially phosphorylated forms of native AtGAD1, (i) the enzyme was fully purified from both -Pi and Pi-sufficient (+Pi) *Arabidopsis* suspension cells using fast protein liquid chromatography (FPLC), and (ii) multiple phosphatases were tested for their ability to *in vitro* dephosphorylate AtGAD1 isolated from the +Pi cells (+P:GAD1). Finally, various mCherry-tagged AtGAD1 clones were generated for transient expression and subsequent imaging of AtGAD1 localization in *Arabidopsis* suspension cells via fluorescence microscopy. Subsequent experiments were directed at assessing the impact of phosphorylation on AtGAD1's specific activity, and impact of AtGAD1 phospho-status on its subcellular localization.

Collectively, this research will expand our knowledge of how plant cells respond to abiotic stresses such as Pi deprivation, especially if GADs across plant taxa are similarly phosphorylated during recovery from other stress conditions. A better understanding of the post-translational control of AtGAD1 during and following plant abiotic and biotic stress, will help us define the physiological functions of the GABA shunt, as well GABA itself as an important plant stress metabolite and signaling molecule.

Table 2-1. V_{max} and K_m(Glu) values reported for various plant GAD preparations. Values measured at optimal acidic pH unless otherwise stated.

Species	*GAD Isozyme*	*Experimental Treatment*	*Phosphorylation Site(s)*	*Reference*
Mus musculus	GAD2	None	S3,S6,S10,S13,S61	(Wiśniewski *et al.* 2010)
Saccharomyces cerivisiae	GAD1	None	S30,S36,S40,S45,T51,S52,S53	(Schreiber *et al.* 2012)
Homo sapiens	GAD2	None	S3,S6,S10,S13	(Namchuk *et al.* 1997)
Oryza sativa L. (seedlings)	GAD1	Abscisic Acid	S8,S10,S13	(Qiu *et al.* 2017)
Oryza sativa L. (suspension cells)	GAD1	None	S10	(Nakagami *et al.* 2010)
Arabidopsis thaliana (suspension cells)	GAD1	Pi resupply to –Pi cells	S4, S8, S10, S13, S16	(Mehta *et al.*, 2021)
Arabidopsis thaliana (suspension cells)	GAD3	None	S10,T361,S368	(Nakagami *et al.* 2010; van Wijk *et al.* 2014)
Arabidopsis thaliana (seedlings)	GAD2	Dehydration	S6, S8, S83, S92	(Umezawa *et al.* 2013)
Arabidopsis thaliana (seedlings)	GAD4	None	T6,S8,S10,S13,S16,S79,Y84,T93	(Hoehenwarter *et al.* 2013)
Arabidopsis thaliana (seedlings)	GAD5	None	S7,S9,Y83,T92,S460,S474	(Mayank *et al.* 2012)
Gossypium hirsutum (leaf)	GAD1	Nitric Oxide	S13	(Fan *et al.* 2014)
Gossypium hirsutum (leaf)	GAD4	Nitric Oxide	S8	(Fan *et al.* 2014)

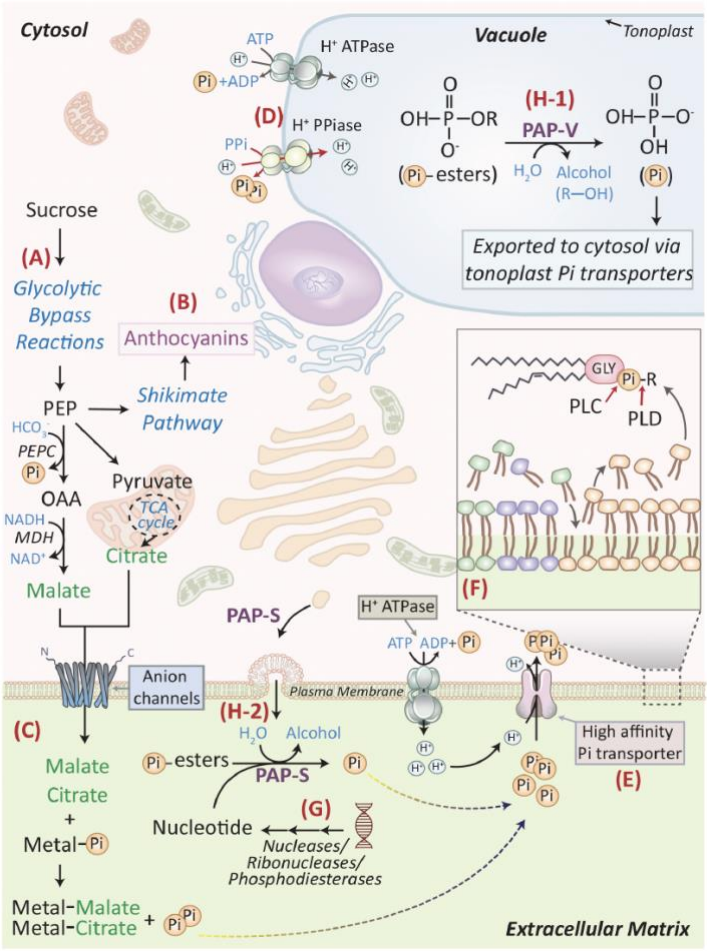

Fig. 2-1. Schematic of various Pi starvation inducible adaptive metabolic processes that help plants acclimate to -Pi conditions. (A) Upregulation of alternative glycolytic bypass reactions allowing for Pi to be recycled more efficiently during cellular respiration. **(B)** Anthocyanin accumulation via the shikimate pathway results in dark green and/or purple colouration of shoots. **(C)** Organic acids (i.e. malate and citrate) are exuded by roots to solubilize and liberate metal-complexed Pi. **(D)** Tonoplast-localized H^+-PPiase replaces the use of H^+-ATPase, thereby recycling Pi from pyrophosphate and conserving ATP. **(E)** -Pi inducible high affinity Pi transporters at the root plasma membrane pump Pi against its concentration gradient from the soil into the cell. **(F)** Typical phospholipids making up the membrane lipid bilayer are replaced with sulfo- and galactolipids so that Pi can be recycled. **(G, H-1)** Enzymes responsible for liberating Pi from various molecules (i.e. DNA, RNA, Pi-esters) are secreted into the soil or **(H-2)** are upregulated in vacuoles to liberate Pi from Pi-esters that have been transported into the vacuole from the cytoplasm.
(Figure reproduced from Dissanayaka *et al.*, 2021, with permission)

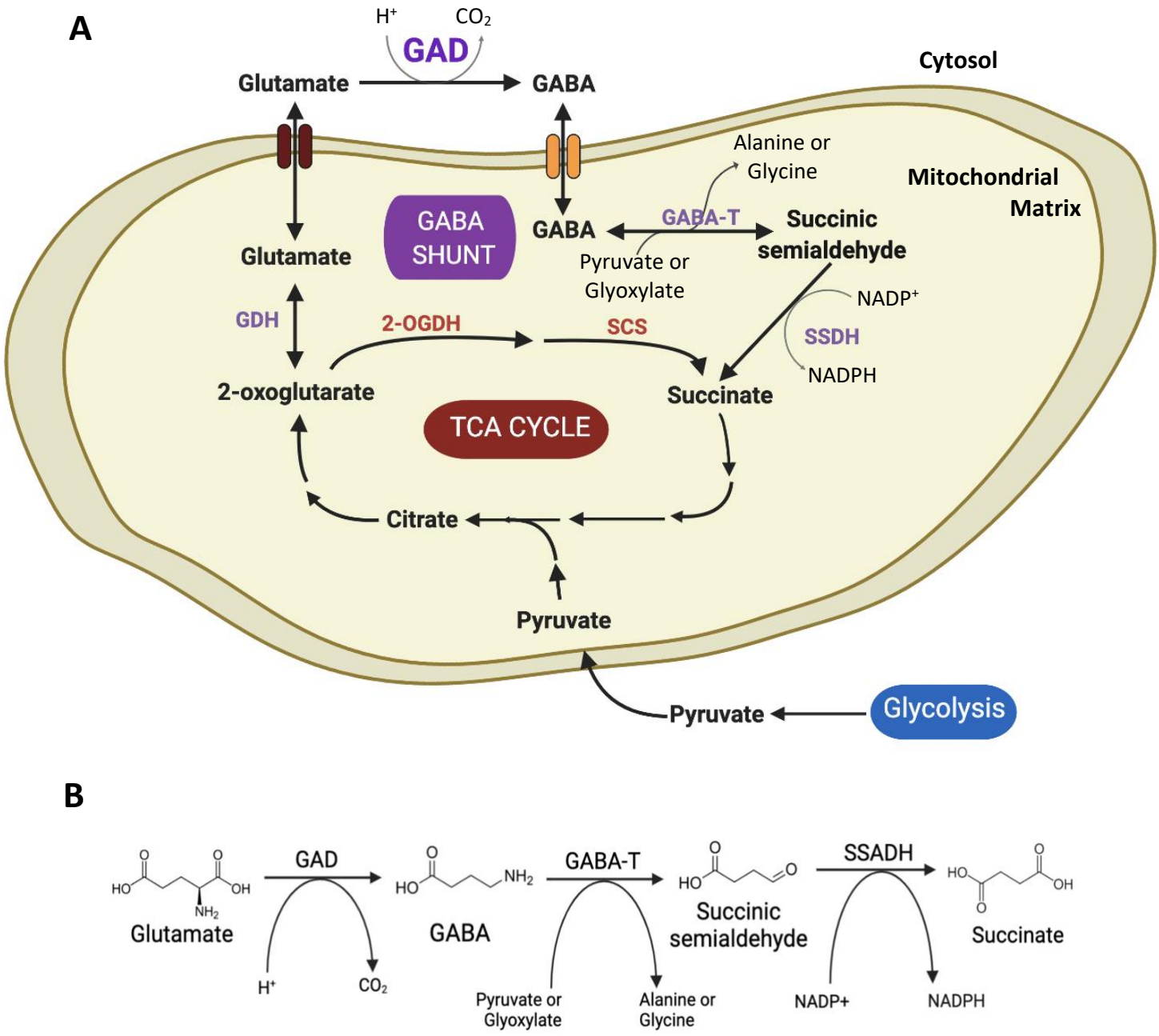

Fig. 2-2. The GABA shunt pathway. (A) The GABA shunt (enzymes denoted in purple) works in parallel with a portion of the TCA cycle (enzymes denoted in red), by providing a bypass of 2-OGDH and succinyl-CoA synthetase (SCS) steps that convert 2-OG into succinate. While the shunt is compartmentalized predominantly in the mitochondria, GAD catalysis of Glu into GABA takes place in the cytosol. **(B)** Molecular structures of GABA shunt intermediates.

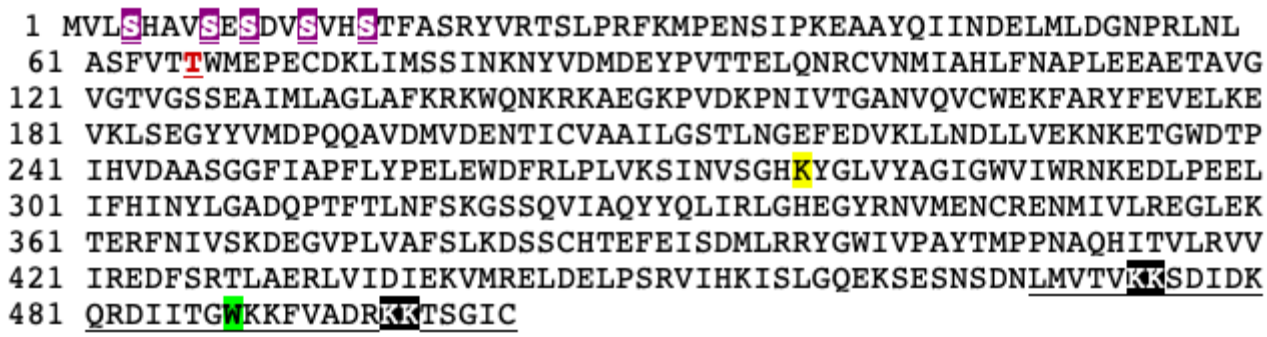

Fig 2-3. Deduced primary structure of AtGAD1 (accession number Q42521) edited manually to highlight residues and domains important for GAD function. Phosphoserine residues identified during LC-MS/MS analysis of tryptic digests prepared from the Pi-resupplied *Arabidopsis* cell cultures are highlighted in purple (Mehta *et al.*, 2021). A putative phosphothreonine-66 residue is bolded in red and underlined, based on sequence alignment with human GAD2. Highlighted in yellow is the PLP-binding Lys277 residue. The CaM binding domain at the C-terminus is underlined, with a key tryptophan residue highlighted in green (Snedden *et al.*, 1995) and conserved flanking positively charged lysine residues highlighted in black (Trobacher *et al.*, 2013).

Chapter 3: Differential *in vivo* phosphorylation activates the glutamate decarboxylase AtGAD1 in phosphate-starved *Arabidopsis thaliana*

Lee-Marie Raytek, Maria Camilo Rodriguez Gallo, Nathan Doner, Micah Grubert Van Iderstine, Robert T. Mullen, R. Glen Uhrig, Barry J. Shelp, Wayne Snedden, & William C. Plaxton

Abstract

GAD is a tightly controlled cytosolic enzyme that catalyzes the first committed step of the GABA shunt, which represents a partial metabolic bypass of the TCA cycle. AtGAD1 is a root-specific, Ca^{2+}/calmodulin-activated GAD isozyme that was recently documented to become *in vivo* hyperphosphorylated at multiple, conserved seryl residues located near the enzyme's N-terminus 48 h following Pi resupply to -Pi *Arabidopsis thaliana* suspension cells. Although *in vivo* phosphorylation of AtGAD1 and its orthologs at analogous residues has been reported in various high-throughput phosphoproteomic studies, nothing is known about the functions or mechanisms of plant GAD phosphorylation. We therefore compared the phospho-status, and physical and kinetic properties of AtGAD from Pi feed (+P:GAD1) and starved (-P:GAD1) cells. Gel filtration and SDS/PAGE demonstrated that both final preparations exist as a 330- or 345-kDa homohexamer composed of identical 57 kDa subunits. However, LC-MS/MS as well as immunoblotting of the respective final preparations with a phosphosite-specific antibody to Ser8 indicated that Pi deprivation triggered AtGAD1 dephosphorylation at Ser8. In contrast, phosphorylation at Ser4, Ser10, and Ser13 increased under -Pi conditions. Interestingly, the specific activity of purified –P:GAD1 was about 60% greater than that of +P:GAD1 at pH 5.8 (32 ±1.0 and 20 ±0.7 units/mg, respectively). *In vitro* dephosphorylation of +P:GAD1 with a commercial phosphatase was unsuccessful. Pi deprivation or resupply did not alter the diffuse cytosolic localization of transiently expressed AtGAD1-mCherry in the *Arabidopsis* cells. We

hypothesize that activation of AtGAD1 by differential phosphorylation mediates increased GABA accumulation and/or GABA shunt flux, and that this represents an important metabolic adaptations of -Pi plants.

3.1 Introduction

The GABA shunt bypasses reactions catalyzed by 2-OGDH and succinyl-CoA synthetase of the TCA cycle by diverting 2-OG through a partially cytosolic pathway (Michaeli *et al.*, 2011; Shelp *et al.*, 2021). GAD catalyzes the first committed step of the GABA shunt by converting glutamate into GABA and CO_2 while consuming a proton, at which point GABA can accumulate and/or be oxidized into succinate by the combined reactions of GABA transaminase and succinic-semialdehyde dehydrogenase (Fig. 1-2A). The GABA shunt has been hypothesized to help ensure that plant cells maintain flux through the TCA cycle – and therefore respiration – whenever 2-OGDH and/or succinyl-CoA synthetase become inhibited (Joshi *et al.*, 2019). For example, salinity stress of wheat seedlings was reported to trigger enhanced GABA shunt flux to bypass the salt-sensitive 2-OGDH of the mitochondrial TCA cycle (Che-Othman *et al.*, 2020).

GABA is an abundant, non-proteinogenic amino acid that is a major inhibitory neurotransmitter in mammals, whereas it confers resistance to acidosis in certain bacteria (Krnjević and Schwartz, 1967; Lund *et al.*, 2014). However, the functions of GABA in plants remain somewhat enigmatic. Levels of the metabolite vary depending on the particular plant tissue and influences from circadian rhythms but can reach the mM range (Ramesh *et al.*, 2017; Yin *et al.*, 2010). Rapid GABA spikes have been documented in plant cells acclimating to various stresses including salinity, cold, heat, insect herbivory, pathogen infection, and oxidative stress; GABA levels may also fluctuate to regulate cytosolic pH or to serve as a buffering mechanism in C/N metabolism (Michaeli and Fromm, 2015; Roberts, 2007; Scholz *et al.*, 2017;

Shelp *et al.*, 2017; Shelp *et al.*, 2012b). GABA also appears to function as a signal metabolite in plants, with evidence for: (i) the requirement of a GABA gradient for tobacco pollen tube growth and development, and (ii) the existence of GABA receptors known as ALMTs and GORK channels (Adem *et al.*, 2020; Ramesh *et al.*, 2017; Yu *et al.*, 2014).

GAD is a ubiquitous cytosolic enzyme in vascular plants that belongs to the largest family of pyridoxal-5'-phosphate (PLP) dependent enzymes: fold I, possessing a PLP-binding Lys residue (Rossignoli *et al.*, 2018). GAD is regulated by a pH-dependent mechanism across all organisms, whereby cytosolic acidification leads to upregulated activity, i.e. as would occur upon mechanical stresses that cause vacuolar lysis and subsequent release of H^+ ions (Bouché *et al.*, 2004; Gut *et al.*, 2009). However, a distinctive kinetic feature of plant GADs is that it is the only enzyme of intermediary metabolism known to be activated by Ca^{2+}/CaM-binding at physiological pH (Snedden *et al.*, 1995). CaM is a prototypical Ca^{2+} sensor protein that plays a central role in Ca^{2+} signaling in eukaryotic cells. In *Arabidopsis thaliana*, three of five GAD isozymes (AtGAD1/2/4) possess a CaM-binding domain at their C-terminus, which consists of a key Trp-Lys-Lys-Phe-Val motif (Fig. 3-3A) (Shelp *et al.*, 2012a). An additional post-translational control mechanism for plant GADs may also exist, however, as numerous phosphoproteomic studies have identified *in vivo* phosphorylated forms of GAD in various plant organs and suspension cells (Table 3-1) (Lin *et al.*, 2015; Mehta *et al.*, 2021; Rayapuram *et al.*, 2018; Wu *et al.*, 2013; Zhao *et al.*, 2019). For example, AtGAD1 became hyperphosphorylated at multiple seryl residues located near its N-terminus (i.e. Ser4, Ser8, Ser10, Ser13, and Ser16) 48 h following resupply of 2 mM Pi to -Pi *Arabidopsis* suspension cells**,** with no significant effect on AtGAD1 protein expression levels (Mehta *et al.*, 2021). Although AtGAD1 is a root-specific isozyme, it was the only GAD detected during LC-MS/MS analysis of the *Arabidopsis*

cell suspension culture (phospho)proteome. Similarly, recovery from short-term salinity stress of maize seedlings was associated with ZmGAD1 phosphorylation at several analogous N-terminal seryl residues (Zhao *et al.*, 2019). Despite abundant phosphoproteomic evidence for *in vivo* phosphorylation of plant GADs, including reports that its phospho-status may be modified during salinity or Pi deprivation stress (Table 3-1) (Zhao *et al.*, 2019; Mehta *et al.*, 2021), nothing is currently known about the functions or mechanisms of plant GAD phosphorylation

Reversible, site-specific phosphorylation is a crucial and widespread PTM that regulates the biological function of numerous proteins involved in all aspects of plant cell biology in response to various extra- or intracellular signals. Phosphorylation may alter an enzyme's substrate saturation kinetics and sensitivity to allosteric effectors, subcellular localization, protein-protein interactions, and/or proteolytic susceptibility (Plaxton and Shane, 2015). Although the role(s) of plant GAD phosphorylation not yet been determined, phosphorylation of human GAD2 (HsGAD2) at similar N-terminal seryl residues (i.e. Ser3, Ser6, Ser10, and Ser13) appears to be a distinguishing feature of membrane-bound HsGAD2 of neurotransmitter-releasing vesicles (Namchuk *et al.*, 1997). It was concluded that these N-terminal phosphosites do not impact HsGAD2's activity or membrane association, whereas HsGAD2 phosphorylation at Thr95 is inhibitory (Namchuk *et al.*, 1997). If N-terminal phosphorylation is indeed evolutionarily significant across kingdoms, HsGAD2 may serve as a model for investigating whether phosphorylation at analogous sites only occurs with membrane-bound plant GADs.

Plant Pi starvation responses (PSRs) arise from complex signaling pathways that integrate altered gene expression with post-transcriptional and post-translational mechanisms. The resultant remodeling of the transcriptome, proteome, and metabolome enhances the efficiency of root Pi acquisition from the soil, as well as the use of assimilated Pi throughout the

plant (Dissanayaka *et al.*, 2021). Studies of the remarkably adaptive mechanisms that contribute to the survival of −Pi plants are facilitating the development of rational strategies and molecular tools for engineering Pi-efficient transgenic crops. Such cultivars are needed to reduce inputs of unsustainable and non-renewable Pi fertilizers for maximum agronomic benefit and long-term global food security and ecosystem preservation. The possible involvement of GAD and the GABA shunt in the PSR was recently assessed by studying the impact of eliminating *AtGAD1* expression in *atgad1* T-DNA insertional mutants on the ability of *Arabidopsis* to acclimate to nutritional Pi deprivation (Benidickson, 2022). Biomass accumulation by –Pi, but not +Pi *atgad1* plants was significantly reduced relative to that of WT controls. Furthermore, Pi deprivation triggered a marked 71% increase in the root GABA concentration of wild-type, but not *atgad1* mutant plants (Benidickson, 2022). These results support the hypothesis that root GABA accumulation and increased GABA shunt flux helps *Arabidopsis* acclimate to nutritional Pi deprivation, and that AtGAD1 plays a significant role in facilitating this process.

The aim of the present study was to assess the impact of differential phosphorylation on the activity and subcellular localization of AtGAD1 in –Pi versus +Pi *Arabidopsis*. Our results indicate that differential phosphorylation activates AtGAD1 in -Pi *Arabidopsis*. However, AtGAD1's phospho-status does not appear to influence its cytosolic localization. Our results have implications not only for the post-translational control of the GABA shunt, but also for the regulation of this CaM-binding, ubiquitous cytosolic enzyme by reversible phosphorylation.

3.2 Materials and Methods

3.2.1 Plant Material

Heterotrophic suspension cells of *Arabidopsis thaliana* (cv. Landsburg erecta) were maintained at 21ºC in the dark, as previously described (Mehta *et al.*, 2021; Veljanovski *et al.*, 2006). Cells used for GAD purification were obtained by scaling up the culture volume: 100 mL aliquots of 7 d-old cells were subcultured into 2.6 L Fernbach flasks containing 400 mL of Murashige-Skoog media supplemented with 1.25 mM KPi; 7 d later 100 mL aliquots were transferred into 400 mL of fresh -Pi (0 mM KPi) or +Pi (5 mM KPi) media. After 7 d cells were harvested by vacuum filtration through Whatman 541 filter paper, washed with ultrapure water, frozen in liquid N_2, and stored at -80ºC. Pi-resupply experiments were conducted as described by Mehta *et al.* (2021). Briefly, 10 mL +Pi cells were initially cultured for 7-d in flasks containing 40 mL of media supplemented with 5 mM KPi; 10 mL aliquots of these cells were then subcultured into flasks that contained 40 mL of fresh media lacking Pi. Three days later, half of these flasks were resupplied with 2 mM Pi while the remaining flasks were maintained under -Pi treatment; 48 h following Pi resupply, all cells were harvested and stored at -80ºC.

3.2.2 GAD Activity and Protein Concentration Determination

GAD activity was assayed using a linked GAD-GABase spectrophotometric assay, as outlined by Miyashita and Good (2008) with a few modifications. The stopped-time GAD assay was carried out for 30 min at 23ºC in a 200 µL reaction mixture containing a mixture of 25 mM MES and 25 mM bis-tris-propane (BTP), along with 10% (v/v) glycerol, 10 mM KCl, 20 mM Glu, and 0.5 mM PLP, at either optimal pH 5.8 or physiological pH 7.2. To assess Ca^{2+}/CaM sensitivity at pH 7.2, either 1 mM Ca^{2+} and/or 1 µM recombinant AtCaM2 (Bender *et al.*, 2013), or 5 mM EGTA was added. Assays were terminated by bringing the assay mixture to pH 1.0 with 70%

(w/v) perchloric acid followed by immediate adjustment to ~pH 8.6 using 3 M KOH, from which 100 µL was transferred to a 96-well microtiter plate. A 100 µL aliquot of a GABase reaction mix (100 mM BTP (pH 8.6) containing 0.16 units/mL GABase, 5 mM 2-OG, 1 mM $NADP^+$) was added to each well (the GABase consists of a mixture of GABA-T and SSA dehydrogenase from *Pseudomonas fluorescens*; MilliporeSigma). Absolute increase in A_{340} was immediately measured using a Molecular Devices Spectromax Plus Microplate spectrophotometer to monitor the reduction of $NADP^+$ to NADPH, a reaction that occurs in a 1:1 stoichiometric ratio with conversion of GABA into succinate. Using a calibration curve generated by known amounts of GABA (Fig. S1A), GAD specific activity was calculated as units/mg protein, where one unit is defined as 1 µmol of GABA produced per min at 23°C. Apparent K_m and V_{max} values were determined using the enzyme kinetics feature of Graphpad Prism. All kinetic parameters are the means of at least three independent experiments, each with triplicate technical assays, and are reproducible to within ±10% of the mean value. Protein concentrations were determined using the Coomassie Blue G-250 colorimetric method with bovine γ-globulin as the protein standard.

3.2.3 Microsomal Fractionation

Microsomal fractionation was carried out according to Fedosejevs *et al.* (2014) with some modifications. Quick frozen -Pi or 48 h Pi-resupplied suspension cells were ground into a fine powder under liquid N_2, then extracted (1:2; w/v) in 50 mM HEPES (pH 7.3) containing 50 mM sucrose, 1 mM EDTA, 1 mM dithiothreitol (DTT), 0.2 mM Na_2MoO_4, 20 mM NaF, 1 mM phenylmethylsulfonyl fluoride (PMSF), and 1% (w/v) poly(vinyl polypyrrolidone) using a Polytron PT-1300 Homogenizer. Homogenates were centrifuged at 4°C and 10,000 x g for 20 min at 4°C, and the resulting supernatant recentrifuged at 96,000 × g for 1 h at 4°C to separate the soluble and microsomal fractions. Microsomal pellets were resuspended in 50 mM HEPES (pH

7.3) containing 50 mM sucrose, 1 mM EDTA, 1 mM DTT, 0.2 mM Na_2MoO_4, 1 mM NaF, 1 mM PMSF, and 0.5% (v/v) Triton X-100. Soluble and microsomal fractions were subjected to immunoblotting with anti-(recombinant petunia-GAD) immune serum (α-GAD) (kind gift of Prof. H. Fromm, Univ. Tel Aviv), which effectively cross-reacts with most plant GADs (Arazi *et al.*, 1995).

3.2.4 Buffers Used During GAD Purification

All buffers were degassed and adjusted to their respective pH values at 23°C, and unless otherwise stated contained a protein-phosphatase inhibitor cocktail (20 mM NaF, 1 mM $NaMoO_4$, 1 mM Na_3VO_4, 1 mM β-glycerophosphate, 5 mM NaPPi); 15 nM microcystin-LR (MC-LR) and 0.2 mM PLP were added to all pooled fractions. Buffer A contained 100 mM HEPES-KOH (pH 7.3), 2 mM EDTA, 20% (v/v) glycerol, 0.2 mM PLP, 15 nM MC-LR, 1 mM PMSF, and 0.5% (w/v) poly(vinyl polypyrrolidone). Buffer B contained 50 mM imidazole-HCl (pH 7.1), 5 mM $MgCl_2$, and 30% (saturation) $(NH_4)_2SO_4$. Buffer C consisted of Buffer B lacking $(NH_4)_2SO_4$ but containing 15% (v/v) ethylene glycol. Buffer D contained 50 mM Hepes-KOH (pH 7.3), 10% (v/v) glycerol, and 0.5 mM DTT. Buffer E was buffer D containing 100 mM KCl, with no phosphatase inhibitors.

3.2.5 GAD Purification

All centrifugation steps were conducted at 27,000 × *g* for 20 min at 4°C and all chromatographic steps were performed at 23°C using an ÄKTA Purifier FPLC (Cytiva). Proteins were routinely concentrated using Millipore Ultra-15 centrifugal filter units (30-kDa cut-off). GAD elution was monitored by immunoblotting every second fraction with α-GAD as described below. Quick-frozen +Pi or -Pi cells (~500 g) were ground to a powder under liquid N_2 using a mortar and

pestle; the powder was then allowed to thaw as it was homogenized (1:1.5; w/v) in buffer A. The extract was further homogenized (1:1.5 w/v) in buffer A using a Polytron PT-1300 homogenizer set at maximum speed (3 × 15 s) and centrifuged. The supernatant fluid was brought to 25% (saturation) $(NH_4)_2SO_4$, stirred for 20 min at 4ºC and centrifuged. The supernatant fluid was adjusted to 75% (saturation) $(NH_4)_2SO_4$, stirred, and centrifuged. The 25–75% (saturation) $(NH_4)_2SO_4$ pellets were resuspended in 150 mL of Buffer B containing 1 mM PMSF. After centrifuging to clarify, the supernatant fluid was loaded at 3 mL/min onto a column (2.5 X 10 cm) of butyl-Sepharose 4 Fast Flow (Cytiva) equilibrated with buffer B. The column was washed until the A_{280} decreased to baseline, and GAD eluted with a linear gradient of buffer C (6 mL/fraction). GAD-containing fractions were pooled, concentrated to ~30 mL, and desalted at 1.5 mL/min on a column (2.5 × 16 cm) of Sephadex G-25 (Cytiva) pre-equilibrated with buffer D. A_{280} absorbing fractions were immediately loaded at 1 mL/min onto a column (1 × 6 cm) of Fractogel EMD DEAE-650(S) (Merck) pre-equilibrated with Buffer D. The column was washed with Buffer D until the A_{280} decreased to baseline, and GAD eluted by applying a linear 0–1 M KCl gradient (60 mL in Buffer D; 1.5 mL/fraction). $CaCl_2$ (2 mM) was added to the pooled peak fractions, before passing the sample twice at 1 mL/min over a column (1 × 3 cm) of CaM-Sepharose (MilliporeSigma) equilibrated with buffer D containing 2 mM $CaCl_2$. The column was washed with equilibration buffer until A_{280} decreased to baseline and GAD eluted with buffer D containing 2 mM EGTA (1 mL/fraction). Pooled peak fractions were concentrated to ~400 μL and applied at 0.5 mL/min onto a Superdex-200 Increase 10/300 GL column (GE Healthcare) equilibrated buffer E lacking protein phosphatase inhibitors (0.75 mL/fraction). Pooled peak fractions corresponding to AtGAD1 from *Arabidopsis* suspension cells were concentrated, frozen in liquid N_2, and stored at -80ºC.

3.2.6 Determination of Native Molecular Mass via Superdex-200 Gel Filtration FPLC

Native M_r determination was performed during Superdex-200 FPLC as described above. The native M_r of -P:GAD1 and +P:GAD1 was estimated from a plot of K_{av} (partition coefficient) against log M_r for the following protein standards: thyroglobulin (669 kDa), ferritin (440 kDa), β-amylase (200 kDa), alcohol dehydrogenase (150 kDa), bovine serum albumin (BSA) (66 kDa), and chymotrypsinogen (25 kDa).

3.2.7 Preparation of Anti-(phosphoSer8-specific AtGAD1) Antibodies

The inoculation and care of rabbits for the preparation of antiserum against the conserved N-terminal phosphorylation domain of AtGAD1 was performed by Animal Care Services (Queen's University) using a synthetic phosphopeptide corresponding to residues 2 through 13 (with a Pi group at the target Ser8 residue) plus an additional Cys residue at the C-terminus to facilitate its conjugation to keyhole limpet hemocyanin (LifeTein). After collection of preimmune serum, conjugated phosphopeptide (2 mg) reconstituted in Pi-buffered saline and TiterMax Gold Adjuvant (MilliporeSigma) was injected subcutaneously into a rabbit. Booster injections (500 μg each) were administered at 4-, 6-, and 8-weeks. At 7 d following the final injection, blood was collected into Vacutainers (Beckton Dickinson) by cardiac puncture. After removal of clotted blood cells by centrifugation at 1,000 X *g*, the anti-(phosphoSer8-specific AtGAD1) immune serum (α-pSer8) was frozen in liquid N_2 and stored at -80^{o}C.

3.2.8 Electrophoresis and Immunoblotting

SDS/PAGE was performed using a Mini-PROTEAN 3 gel electrophoresis minigel rig (Bio-Rad) at 200 V for 50 min. Unless otherwise stated all gels were composed of 4 and 10% (w/v) acrylamide stacking and resolving gels, respectively. Following PAGE, gels were either stained

for total (phospho)proteins or electroblotted onto poly(vinylidene) difluoride (PVDF) membranes for immunoblotting. Phosphoprotein staining was conducted using Phos-Tag™ Phosphoprotein Gel Stain (ABP Biosciences) according to the manufacturer's protocol; phosphoprotein detection was accomplished using fluorescent imaging with a Typhoon 8600 (Cytiva). Phos-Tag stained and imaged gels were then stained with Coomassie Brilliant Blue G-250 for total protein detection. For immunoblots probed with α-GAD antisera, PVDF membranes were blocked with 3% (w/v) skim milk powder, whereas 1% (v/v) BSA (BioShop) was used to block blots probed with phospho-specific antibodies. Rabbit α-GAD (kind gift of H.Fromm), and rabbit α-pSer8 antisera were diluted 1:1000, and 1:500, respectively, in Tris-buffered saline (20 mM Tris (pH 7.5), 150 mM NaCl) with 0.1% (v/v) Tween-20 (TBST) containing 1% (w/v) BSA, and 0.05% (w/v) NaN_3. Immunoreactive polypeptides were visualized using an alkaline-phosphatase linked secondary antibody, and chromogenic detection as previously described (Veljanovski *et al.*, 2006).

3.2.9 *In vitro* Dephosphorylation of AtGAD1

Dephosphorylation of purified +P:GAD1 was attempted using λ phosphatase (NEB; P0753S) with 1X NEBuffer (with 1 mM $MnCl_2$) or calf intestinal alkaline phosphatase (CIP) (Sigma Aldrich) in buffer (50 mM Tris, 50 mM NaCl, 10 mM $MgCl_2$) according to the manufacturer's protocols. For λ phosphatase treatment, 0.2 μg/μL of +P:GAD1 was added to the manufacturer's reaction mix and incubated with 0.5 unit/μg GAD of phosphatase at 30°C for 1 h. For CIP treatment, 0.2 μg/μL of +P:GAD1 along with 1 unit/μg GAD of CIP were added to the reaction mixtures and incubated for 2 h at 37°C at a range of pHs (6.5, 7, or 9) in the presence or absence of 1 mM Ca^{2+} with 1 μM CaM. Boiled samples were subjected to SDS-PAGE and stained with Phos-Tag phosphoprotein stain, followed by total protein staining with Coomassie Blue G-250.

Imaging of Phos-Tag stained phosphoproteins was accomplished using fluorescent imaging with a Typhoon 8600.

3.2.10 LC-MS/MS Analysis of AtGAD1 Phosphosites

Purified +P:GAD1 and –P:GAD1 (5 µg each) were subjected to SDS-PAGE and stained with Coomassie Blue G-250. Gel slices corresponding to protein-stained 57 kDa AtGAD1 polypeptides were excised and stored in microfuge tubes prior to processing. In-gel trypsin digestion was performed on the samples, which included: reduction (10 mM β-mercaptoethanol in 100 mM triethylammonium biocarbonate) for 10 min at 95°C and alkylation (55 mM iodoacetamide in 100 mM bicarbonate) for 30 min at 23°C. After dehydration, trypsin (6 ng/µl, Promega Sequencing Grade - V5113) was added to just cover the gel pieces, with digestion occurring overnight (~16 h) at 37°C. Tryptic peptides were first extracted from the gel using 97% (v/v) water / 2% (v/v) acetonitrile (ACN) / 1% (v/v) formic acid (FA) followed by a second extraction using 50% (v/v) of the extraction buffer and 50% (v/v) ACN. Isolated peptides were then dried, re-suspended and desalted using ZipTip C18 pipette tips (ZTC18S960; Millipore) as previously described (Uhrig *et al.*, 2019). All peptides were then dried and resuspended in 3% (v/v) ACN / 0.1% (v/v) FA immediately prior to MS analysis. Resuspended tryptic peptides were analyzed using nanoflow HPLC (Easy-nLC 1000, Thermo Scientific) with an EASY-Spray capillary HPLC column (PepMap RSLC C18, 75um x 25cm, 100 Å, 2 µm, Thermo Scientific) coupled to a Q Exactive Orbitrap mass spectrometer (Thermo Scientific). Dissolved samples were injected using an Easy-nLC 1000 system (Thermo Scientific). The column was equilibrated with 100% solvent A (0.1% formic acid (FA), 4% ACN in water). Peptides were eluted using the following gradient of solvent B (0.1% FA in 80% ACN): 0–18% B, 0–73 min; 18–30% B, 73-101 min; 30–46% B, 101–120 min; 46–100% B, 120-123, min at a flow rate of 0.35 µL/min at

50°C. High-accuracy mass spectra were acquired in data-dependent acquisition mode. All precursor signals were recorded in a mass range of 300–1700 m/z and a resolution of 35 000 at 200 m/z. The maximum accumulation time for a target value of 1×10^6 was set to 120 ms. Up to 12 data-dependent MS/MS were recorded using quadrupole isolation with a window of 2 Da and higher-energy collisional dissociation fragmentation with 26% fragmentation energy. A target value of 5×10^4 was set for MS/MS using a maximum injection time of 250 ms and a resolution of 17 500 at 200 m/z. Precursor signals were selected for fragmentation with charge states from +2 to +7 and a signal intensity of at least 1×10^4. All precursor signals selected for MS/MS were dynamically excluded for 30 s.

Data was processed using MaxQuant 1.6.14.0 (http://www.maxquant.org/), using the Araport 11 database (https://www.araport.org/) with the reverse decoy option selected. Search parameters included a peptide, protein and PSM false discovery rate (FDR) of 1%, a precursor mass tolerance of 10ppm and a fragment mass tolerance of 0.01 Da and a total of 2 missed cleavages. Peptides were searched with carbamidomethyl cysteine as a fixed modification and oxidized methionine and phosphorylated serine, threonine and tyrosine as variable modifications. A PTM site localization score threshold ≥ 0.75 was used to determine PTM site reliability.

3.2.11 Isolation of AtGAD1 cDNA, Construction of Plasmids, Transient Expression, and Fluorescence Imaging of Arabidopsis Suspension Cells

A full-length *AtGAD1* clone inserted into *pET15b* in frame with a 6-His tag at the N-terminal end was kindly provided by Prof. Barry Shelp (University of Guelph). To generate fluorescent-protein tagged AtGAD1, the full-length *AtGAD1* coding sequence (amplified from *pET15b:AtGAD1*) was cloned into *pRTL2* vector encoding *mCherry*. Two constructs were made

to generate AtGAD1 with mCherry fused to either the N- or C-terminus using *BamHI/XbaI* or *XmaI/NheI* restriction enzymes, respectively. *Arabidopsis* suspension cells were cultured in +Pi Mursashige-Skoog media (containing 5 mM K_2HPO_4) for 6 d, then subcultured into –Pi media for a further 3 d. Cells were collected by centrifugation to remove the media, then resuspended in fresh media containing 0.25 M mannitol and either 0 or 2 mM K_2HPO_4. Cells were spread on Whatman filter paper in a petri dish and biolistically bombarded with tungsten particles coated with plasmid DNA encoding one of the two *AtGAD1-mCherry* constructs. Some cells were co-bombarded with a GFP-tagged mitochondrial marker protein (mito-GFP). After incubating on the plate for 48 h, cells were fixed in 0.5X PBS containing 4% formaldehyde for 1 h, then washed 3 times in 1X PBS. Fixed cells were imaged using epifluorescence microscopy as previously described (Lingard *et al.*, 2008).

3.2.12 Bioinformatic Analyses

Deduced amino acid sequences for AtGAD1-5 (AT5G17330, AT1G65960, AT2G02000, AT2G02010, AT3G17760, respectively) were retrieved from The Arabidopsis Information Resource (TAIR, https://www.arabidopsis.org), and the sequences of AtGAD1 orthologs from other species were obtained via the National Center for Biotechnology Information (NCBI) Protein Database (https://www.ncbi.nlm.nih.gov/protein/). PhosphoSVM (http://sysbio.unl.edu/PhosphoSVM/prediction.php) was used to predict phosphorylation sites, and Phosphat 4.0 and the Eukaryotic Phosphorylation Site Database (EPSD, http://epsd.biocuckoo.cn) were used to identify experimental and predicted phosphorylation sites of AtGAD1-5 and their orthologs. *Arabidopsis thaliana* Expression Atlas (ATHENA, http://athena.proteomics.wzw.tum.de:5002/master_arabidopsisshiny/) supplemented predicted phosphorylation sites while providing tissue-specific expression data for the AtGAD1-5

polypeptides using intensity based absolute quantification proteomics (iBAQ). The EPSD Lipid Modification (http://gpspalm.biocuckoo.cn) and Methylation (http://msp.biocuckoo.org/#) predictors were also employed. Subcellular localization prediction was performed via the Subcellular Localization Database for Arabidopsis Proteins (SUBA, https://suba.live) subcellular localization predictor, which compiles experimental and sequence data to provide the most probable localization sites.

3.2.13 Statistics

All data were plotted as histograms with error bars representing SEM, and analyzed using one-tailed, unpaired student's *t*-test and deemed statistically significant at $*P < 0.05$, $**P < 0.001$, $***P < 0.0001$.

3.3 Results

3.3.1 Bioinformatic Analysis of GAD Sequences and Phosphorylation Sites

Alignment of the N-terminal amino acid sequence of various AtGAD1 orthologs revealed substantial conservation within plants as measured by Euclidian distance, with sequence dissimilarity increasing in more phylogenetically distant relatives (Fig. A-1). We were also interested in comparing AtGAD1 with human GAD2 (HsGAD2) which also undergoes *in vivo* phosphorylation at multiple seryl residues located near its N-terminus (Table 3-1) (Namchuk *et al.*, 1997). HsGAD2 and AtGAD1 share 22.4% sequence identity, but pairwise sequence alignment using EMBOSS Matcher aligned the N-terminal phosphoserine residues of both proteins, as well as a Thr95 residue that is also phosphorylated in HsGAD2 (Fig. 3-1A) (Chou *et al.*, 2017).

The phosphosite predictor PhosphoSVM identified Ser4, Ser8, and Ser10 as putative AtGAD1 phosphosites; Ser4, Ser8, Ser10 and Ser13 as AtGAD3 and AtGAD4 phosphosites; and

Thr5, Ser7, and Ser9 as AtGAD5 phosphosites. Interrogation of PhosPhAt 4.0, EPSD, and ATHENA phosphoproteomic databases revealed that AtGAD1 is frequently *in vivo* phosphorylated at Ser4, Ser8, Ser10, Ser13, Ser16, and Ser20 under a variety of conditions, with different combinations of residues being phosphorylated both at baseline and following recovery from abiotic stress (Table 3-1) (Lin *et al.*, 2015; Menz *et al.*, 2016; Wu *et al.*, 2013). High throughput studies that focused on mitogen activated protein kinases (MAPK) suggested that AtGAD1's Ser10 and Ser12 residues are phosphorylated by MAPKs, while another study identified AtGAD1's N-terminus as being a shared target of the MAPKs MPK3, MPK4 and MPK6 (Hoehenwarter *et al.*, 2013; Rayapuram *et al.*, 2018; Rayapuram *et al.*, 2014). Data compiled from EPSD identified multiple N-terminal seryl phosphorylation sites that have been mapped on AtGAD1-5, as well as several GAD orthologs from other species (Table 3-1).

3.3.2 AtGAD1 Co-expression and Subcellular Localization *In Silico* Prediction

The EPSD lipid modification predictor suggested C-terminal lipid modification may occur on Cys502 of AtGAD1, ranking cluster B S-palmitoylation and non-consensus S-farnesylation as the most likely modifications. No methylation in the AtGAD1 sequence was predicted by the EPSD Methylation predictor and has never been identified experimentally. GeneMania protein interaction analysis highlighted the co-expression of AtGAD1 and ALMT1 as well as AtGAD2 and ALMT5, in addition to the experimentally proven physical interaction between AtGAD1 and CaM (co-expression coefficients were unavailable due to the non-specific nature of the data-scraping tools used to populate the GeneMania program). SUBA subcellular localization analysis of AtGAD1 and AtGAD2 suggested that they are cytosolic proteins, which is consistent with most GAD localization studies (Breitkreuz and Shelp, 1995; Ito *et al.*, 2011; Wallace *et al.*, 1984); however, a hit on a high throughput

proteomics study identified the presence of both isozymes in *Arabidopsis* root extracellular matrix or cell wall protein extracts (Nguyen-Kim *et al.*, 2016). Hydropathy plots of deduced AtGAD1-5 polypeptides generated by EPSD indicated the hydrophobicity of the first 10 amino acids of their N-termini, as well as a domain at about residue 210, are above the transmembrane domain cut-off.

3.3.3 AtGAD1 Localizes Predominantly to the Cytosol of *Arabidopsis* Suspension Cells Irrespective of Nutritional Pi Status

To determine the subcellular location of AtGAD1, its coding region was cloned to yield either a C- or N-terminal fusion protein in-frame with an mCherry reporter protein and transiently expressed via biolistic bombardment in –Pi and Pi-resupplied *Arabidopsis* suspension cells, under the control of the *cauliflower mosaic virus 35S* promoter. Epifluorescence microscopy revealed that AtGAD1-mCherry localized exclusively to the cytosol irrespective of the cell's Pi status (Fig. 3-2A). This is consistent with most of the bioinformatics analyses of AtGAD1's amino acid sequence, which failed to predict the presence of any membrane-spanning domains or mitochondrial or plastid targeting peptides at its N-terminus, besides the predicted lipid modification of Cys502. Although mCherry-AtGAD1 similarly localized throughout the cytosol, it also appeared to associate with some puncta to a small degree (Fig. 3-2B). When co-expressed with a mitochondrial-green fluorescent protein (mito-GFP) marker, the mCherry-AtGAD1 fluorescing puncta were distinct from any mitochondrial structures (Fig. 3-2B). Nevertheless, the puncta localization of mCherry-AtGAD1 was not impacted by the Pi status of the cells.

To determine whether any GAD is associated with endomembranes, microsomes and corresponding soluble fractions were isolated from freshly harvested –Pi and 48 h-Pi resupplied

cells and subjected to immunoblotting with anti-petunia GAD immune serum (α-GAD). Immunoreactive 57 kDa GAD polypeptides (p57) were predominantly detected in the soluble rather than microsomal fractions, and the cell's nutritional Pi-status had no obvious impact on GAD's partitioning into the either fraction (Fig. 3-2C).

3.3.4 Pi-resupply to Pi-starved *Arabidopsis* Suspension Cells Attenuates Extractable GAD Activity

GAD activity and Ca^{2+}/CaM- sensitivity was initially analysed using clarified, desalted extracts from -Pi and 48 h Pi-resupplied *Arabidopsis* cells, from which AtGAD1 was previously identified to possess a hypo- and hyper-phosphorylated N-terminus, respectively (with no change in AtGAD1 abundance) (Mehta *et al.*, 2021). Assays were performed using a stop-timed GAD-GABase linked activity assay as previously described (Miyashita and Good, 2008). The microplate reader-based spectrophotometric GAD assay was optimized, calibrated, and validated by showing that the amount of GABA produced by a desalted *Arabidopsis* cell-culture extract was proportional to assay time (Fig. A-2). Desalting effectively eliminated glutamate-independent $NADP^+$ reductase activity from the clarified extracts.

At optimal pH 5.8, extractable GAD activity of the -Pi cells was 40% higher ($p < 0.02$; Students' *t*-test) than that of 48 h Pi-resupplied cells (Fig. 3-3). At physiological pH 7.2, addition of either 5 mM EGTA or 1 mM Ca^{2+} resulted in a 70% and 30% increase in activity ($p < 0.05$; Students' *t*-test), respectively, of -Pi compared to Pi-resupplied cells. However, at pH 7.2, addition of 1 mM Ca^{2+} with 1 μM purified recombinant AtCaM2 did not yield a significant difference in GAD activity of the respective extracts likely due to presence endogenous CaM in clarified extracts ($p > 0.05$, Students' *t*-test).

3.3.5 AtGAD1 Purification from Pi-starved versus Pi-replete *Arabidopsis* Suspension Cells

To assess the impact of Pi deprivation on AtGAD1 more thoroughly, the enzyme was purified 500- to 2,000-fold from quick-frozen +Pi and –Pi suspension cells (Tables B-1 and B-2). The final specific GAD activities of 20 and 32 units/mg obtained for +P:GAD1 and –P:GAD1, respectively, compare favorably with values reported for homogeneous GADs isolated from a range of plant sources (Table 2-1). To negate possible *in vitro* GAD dephosphorylation by co-purifying phosphatases, a phosphatase-inhibitor cocktail was included in all purification buffers (other than that used for the final Superdex 200 Increase gel filtration step). When the final preparations were denatured and subjected to SDS-PAGE, major 57-kDa protein-staining polypeptides (p57) were isolated that strongly cross-reacted with α-GAD (Fig. 3-4A and B). LC-MS/MS analysis of the respective tryptic digests identified the p57 of both preparations as AtGAD1 (AT5G17730.1) (Table 3-2).

The native M_r of +P:GAD1 and –P:GAD1 was estimated to be 330 kDa and 345 kDa, respectively, via analytical gel-filtration using a calibrated Superdex 200 column (Fig. 3-5). Thus, similar to other plant as well as *E. coli* GADs (Astegno *et al.*, 2015; Capitani *et al.*, 2003; Gut *et al.*, 2009), native AtGAD1 isolated from +Pi or –Pi *Arabidopsis* suspension cells appears to exist as a homohexamer composed of identical p57 subunits.

3.3.6 Purified +P:GAD1 and –P:GAD1 are Differentially Phosphorylated

LC-MS/MS analyses of p57 subunits excised from SDS gels revealed that +P:GAD1 was more significantly phosphorylated at Ser8, whereas phosphorylation at Ser4 was far more prevalent with the –P:GAD1 (Fig. 3-4D, Table 3-2). Additionally, phosphorylation of Ser10 and Ser13 increased slightly in -P:GAD1.

A phospho-Ser8-specific antibody (α-pSer8) was raised against a synthetic phosphopeptide corresponding to residues 2–13 of AtGAD1 (Fig. 3-6A). The α-pSer8 detected as little as 250 ng of the phosphopeptide on dot blots but did not cross-react with up to 1000 ng of the corresponding dephosphopeptide (Fig. 3-6B). The cross-reaction with the phosphopeptide was abolished when a parallel dot blot was incubated with α-pSer8 containing 10 µg/mL of the blocking phosphopeptide. Our use of α-pSer8 was complemented with the antibody raised against recombinant petunia GAD (α-GAD) that cross-reacts with GAD polypeptides irrespective of their phosphorylation status (Fig. 3-4B and C), thus allowing for standardization of total AtGAD1 on immunoblots. The immunoblot presented in Fig. 3-4C corroborated the LC-MS/MS results (Fig. 3-4D, Table 3-2) indicating that purified +P:GAD1 was significantly more phosphorylated at Ser8 than –P:GAD1. Inclusion of 10 µg/mL of the blocking phosphopeptide quenched the cross reaction of α-pSer8 with +P:GAD1 (Fig. 3-4C). Collectively, these data indicate the specificity of the α-pSer8 antisera and clearly demonstrate that AtGAD1 is significantly phosphorylated at Ser8 in +Pi suspension cells.

3.3.7 Pi Deprivation Activates AtGAD1

Each round of assays comparing GAD activity of +P:GAD1 versus -P:GAD1 was conducted alongside α-GAD immunoblots to ensure normalization of the respective amounts of AtGAD1 that were being assayed. Specific activities of the final preparations were measured under a range of conditions (pH 5.8; pH 7.2, $\pm Ca^{2+}$/CaM). The -P:GAD1 exhibited significantly greater activity than +P:GAD1 at most conditions assayed, but this difference was most pronounced at pH 5.8 (Fig. 3-7). At this optimal pH, regardless of Ca^{2+}/CaM presence, +P:GAD1 exhibited a specific activity of 20 ±0.7 units/mg while -P:GAD1 was more active at 32 ±1.0 units/mg, indicating that Pi deprivation triggered an ~60% increase in AtGAD1 activity.

These results corroborate those of Fig. 3-3 in which total GAD activity of desalted clarified extracts of –Pi cells was about 40% greater than that of Pi-resupplied cells. At pH 7.2 with Ca^{2+}/CaM addition, activity of +P:GAD1 was 12 ±0.5 units/mg, which increased by about 23% to 15 ±0.8 units/mg with -P:GAD1. There was no significant difference in the low baseline activity at pH 7.2 in the presence of EGTA. Fold-activation from baseline levels upon Ca^{2+}/CaM addition at pH 7.2 was 3.5- and 2.8-fold for -P:GAD1 and +P:GAD1, respectively. A glutamate saturation curve was generated for -P:GAD1 at optimal pH 5.8 (Fig. B-6). The -P:GAD1 exhibited V_{max} and K_m(Glu) values of 33 ± 2.2 units/mg and 3.9 ± 0.66 mM, respectively. Unfortunately, glutamate saturation kinetics of the +P:GAD1 were not determined owing to insufficient amounts of the purified enzyme.

3.3.8 AtGAD1 Phosphosites are Recalcitrant to Exogenous Phosphatases

Attempts at *in vitro* dephosphorylation of +P:GAD1 using either λ phosphatase or CIP were unsuccessful. Neither treatment effectively dephosphorylated +P:GAD1 as judged by SDS-PAGE and Phos-Tag phosphoprotein staining (Fig. A-3).

Table 3-1. Experimentally identified phosphorylation sites of eukaryotic GAD orthologs.

Species	*GAD Isozyme*	*Experimental Treatment*	*Phosphorylation Site(s)*	*Reference*
Mus musculus	GAD2	None	S3,S6,S10,S13,S61	(Wiśniewski *et al.*, 2010)
Saccharomyces cerivisiae	GAD1	None	S30,S36,S40,S45,T51,S52,S53	(Schreiber *et al.*, 2012)
Homo sapiens	GAD2	None	S3,S6,S10,S13	(Namchuk *et al.*, 1997)
Oryza sativa L. (seedlings)	GAD1	Abscisic Acid	S8,S10,S13	(Qiu *et al.*, 2017)
Oryza sativa L. (suspension cells)	GAD1	None	S10	(Nakagami *et al.*, 2010)
Arabidopsis thaliana (suspension cells)	GAD1	Pi resupply to –Pi cells	S4, S8, S10, S13, S16	(Mehta *et al.*, 2021)
Arabidopsis thaliana (suspension cells)	GAD3	None	S10,T361,S368	(Nakagami *et al.*, 2010; van Wijk *et al.*, 2014)
Arabidopsis thaliana (seedlings)	GAD2	Dehydration	S6, S8, S83, S92	(Umezawa *et al.*, 2013)
Arabidopsis thaliana (seedlings)	GAD4	None	T6,S8,S10,S13,S16,S79,Y84,T93	(Hoehenwarter *et al.*, 2013)
Arabidopsis thaliana (seedlings)	GAD5	None	S7,S9,Y83,T92,S460,S474	(Mayank *et al.*, 2012)
Gossypium hirsutum (leaf)	GAD1	Nitric Oxide	S13	(Fan *et al.*, 2014)
Gossypium hirsutum (leaf)	GAD4	Nitric Oxide	S8	(Fan *et al.*, 2014)

Table 3-2. Phosphosite mapping data for +P:GAD1 and -P:GAD1 as determined via Orbitrap LC-MS/MS.

Protein Accession	*Phosphorylated residue*	*Localization Probability*	*Intensity +P:GAD1*	*Intensity –P:GAD1*	*GAD -P/+P Log2FC*
AT5G17330.1	Ser4	0.62	0	6.71×10^6	22.7
AT5G17330.1	Ser8	1.00	1.29×10^9	2.10×10^7	-5.9
AT5G17330.1	Ser10	0.87	8.34×10^7	3.61×10^8	2.1
AT5G17330.1	Ser13	1.00	7.35×10^7	1.26×10^8	0.78

A

```
AtGAD1     4 SHAVSE--S-DVSVHS--TFASR-Y--V-R--TS-L--PRF---------     30
             |.. ||  | | | .:  | | | :  | :  |. :   :.
HsGAD2    10 SFG-SEDGSGD-S-ENPGT-A-RAWCQVAQKFTGGIGN-KLCALLYGDAE     53

AtGAD1    31 KMP-EN--S--IPKEAAYQIINDELML--DGN-P-R-L----NLASFV-T     65
             | | |:  |   |: || .  . :...  | . | . .    |.| |: .
HsGAD2    54 K-PAESGGSQP-PR-AA-A--R-KAACACD-QKPCSCSKVDVNYA-FLHA     94

AtGAD1    66 TWME--PECD-K---L-IMSSI-N-K--NYV----DM-----D-EYPVTT     94
             |  :  |.|| :   | .:..: | .   ||    |.     | .|| .
HsGAD2    95 T--DLLPACDGERPTLAFLQDVMNILLQ-YVVKSFDRSTKVIDFHYP-N-    139
```

B

Source	N-terminal Sequence	UniProt Accession Number
AtGAD5	MVLA--TNSDSDEHLHSTFA	Q9LSH2
ZmGAD1	MVLSHGVGGSDESVHSTFAS	B4F972
AtGAD2	MVLTKT-A-TNDESVCTMFG	Q42472
AtGAD1	MVLSHAVS-ESDVSVHSTFA	Q42521
NtGAD1	MVLSKTAS-ESDVSIHSTFA	P93369
PhGAD1	MVLSKTVS-QSDVSIHSTFA	Q07346.1
AtGAD3	MVLSKTAS-KSDDSIHSTFA	Q9ZPS4
AtGAD4	MVLSKTVS-ESDVSIHSTFA	Q9ZPS3
MdGAD1	MVISTTSAEGRGEQVNCTFA	V9SI88

Fig. 3-1 AtGAD1's N-terminal seryl phosphorylation sites are widely conserved in plant and mammalian GADs. (A) Pairwise sequence alignment of N-termini of *Arabidopsis* AtGAD1 and human GAD2 (HsGAD2; accession number Q05329) computed using EMBOSS Matcher. Phosphosites of native AtGAD1 and HsGAD2 that have been identified (Namchuk *et al.*, 1997) are underlined and either highlighted in purple (for pSer) or red (for pThr). AtGAD1's putative phosphoThr66 residue is based on its alignment with HsGAD2. **(B)** Multiple sequence alignment of the identified Ser4, Ser8, Ser10, Ser13, and Ser16 phosphosites of AtGAD1 (Mehta *et al.*, 2021) with other members of the AtGAD family, as well as GAD orthologs from *Petunia hybrida*, *Zea mays*, *Nicotiana tabacum*, and *Malus domestica* using Clustal Omega (version 1.2.4). Conserved N-terminal serine residues are bolded in purple, with underlined residues indicating evidence of phosphorylation occurring there (https://phosphat.uni-hohenheim.de/).

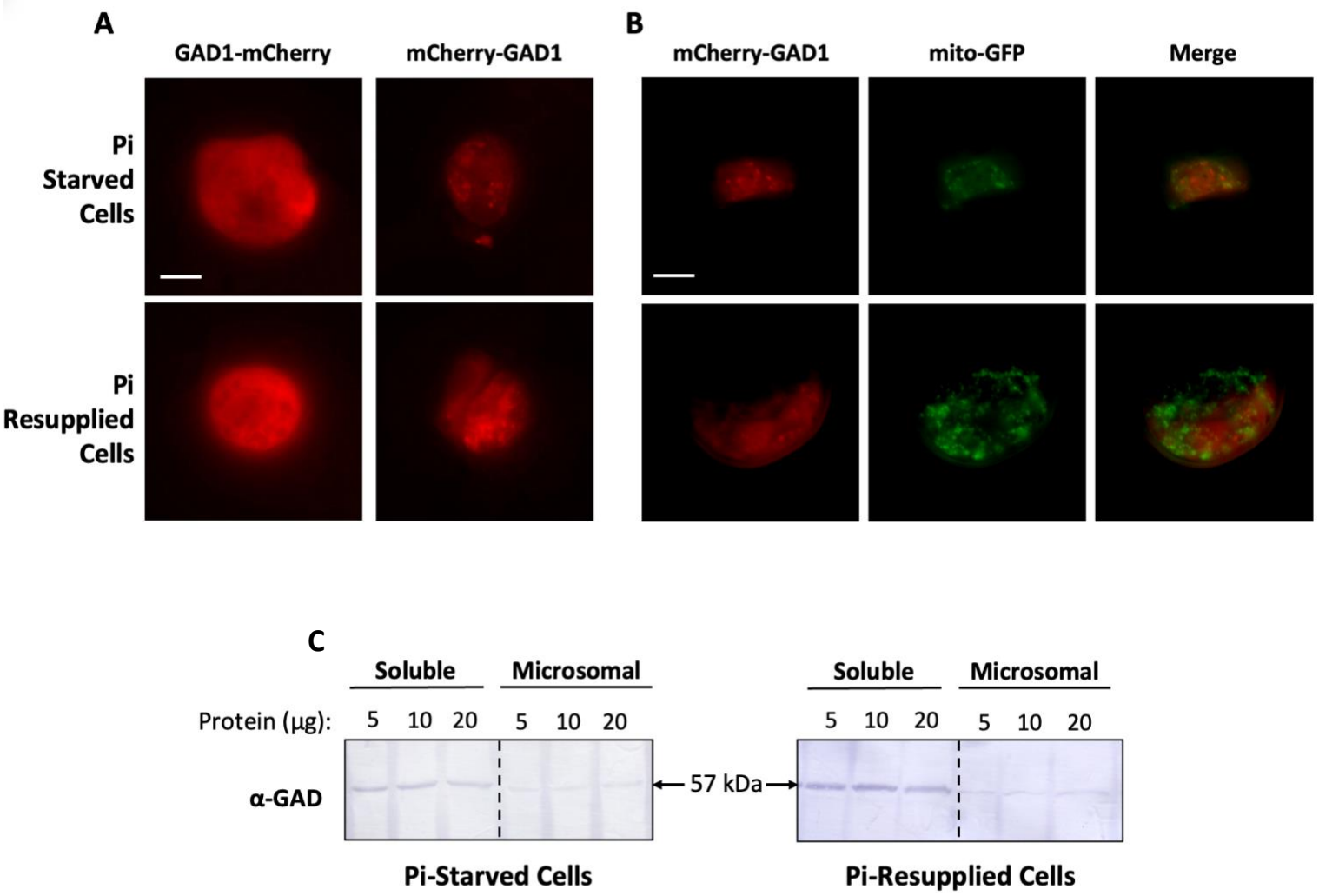

Fig. 3-2. AtGAD1 localizes to cytosolic and soluble fractions of –Pi or Pi-resupplied *Arabidopsis* suspension cells. (A) Representative images of AtGAD1-mCherry and mCherry-AtGAD1 localization in –Pi versus 48 h Pi-resupplied *Arabidopsis* suspension cells. Following bombardment, cells were incubated for 48 h to allow for gene expression and protein sorting, then fixed in formaldehyde and viewed using epifluorescence microscope. **(B)** Epifluorescence microscopy images of mCherry-GAD1 and mito-GFP merged. Images shown in panels A and B are representative of each GAD1-mCherry and mCherry-GAD1 under different Pi conditions. White scale bars represent 10 μm**. (C)** Soluble and microsomal membrane fractions were rapidly prepared from –Pi and 48 h Pi-resupplied cells as described in the Materials and Methods, and subjected to SDS-PAGE and immuoblotting with α-GAD antiserum**.**

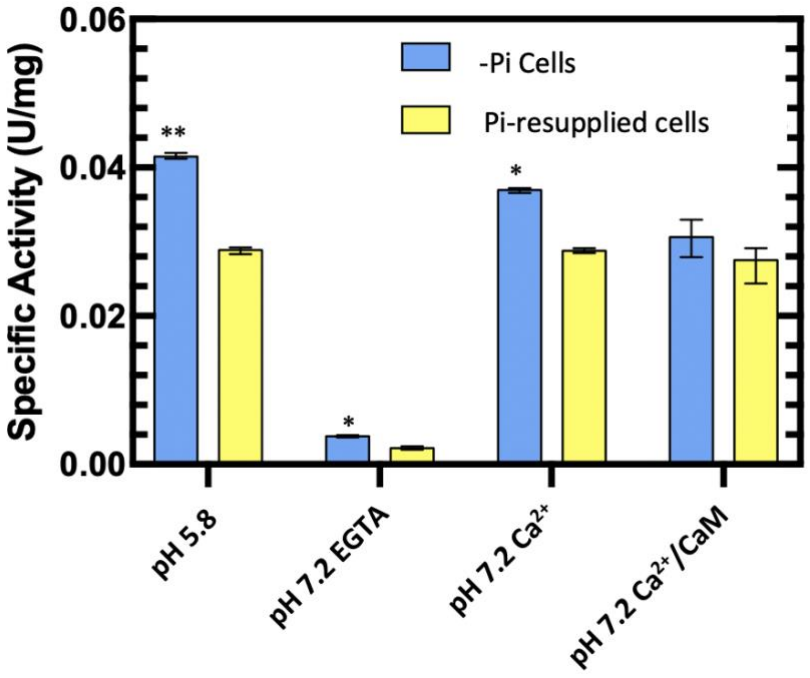

Fig. 3-3. Specific GAD activity of clarified desalted extracts prepared from -Pi versus 48 h Pi-resupplied *Arabidopsis* suspension cells. Spectrophotometric assays were conducted as outlined in the Materials and Methods by adding 20 μL of extract to a 180 μL GAD reaction mixture at either optimal pH 5.8 or physiological pH 7.2. Ca^{2+}/CaM-sensitivity was tested at pH 7.2 by the addition of either 1 mM Ca^{2+} ±1 μM CaM, or 5 mM EGTA. All values represent means ±SEM of $n = 3$ separate assays; asterisks indicate significant differences (* = $p < 0.05$; ** = $p < 0.02$; one-tailed students' *t*-test) between -Pi and the Pi-resupplied cells.

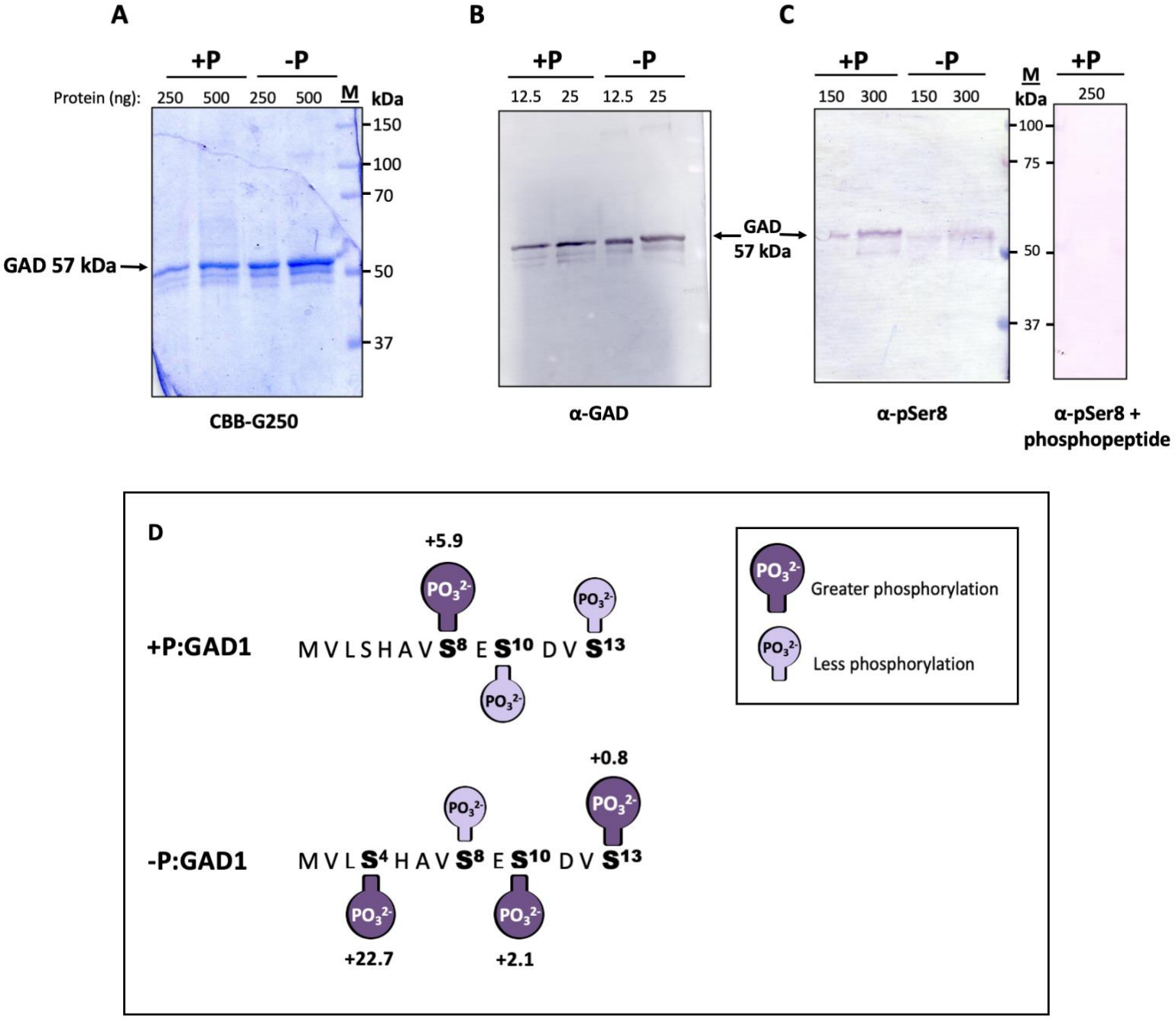

Fig. 3-4. SDS-PAGE, immunoblotting, and phosphosite analysis of purified AtGAD1 from –Pi and +Pi *Arabidopsis* suspension cells. SDS-PAGE of the final +P:GAD1 and –P:GAD1 preparations was followed by: **(A)** total protein staining with Coomassie brilliant blue G-250 (CBB G-250), or immunoblotting with **(B)** α-GAD, or **(C)** α-pSer8. **(D)** Schematic diagram of LC-MS/MS mapped phosphosites revealing differences in +P:GAD1 versus –P:GAD1 phosphorylation. (Top) +P:GAD1 was phosphorylated at three N-terminal sites: Ser8, Ser10, and Ser13. (Bottom) -P:GAD1 was phosphorylated at four sites: Ser4, Ser8, Ser10, and Ser13. Dark purple Pi groups denote greater phosphorylation while light purple Pi groups denote reduced phosphorylation. Values indicate AtGAD1 -Pi/+Pi_Log2FC (Table S2).

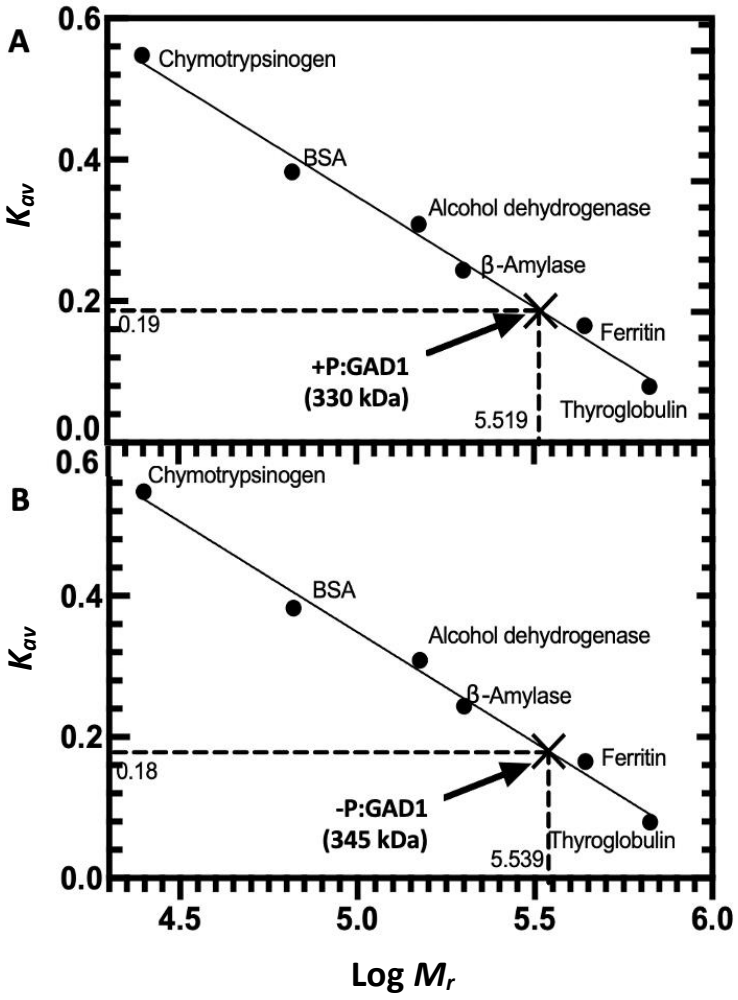

Fig. 3-5. Native molecular mass determination for AtGAD1 purified from +Pi versus –Pi *Arabidopsis* suspension cells as determined via analytical Superdex 200 Increase 10/300 gel filtration FPLC. Native molecular masses of (**A**) +P:GAD1 and (**B**) –P:GAD1 were estimated from a plot of K_{av} versus log M_r for the indicated protein standards as described in the Materials and Methods.

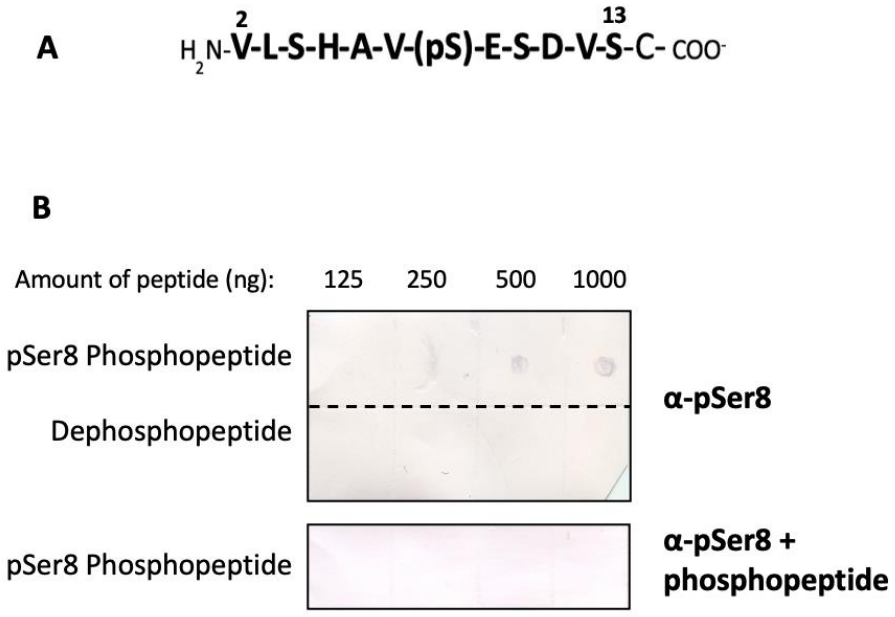

Fig. 3-6. Preparation of phosphosite-specific antibody against AtGAD1 pSer8.
(A) Sequence of synthetic phosphopeptide that was covalently coupled to KLH and used for rabbit immunization. The peptide was synthesized with an extra N-terminal Cys residue to facilitate its conjugation to KLH. The Ser8 phosphorylation site is indicated. (**B)** Dot blots (immunoblots) of varying amounts of the synthetic phosphopeptide and corresponding dephosphopeptide were probed with α-pSer8 antiserum in the presence and/or absence of 10 μg/mL of the phosphopeptide.

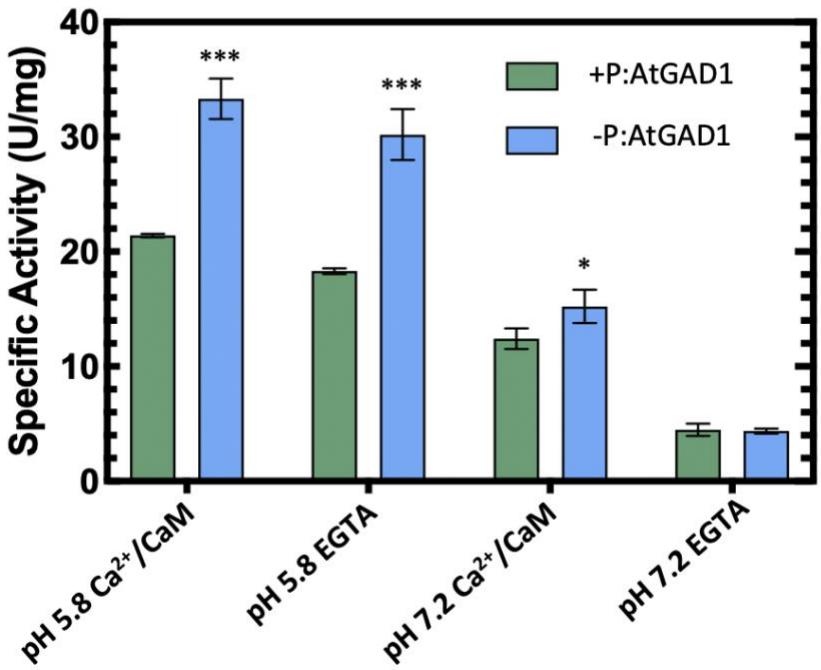

Fig. 3-7. Specific GAD activity of +P:GAD1 versus –P:GAD1 at optimal and physiological pH in presence and absence of Ca^{2+}/CaM. Spectrophotometric GAD-GABase linked enzyme assays were conducted using 200 ng of each sample. Assays were conducted at optimal pH 5.8 and physiological pH 7.2, testing Ca^{2+}/CaM-activation. All values represent means ±SEM of n = 3 separate assays; asterisks indicate significant differences (* = $p < 0.05$; ** = $p < 0.01$; *** = $p < 0.001$; one-tailed students' t-test) between +P:GAD1 and –P:GAD1.

3.4 Discussion

As the entry point to the GABA shunt, a pathway involved in abiotic and biotic stress responses (Bown *et al.*, 2002; Che-Othman *et al.*, 2020; Mekonnen *et al.*, 2016; Park *et al.*, 2010; Scholz *et al.*, 2017; Seifi *et al.*, 2013; Yin *et al.*, 2010), GAD is an important enzyme linking Ca^{2+}-signalling and GABA biosynthesis. Our recent analysis of the phosphoproteome of heterotrophic *Arabidopsis* cell suspension cultures identified AtGAD1 as the most hyperphosphorylated protein 48 h following Pi resupply to -Pi cells, with no significant change in the overall abundance of AtGAD1 polypeptides (Mehta *et al.*, 2021). We further explored the properties and role of AtGAD1 phosphorylation using subcellular localization analysis, phosphosite-specific antisera, and activity assays on native AtGAD1 purified from -Pi or +Pi cells.

To date, plant GADs have been predominantly characterized as cytosolic based on subcellular fractionation studies, although these extractions can be quite harsh and are sometimes prone to contamination by organellar contents (Breitkreuz and Shelp, 1995; Ito *et al.*, 2011; Wallace *et al.*, 1984). We could find only a single report identifying AtGAD1 in cell wall protein extracts from non-stressed *Arabidopsis* roots (Nguyen-Kim *et al.*, 2016). Although the low pH optima for GAD activity is consistent with the acidic environment of the apoplast, a cell wall localization seems unlikely and most studies suggest that plant GADs are cytosolic enzymes (Breitkreuz and Shelp, 1995; Ito *et al.*, 2011; Shelp *et al.*, 2017). Surprisingly, *in vivo* localization studies using fluorescent microscopic imaging of plant GAD-fluorescent protein fusions have never been described. The multisite phosphorylation at the N-terminus of human HsGAD2 occurs after anchoring of GAD to membranes of neurotransmitter-releasing vesicles, but the specific role of HsGAD2 phosphorylation remains unclear (Namchuk *et al.*, 1997). In

animals, vesicle-bound GAD allows for more efficient and rapid GABA production and subsequent packaging into vesicles for release into the synaptic cleft. Given the partial conservation of N-terminal phosphorylation sites on AtGAD1 compared to HsGAD2 (Fig. 3-1A), we investigated the subcellular localization of AtGAD1-mCherry and mCherry-AtGAD1 using *in vivo* fluorescence imaging of -Pi versus 48 h Pi-resupplied *Arabidopsis* suspension cell cultures (Fig. 3-2A and B). As a dramatic increase in phosphorylation at Ser4, Ser8, Ser10, Ser13, and Ser16 occurred 48 h following Pi-resupply to -Pi *Arabidopsis* cells (Mehta *et al.*, 2021), we tested the hypothesis that changes in the phosphorylation status of AtGAD1 due to Pi nutrition might impact its subcellular association with membranes. As GABA produced by GAD can be transported into mitochondria and subsequently metabolized into succinate, or exported from cells we reasoned that GAD might associate with membranes (i.e. microsomal fraction) of -Pi cells that facilitate efficient GABA transport and/or flux through the GABA shunt (Michaeli *et al.*, 2011; Ramesh *et al.*, 2018). Subcellular fractionation and α-GAD immunoblot analysis using suspension cells grown either under -Pi or 48 h Pi-resupplied conditions revealed that 57 kDa immunoreactive GAD polypeptides predominantly associated with the soluble fraction and there was no apparent difference in GAD partitioning between the soluble and microsomal fractions between -Pi and Pi-resupplied cells (Fig. 3-2C). This result is consistent with previous reports indicating that GAD is a cytosolic protein (Breitkreuz and Shelp, 1995; Ito *et al.*, 2011; Wallace *et al.*, 1984). However, given the harshness of fractionation protocols, we also explored the *in vivo* localization of fluorescent protein (i.e. mCherry) tagged AtGAD1 in intact -Pi versus Pi-resupplied *Arabidopsis* suspension cells.

AtGAD1, fused to mCherry fluorescent protein at either its N- or C-terminus, localized predominantly to the cytosol when expressed in heterotrophic *Arabidopsis* suspension cells (Fig.

3-2A and B). Interestingly, mCherry-GAD1 also appeared to localize with some puncta. When co-expressed with a mito-GFP marker protein, there was only minor apparent overlap in fluorescence, and thus the identity of these punctate structures remains unclear. Importantly, cytosolic partitioning of either N- or C-terminal AtGAD1-mCherry fusion proteins was not influenced by Pi nutrition (Fig. 3-2A and B). To the best of my knowledge, these are the first *in vivo,* subcellular localization images of a GAD isozyme in plant cells. Our subcellular fractionation data and *in vivo* imaging indicate that AtGAD1 is a cytosolic enzyme, and that its localization is not impacted by Pi nutrition or phosphorylation status. Moreover, our empirical data suggest that the weak *in silico* transmembrane predictions are likely unreliable.

In order to explore the biochemical properties and impact of phosphorylation status on AtGAD1's activity and subunit structure, I developed and optimized a FPLC-based purification protocol for native AtGAD1, using either +Pi or -Pi *Arabidopsis* suspension cell cultures to obtain differentially phosphorylated forms of the enzyme. Using a series of FPLC steps (Appendix B), I purified AtGAD1 to homogeneity from cells grown under each condition and verified its identity via α-GAD immunoblotting and LC-MS/MS analysis (Fig. 3-4; Table 3-2). This strategy offers the advantage of analyzing changes in AtGAD1 phosphorylation triggered by Pi status, rather than relying on *in vitro* dephosphorylation assays to strip Pi groups off AtGAD1. Indeed, we observed marked changes in the phosphorylation profile of AtGAD1 where the phosphorylation status of certain residues increased in abundance under one Pi growth condition, whereas others decreased (Fig. 3-4D; Table 3-2). This is intriguing, and somewhat surprising, given that all four identified phosphosites are clustered within one very short 12 amino acid region near AtGAD1's N-terminus and yet are not up- or down-regulated in a synchronized manner. The underlying physiological implications of this apparent differential

AtGAD1 phosphorylation in response to nutritional Pi status remain unclear. In addition, the identities of the responsible protein kinase(s) and phosphatase(s) are unknown. While AtGAD1 has been identified in a small number of high-throughput studies mining for putative MAPK targets, this lead has never been followed up on but may merit future investigation (Hoehenwarter *et al.*, 2013; Rayapuram *et al.*, 2018).

With respect to differential phosphorylation, I observed that phosphorylation of Ser8 was about 6-fold greater in purified +P:GAD1, whereas phosphorylation at Ser10, Ser13, and especially Ser4 was enhanced in -P:GAD1 (Fig. 3-4D). It should be noted that this pattern of differential phosphorylation contrasts with what was previously observed from -Pi and 48 h Pi-resupplied cells, where each of these seryl residues, as well as Ser16, appeared to be hyperphosphorylated upon Pi-resupply (Mehta *et al.*, 2021). It is possible that the different growth conditions used between these studies underlie the patterns observed; in my analyses, I used cells cultured in either -Pi or +Pi liquid media for 7 d as this allowed for the high density of cell cultures needed to accumulate significant biomass for native AtGAD1 purification. By contrast, the Mehta *et al.* (2021) study focused on recovery (i.e. refeeding Pi to -Pi cells for 48 h) from -Pi conditions. Future work could explore the effect of different Pi regimes on AtGAD1's phosphorylation status as well as expanding the breadth of abiotic stress conditions tested.

Hyperphosphorylation, particularly at Ser4 and Ser16, may be mechanisms needed during or for recovery from -Pi stress, whereas phosphoSer8 could be critical under normal conditions to return AtGAD1 activity to baseline levels. Bioinformatic analyses identified similar N-terminal multisite phosphorylation of AtGAD1 and other plant GAD orthologs under a range of conditions (Fig. 3-1B; Table 3-1). Rice seedlings treated with abscisic acid exhibited OsGAD1 phosphorylation at Ser8, Ser10, and Ser13, and various GAD isozymes in cotton leaf exposed to

nitric oxide exhibited some N-terminal phosphosites (Fan *et al.*, 2014; Qiu *et al.*, 2017). Interestingly, iron deficiency in *Arabidopsis* roots was associated with phosphorylation of AtGAD1 at Ser8, Ser10, and Ser13, similar to what we have observed with Pi deficiency (Lan *et al.*, 2012). One study comparing the phosphoproteomes of WT, *mpk3*, *mpk4* and *mpk6* *Arabidopsis* plants identified AtGAD1 N-terminal phosphosites as potential shared targets of all three MAPKs (Rayapuram *et al.*, 2018). It is fascinating that Ser3, Ser6, Ser10, Ser13, and Ser16 are also reported phosphosites in both human and mouse GAD2 under normal conditions (Namchuk *et al.*, 1997; Wiśniewski *et al.*, 2010). We hypothesized that this could be evidence of a conserved function of GAD N-terminal phosphorylation not just in plants, but across kingdoms. While animal GAD N-terminal phosphorylation is known to occur following its anchoring to vesicular membranes, like plant GADs, the function of animal GAD N-terminal phosphorylation is unclear (Namchuk *et al.*, 1997). In future, it will be interesting to determine if the physiological roles of GAD phosphorylation are evolutionarily conserved.

Given that phosphorylation can impact enzymatic activity, I first developed and optimized a method to detect and quantify GAD activity using a stopped-time GAD-GABase linked spectrophotometric assay, which is frequently used in place of the 1-[^{14}C]-glutamate-based radiometric assay (Li *et al.*, 2018; Miyashita and Good, 2008; Zhang and Bown, 1997). While this method may not be as sensitive as directly measuring $^{14}CO_2$ released by GAD from 1-[^{14}C]-glutamate, I was able to validate the linked enzyme assay (Fig. A-2), allowing us to circumvent the handling of radioisotopes. I first compared extractable GAD activity in desalted clarified extracts of-Pi and 48 h Pi-resupplied cells, conditions under which previous LC-MS/MS analysis found no differences in AtGAD1 abundance (Mehta *et al.*, 2021), and determined that overall, GAD activity was significantly higher in -Pi cell extracts under a range of assay

conditions (Fig. 3-3). To further evaluate whether this impact was due to differences in phospho-status of AtGAD1, the native enzyme was purified from both +Pi and -Pi cells (+P:GAD1 and -P:GAD1, respectively), in which it exhibits a markedly different pattern of phosphorylation (Fig. 3-4). Initial enzyme activity assays revealed that -P:GAD1 was up to 60% more active than +P:GAD1 at optimal pH 5.8 (~32 versus ~20 units/mg) (Fig. 3-7). This effect became less pronounced at physiological pH 7.2, but -P:GAD1 was still ~23% more active than +P:GAD1 in the presence of Ca^{2+}/CaM (15 versus 12 units/mg), suggesting that phospho-status of the enzyme could influence its pH-responsiveness.

The specific GAD activity obtained for the final preparation of purified -P:AtGAD1 is comparable to that previously reported for purified recombinant AtGAD1 (rAtGAD1): ~55 units/mg at pH 5.8 versus ~33 units/mg at pH 7.2 with Ca^{2+}/CaM (Table 2-1) (Astegno *et al.*, 2015). However, the measured differences in activity between the recombinant enzyme used in the Astegno *et al.* (2015) study and the native enzymes in the present work might be attributed to different PTMs, such as the inability of rAtGAD1 to undergo N-terminal multisite phosphorylation in *E. coli*. In addition, another study measured specific GAD activity of rAtGAD1 at pH 7.2 with Ca^{2+}/CaM to be as high as 70 units/mg when assayed at 30^{o}C (Turano and Fang, 1998). In contrast, recombinant petunia GAD yielded a specific activity of ~20 units/mg at physiological pH in the presence of Ca^{2+}/CaM (Snedden *et al.*, 1996). Zhang *et al.* (2007) purified GAD from rice germ to apparent homogeneity with the final preparation exhibiting a lower specific activity of 7.5 units/mg at its optimal pH 5.6. Similarly, native rice bran GAD purified 130-fold had a specific activity of 7.7 units/mg (Wang *et al.*, 2010). In general, the specific activity of my pure, native +P:GAD1 and -P:GAD1 preparations are within the range of purified plant GADs described elsewhere.

Although a full comparison of the kinetic properties of AtGAD1 isolated from +Pi vs -Pi cells was planned, I was limited by the amount of available +P:GAD1 preparation. Nevertheless, I had sufficient -P:GAD1 sample for analysis and thus generated a Glu saturation curve in order to estimate its V_{max} and K_m(Glu) values. The -P:GAD1 preparation yielded a K_m(Glu) of 3.9 mM, which is consistent with reported values for other plant GADs (Table 2-1) which range from about 3-9 mM (Inatomi and Slaughter, 1975; Satyanarayan and Nair, 1985; Snedden *et al.*, 1995; Snedden *et al.*, 1996). Meanwhile, rice germ GADs appear to have unusually high K_m(Glu) of about 30 mM (Wang *et al.*, 2010; Zhang *et al.*, 2007). Further, I determined V_{max} of -P:AtGAD1 to be 33 units/mg (Fig. B-6), which is comparable to the measured specific activity of ~32 units/mg obtained with the final preparation at saturating (20 mM) glutamate at pH 5.8 (Fig. 3-7). My data suggest that purified -P:GAD1 is about 60% more active compared to +P:GAD1, and this correlates with differences in their respective phosphorylation status (Fig. 3-4D). It remains unclear, however, whether the phosphosite differences I have identified are directly responsible for the kinetic differences in purified AtGAD1 specific activity. Further analysis via *in* vitro dephosphorylation or using point-mutations at these sites, or related approaches, are needed before firm conclusions can be drawn.

It is noteworthy, that these observations align with recent (unpublished) evidence indicating that *atgad1* KO mutants with low root GABA content exhibited reduced growth under -Pi, but not +Pi conditions compared to WT (Benidickson, 2022). Under -Pi conditions, a more active GAD would enable GABA accumulation and/or enhanced flux through the GABA shunt, both of which are scenarios that have previously been reported to be correlated with or directly responsible for enhanced tolerance to a variety of abiotic and biotic stresses including drought, hypoxia, salinity, and herbivory (Bown *et al.*, 2002; Mei *et al.*, 2016; Mekonnen *et al.*, 2016;

Shelp *et al.*, 2012a). Similarly, increases in GABA content of tissues of various plant species exposed to -Pi stress have been documented for barley roots and shoots, tomato xylem sap, common bean roots, and *Arabidopsis* roots (Benidickson, 2022; Hernández *et al.*, 2007; Huang *et al.*, 2008; Sung *et al.*, 2015). While the physiological consequences of GABA accumulation are unknown, the recent identification of GABA receptors in plants (ALMTs, GORKs) indicates a role in signalling, suggesting that GABA is far more than a marker of stress (Adem *et al.*, 2020; Ramesh *et al.*, 2015). Additionally, some researchers have hypothesized that the GABA shunt serves as a bypass mechanism to support cellular respiration under stresses (i.e. salinity or Pi deprivation) that may impair 2-OGDH or succinyl-coA synthetase activities of the mitochondrial TCA cycle (Fig. 2-1) (Che-Othman *et al.*, 2020; Joshi *et al.*, 2019). Given that GAD catalyzes the first committed step of the shunt, upregulated activity would elicit GABA accumulation and/or increased GABA shunt flux under various stresses, including Pi deprivation. While most plant GAD isoforms are activated by Ca^{2+}/CaM-binding, the enzyme is a critical inflection point in stress metabolism and differential phosphorylation could further contribute to fine-tuning of its activity.

As I was able to purify AtGAD1 from cells grown under different Pi nutrient conditions, I attempted *in vitro* dephosphorylation assays using exogenous phosphatases with the aim of providing a source of dephosphorylated AtGAD1 for comparative kinetic analyses. I tested the use of the robust λ phosphatase using the provided commercial reaction buffer at near neutral pH 7.5, as well as CIP which works optimally at alkaline pH 9 (Fig. A-3). However, I observed no dephosphorylation occurring using λ phosphatase under the optimal conditions as outlined by the manufacturer's protocols (λ phosphatase is a phosphatase of phage λ that can efficiently dephosphorylate phosphorylated Ser, Thr, and Tyr residues of phosphoproteins). Its inability to

dephosphorylate purified +P:GAD1 (Fig. A-3) indicates that AtGAD1's phosphorylated N-terminal seryl residues may not be solvent accessible, or that λ phosphatase is unable to catalyze *in vitro* +P:GAD1 dephosphorylation owing to steric hindrance caused by its multiple, closely spaced phosphorylated seryl residues. Subsequent test assays using CIP at varying pH's (6.5, 7, 9), indicated that +P:GAD1 became slightly less phosphorylated at acidic pH (Fig. A-3B). I also tested the hypothesis that AtGAD1conformation and/or oligomerization could affect the accessibility of the N-terminal phosphosites. However, the presence of Ca^{2+}/CaM, which induces hexamerization of GAD similar to acidic pH, had no effect on +P:GAD1 dephosphorylation by CIP (Fig. A-3B). The AlphaFold model for a single AtGAD1 subunit predicts the structure of the first 12 residues with low or very low confidence (https://alphafold.ebi.ac.uk/entry/Q42521). The PDBe-KB database models AtGAD1 in its hexameric form, but lacks the first 11 residues, although Val12 is predicted to be exposed to the surface of the complex (https://www.ebi.ac.uk/pdbe/pdbe-kb/proteins/Q42521). In future, it might be prudent to assess GAD dephosphorylation using an acid phosphatase, ideally one from a plant source, such as potato tuber which we previously purified and characterized as a highly effective protein phosphatase (Gellatly *et al.*, 1994). In this study I was limited by the amount of purified AtGAD1 enzyme available, as well as access to a reliable source of potato acid phosphatase. The identity of the protein kinase(s)/phosphatase(s) responsible for differential AtGAD1 phosphorylation are presently unknown, and similar questions remain for the other AtGAD isozymes that also appear to undergo some form of N-terminal phosphorylation *in planta* (Table 3-1).

Future Directions

My data indicate that AtGAD1 undergoes differential phosphorylation near its N-terminus in +Pi versus -Pi *Arabidopsis* suspension cells. The phosphorylation status of AtGAD1 doesn't appear to alter its subcellular localization, but does seem to influence its specific activity, so a future +P:GAD1 purification should be carried out to thoroughly compare its kinetic properties (e.g. K_m(Glu), V_{max}) with purified -Pi:GAD1. Further analyses should also be conducted to assess additional differences in kinetic properties at physiological pH in the presence of Ca^{2+}/CaM, as well as susceptibility to allosteric effectors between +P:GAD1 and -P:GAD1. Future experiments could also be performed using recombinant phospho-ablative and -mimetic AtGAD1 mutants, which would provide a simpler means of purifying ample amounts of enzyme. Aside from further investigations into enzyme kinetics, other aspects of AtGAD1 regulation by phosphorylation should also be considered, including susceptibility to proteolysis or promotion of protein-protein interactions. In *Arabidopsis*, phospho-status of the immune signaling protein kinase, botrytis-induced kinase-1, can regulate whether it is targeted for polyubiquitination and subsequent degradation (Wang *et al.*, 2018). Alternately, *in vivo* phosphorylation of sucrose synthase-1 at Ser11 in developing castor beans appears to protect it from proteolytic turnover (Fedosejevs *et al.*, 2014). It is conceivable that AtGAD1 phosphorylation dictates its turnover, although our previous phosphoproteomics study did not detect any change in AtGAD1 protein levels 48 h following Pi-resupply to the -Pi cells (Mehta *et al.*, 2021). Alternatively, phosphorylation has also been shown to play a role in protein-protein interactions, such as in the Abl SH3 domain, wherein phosphorylation can impede its ability to bind to its interaction partner (Chen *et al.*, 2008). Perhaps phosphorylation could be involved in

regulating AtGAD1 binding to Ca^{2+}/CaM, or to some other as of yet unidentified binding partner.

It would also be of value to extend our discovery of the complexity of N-terminal multisite phosphorylation of AtGAD1 in *Arabidopsis* cells to seedlings grown in liquid culture, or in soil and perhaps even to AtGAD1 paralogs, and GAD orthologs from other species. Such comparative biochemistry would further support a rationale for the identification of the protein kinases/phosphatases that target the specific Ser residues of AtGAD1's N-terminus. I have preliminary evidence suggesting that *in vitro* AtGAD1 dephosphorylation requires acidic pH, which may be indicative of the involvement of an acid phosphatase, and this could be further tested *in vitro* using either commercial acid phosphatases or native *Arabidopsis* enzymes.

Concluding Remarks

As a Ca^{2+}/CaM-regulated enzyme that catalyzes the first committed step of the GABA shunt, GAD is a unique enzyme of central plant metabolism. The identification and characterization of AtGAD1 phosphorylation provides an added layer of complexity to the tight control of GABA biosynthesis and GABA shunt flux – both of which are important during times of biotic and abiotic stress, and now evidently during -Pi stress. According to LC-MS/MS analyses of purified +P:GAD1 and -P:GAD1 the root-specific AtGAD1 isozyme of *Arabidopsis* suspension cells undergoes N-terminal multisite phosphorylation at Ser4, Ser10, and Ser13, but is dephosphorylated at Ser8 in response to nutritional Pi deprivation. This intriguing shift in phospho-status of the enzyme was correlated with a change in specific activity of purified native enzymes Preparations of -P:GAD1 were more active than +P:GAD1, and preliminary evidence suggests that this effect is pH-dependent, wherein a drop in pH led to enhanced activation.

Furthermore, *in vivo* fluorescence microscopy revealed that mCherry-tagged AtGAD1 is cytosolic in *Arabidopsis* cells irrespective of Pi nutrition, corroborating previous data obtained from cell fractionation studies. An understanding of the mechanisms and functions of GAD and GABA shunt regulation will shed some light on the physiological role and significance of GABA and its metabolic pathway in plants, which to this day remain elusive.

3.6 Acknowledgements

This work was kindly funded by grants to WCP, WS, RTM, and RGU from the Natural Science and Engineering Research Council of Canada (NSERC), and Queen's and Guelph Research Chair programs. We are also thankful to have received polyclonal α-recombinant petunia GAD antibody (α-GAD) from Prof. Hillel Fromm (Tel Aviv Univ.).

Chapter 4: General Discussion

In plants, GABA and GAD have been studied in relation to various abiotic and biotic stresses (Seifikalhor *et al.*, 2019; Shelp *et al.*, 2021; Shelp *et al.*, 2012a; Zhao *et al.*, 2019). However, the role of GAD during the plant PSR has received little attention. Recently, LC-MS/MS analysis detected a drastic shift in multisite AtGAD1 phosphorylation at its N-terminus in response to altered Pi nutrition of *Arabidopsis* suspension cells (Mehta *et al.*, 2021). Although AtGAD1 phosphorylation provides a potential means of rapid and reversible post-translational control, the function of the PTM has not been reported in the literature. Reversible phosphorylation of proteins is a control mechanism that integrates the regulation of metabolism and development, with the control of gene expression, signal transduction, and stress responses in multicellular eukaryotes (Plaxton and Shane, 2015). Despite this, phosphorylation of GABA shunt enzymes as a regulatory mechanism has never been reported. GAD is the pacemaker enzyme of this pathway, and thus its regulation is particularly important. Most plant GADs are regulated by Ca^{2+}/CaM, however, the discovery of N-terminal multisite phosphorylation in plant GAD and GADs from other organisms (Table 3-1) points to an added strategy for rapid fine-tuning of GABA accumulation and/or controlling flux through the GABA shunt that may be evolutionarily conserved.

4.1 Purification and Characterization of AtGAD1's Phospho-Status in +Pi versus –Pi *Arabidopsis* suspension cells

Detailed *in vitro* characterization of native AtGAD1's physical, immunological, and kinetic/regulatory properties (including PTMs) is greatly facilitated by purifying the enzyme away from contaminating proteins and metabolites. Isolating native purified enzymes from plants

(especially the diminutive *Arabidopsis thaliana*) is a challenge due to difficulties in acquiring adequate biomass of tissue as well as the development and optimization of a laborious and multistep chromatography workflow. The use of *Arabidopsis* for protein purification is uncommon given the small size of the plant and its 6-8 week generation time; however, our lab has adopted the use of heterotrophic *Arabidopsis* cell cultures, enabling rapid accumulation of kilograms of healthy +Pi cells relatively quickly in comparison. One particular advantage of purifying native plant proteins from cell suspension cultures is the conservation of PTMs that might otherwise be absent or distorted when using recombinant proteins from bacteria or other heterologous sources. Despite the caveat that cell cultures are an artificial system and not necessarily representative of whole-plant physiology, this strategy has proven to be a simple, efficient, and valuable tool for prospecting various aspects of plant cell biology, including the metabolic adaptations of -Pi plants and the occurrence and functions of novel PTMs, that can be subsequently expanded upon using whole plants. Our recent phosphoproteomic study comparing the phosphoproteomes of -Pi vs 48 h Pi-resupplied *Arabidopsis* suspension cells identified AtGAD1 as one of the most differentially phosphorylated enzymes. Although N-terminal multisite phosphorylation of this enzyme has been reported in phosphoproteome datasets, this aspect of GAD regulation has never been explored in any depth (Table 3-1) (Mehta *et al.*, 2021). A primary objective of this thesis research was to purify native AtGAD1 from +Pi versus -Pi *Arabidopsis* cell cultures to study the role of phosphorylation, and ultimately, broaden these findings using *Arabidopsis* seedlings.

Purification of AtGAD1 was carried out using +Pi cells in place of 48 h Pi-resupplied cells due to logistical reasons, as biomass becomes difficult to accumulate when cells are exposed to -Pi stress. Based on the GAD activity assays, SDS-PAGE analysis – which revealed a

single protein staining polypeptide at ~57 kDa (Fig. 3-4A), the predicted M_r of a single AtGAD1 subunit – immunodetection by α-pSer8 (Fig. 3-4C), and most conclusively LC-MS/MS analysis, the purified preparations from both +Pi and -Pi cells were confirmed AtGAD1 isozymes. Both preparations experienced some limited proteolytic degradation, as evidenced by slight staining of minor lower molecular weight bands by CBB G-250 (Fig. 3-4A). However, these were also detected by α-GAD antiserum, indicating they were degraded polypeptides of AtGAD1, with C-terminal ends likely being cleaved off (Fig. 3-4B). To the best of my knowledge, this is the first report of native GAD purification from *Arabidopsis*. In fact, only a few plant native GADs have been fully purified, including GAD from rice germ (Wang *et al.*, 2010; Zhang *et al.*, 2007), potato tuber (Satyanarayan and Nair, 1985), and squash (Matsumoto *et al.*, 1996). Analytical gel-filtration coupled with SDS-PAGE indicated that both +P:GAD1 and -P:GAD1 exist as a ~330-345 kDa homohexamer composed of 57 kDa subunits (Fig. 3-5). This is consistent with a previous study in which recombinant AtGAD1 eluted from a gel-filtration column as either a less active 140 kDa homodimer or more active 340 kDa homohexamer (Astegno *et al.*, 2015).

Although AtGAD1 has been identified in a number of high-throughput studies as a putative MAPK target, this connection has never been experimentally shown (Hoehenwarter *et al.*, 2013; Rayapuram *et al.*, 2018). MAPKs are involved in some (a)biotic stress signal transduction pathways, as well as hormone signaling, which would support the model that the GABA shunt plays an important role particularly during times of stress. Because MAPKs are involved in a remarkable breadth of processes in plant cells, most identified motifs have been implicated as putative MAPK consensus motifs (Xi *et al.*, 2021). The S-E motif is one such example, with AtGAD1 Ser8 falling into this category. It remains to be seen whether the protein kinase/phosphatase pair targeting Ser8 are root-specific, or are expressed in other tissues,

although similar N-terminal phosphosites have been reported in other AtGAD isozymes, suggesting they may not be root-specific (Table 3-1). If differential phosphorylation of GAD is an important regulatory mechanism of the GABA shunt across species, and a survey of phosphoproteome databases does indeed support such an hypothesis (Table 3-1), the identification of the responsible protein kinase and phosphatase orthologs should be a focus of future studies.

4.2 What is the Role of the GABA Shunt and How is it Impacted by AtGAD1 Phosphorylation?

It remains unclear whether GABA accumulation, enhanced GABA shunt flux, or both, are critical under -Pi stress, but it could be expected that enhanced GAD activity would be required under either case. If differential phosphorylation of AtGAD1 under -Pi stress is in fact responsible for enhancing activity under certain conditions (Fig. 3-7), this would support findings on GABA accumulation in response to -Pi stress in WT *Arabidopsis* roots (Benidickson, 2022). Importantly, *atgad1* KO plants unable to accumulate GABA in roots under -Pi conditions grew significantly less compared to WT plants. If N-terminal phosphorylation plays the same role across GAD isozymes under various stressors, which I suspect is likely, GADs may be rapidly and tightly activated to different degrees in a tissue-specific manner. Given that the ability to synthesize GABA in response to osmotic stresses (i.e. salinity and drought) enhances tolerance, it has long been speculated that GABA may serve as an osmoprotectant. However, the fact that it does not accumulate close to levels seen with proline, the classical osmolyte, it may have a different purpose altogether, or perhaps enhanced flux through the GABA shunt becomes more critical under these conditions (Che-Othman *et al.*, 2020; Mekonnen *et al.*, 2016). Additionally, because GABA production consumes protons, it is expected to play an important

role as a pH buffer, as is the case in bacteria exposed to acidosis (Castanie-Cornet *et al.*, 1999). In this study, I measured the highest fold-change in activity between the two phosphoforms of AtGAD1 at pH 5.8 compared to physiological pH 7.2 (Fig. 3-7). If AtGAD1 phosphorylation shifts similarly in response to changes in pH as it does to Pi deprivation, GAD may be maximally activated not only by the drop in pH but also by phosphorylation enhancing its pH-responsiveness under this condition, enabling faster consumption of acidic H^+ as GABA is produced. Following neutralisation, GABA can then be metabolized, transported out the cell, or used in a downstream pathway.

With strong evidence that ALMT channels can serve as GABA receptors, GABA accumulation and subsequent signal transduction may be a broad-range stress response in plants under conditions that promote accumulation (Ramesh *et al.*, 2017). Certainly with respect to drought stress, GABA signaling can regulate stomatal conductance, potentially via binding to guard cell-localized AtALMT6, 9, and 12, which have also been implicated in stomatal regulation (Abdel Razik *et al.*, 2021; Mekonnen *et al.*, 2016; Sasaki *et al.*, 2010; Sharma *et al.*, 2016; Xu *et al.*, 2021). Interestingly, *AtALMT1* is expressed in the root apex, and its transcription is upregulated by low Pi, high Fe^{3+}, or high Al^{3+} (Balzergue *et al.*, 2017; Sawaki *et al.*, 2009). GABA binding inhibits ALMT1 from transporting malate out the cell into the soil, which is a crucial mechanism for enhancing Pi acquisition during -Pi stress in order to liberate soluble Pi from insoluble metal cation-Pi complexes (Dissanayaka *et al.*, 2021; Ramesh *et al.*, 2015). Ramesh *et al.* (2015) reported that GABA did not accumulate under Al^{3+} stress, while malate efflux increased , but although low Pi upregulates *AtALMT1* transcription similarly to high Al^{3+}, recent data has documented GABA accumulation in roots of *Arabidopsis* seedlings exposed to -Pi stress which agrees with my findings that -P:GAD1 is generally more active than +P:GAD1

(Fig. 3-7) (Benidickson, 2022). High GABA levels appear to contradict the need for active ALMT1 channels to exude malate during Pi deprivation; however, wheat TaALMT1 is also regulated by phosphorylation (Long *et al.*, 2020). It is conceivable that phosphorylation might relieve allosteric inhibition of ALMT1 channels by GABA, which is one scenario that would reconcile elevated GABA levels and unhindered malate efflux via ALMT1, if such phosphorylation occurs under low Pi conditions.

While the precise roles of GABA and the GABA shunt remain elusive, some have speculated that the shunt serves as a critical bypass that is upregulated during times of stress to support cellular respiration. Che-Othman *et al.* (2020) measured increased flux through the GABA shunt in wheat leaves after exposure to salt stress for 11 d. This was demonstrated by observing heightened extractable GAD activity in salt-stressed leaf clarified extracts in conjunction with reduced (~20%) rates of respiration upon application of either vigabatrin (GABA-T inhibitor) or 3-mercaptopropionic acid (GAD inhibitor) to salt-treated but not control excised wheat leaves. While pharmacological agents can exert non-specific effects, the comparable impact of the two reagents on respiration rate point to a putative role for the GABA shunt under these conditions. Additionally, the mitochondrial 2-OGDH complex was highly salt-sensitive; its activity was significantly inhibited by 50 mM NaCl and almost completely inhibited by 300 mM NaCl, whereas GAD remained 70% active in the presence of 150 mM NaCl, providing further support for the hypothesis that the GABA shunt is a required bypass to maintain respiration when the TCA cycle is impaired (Che-Othman *et al.*, 2020). Recently, it was hypothesized that a similar bypass mechanism may become necessary during times when TPP, an important co-factor of 2-OGDH (Fig. 2-2A), becomes depleted (Joshi *et al.*, 2019). This scenario was proposed to arise during -Pi stress, as pools of most Pi-containing compounds are

recycled to liberate free Pi. If this is the case, similar reliance on upregulated flux through the GABA shunt could be critical for supporting cellular respiration. However, further empirical biochemical and genetic studies are needed to assess the levels and importance of TPP metabolism during -Pi stress and other abiotic stresses before a role for this cofactor and its relation to GABA shunt activity can be confidently stated.

As well, further analyses are necessary before drawing any conclusions regarding the regulation of GAD activity and the GABA shunt by phosphorylation, as we have yet to analyze the full kinetic properties of +P:GAD1 compared to -P:GAD1. Moreover, while AtGAD1 is not predicted to be methylated, roles for other PTMs not assessed in the current study may also come into play during the PSR. As aforementioned, the EPSD lipid modification predictor suggested Cys502 of AtGAD1 may undergo lipid modification; however, this has never been experimentally shown, and seems unlikely in light of my subcellular localization work corroborating evidence of multiple studies that GAD is cytosolic (Fig. 3-2A and B). Arguably, a more compelling and definitive way to investigate the potential impact of phosphorylation on kinetic properties would have been to dephosphorylate a preparation of +P:GAD1, given that, as noted above, there may be other undetected differential PTMs present in the +P- and -P:GAD1 preparations. Due to limiting amounts of the +P:GAD1 preparation – much of which was used up attempting *in vitro* dephosphorylation assays using exogenous CIP or λ phosphatase – I was unable to generate a Glu saturation curve to compare its V_{max} and K_m(Glu) values with that of -P:GAD1 (35 units/mg; 4.7 mM) (Fig. B-6). Despite this, the preliminary evidence presented here suggests that there may be a pH-dependent impact of a differentially phosphorylated N-terminus on certain aspects of AtGAD1 kinetic properties.

4.3 Future Directions

Owing to difficulties in accumulating biomass for repeat purifications, the LC-MS/MS data reported here are the result of single biological replicate measurements for each +P:GAD1 and -P:GAD1. Despite the challenge of purifying native AtGAD1, it would be prudent to investigate the reproducibility of the pattern of differential AtGAD1 phosphorylation I have observed I cells grown under +Pi versus -Pi conditions. Importantly, going forward a priority should be to assess whether N-terminal multisite phosphorylation of AtGAD1 occurs *in planta* in roots in a manner similar to what we have observed using suspension cell cultures. To further parse the impact of N-terminal phosphorylation on AtGAD1, phospho-ablative and phosphomimetic recombinant GAD can be generated, namely, mutating either Ser4 or Ser8 – the two phosphosites that exhibited that largest change in phosphorylation as measured by LC-MS/MS. These mutants can be used to analyze effects on AtGAD1 kinetic properties, as well as susceptibility to proteolysis or protein-protein interactions (eg. sensitivity to CaM binding/regulation). In addition to biochemical strategies to investigate the role of phosphorylation, genetic approaches will also prove important. For example, by transforming *atgad1* KO mutants to overexpress various AtGAD1 phosphomimetic/ablative transgenes, future studies can compare the phenotypes of these mutants to WT plants under different stress conditions, including Pi stress. In conjunction with comparative metabolomics, (e.g. GABA content), such studies will help to paint a clearer picture on the impact that GAD phosphorylation has not only on GABA shunt regulation, but also on the role that the shunt plays as a component of the PSR.

Literature Cited

Abdel Razik, E.S., Alharbi, B.M., Pirzadah, T.B., Alnusairi, G.S.H., Soliman, M.H., and Hakeem, K.R. 2021. γ-Aminobutyric acid (GABA) mitigates drought and heat stress in sunflower (Helianthus annuus L.) by regulating its physiological, biochemical and molecular pathways. *Physiol Plant 172*, 505-527.

Adem, G.D., Chen, G., Shabala, L., Chen, Z.-H., and Shabala, S. 2020. GORK channel: a master switch of plant metabolism? *Trends Plant Sci 25*, 434-445.

Akihiro, T., Koike, S., Tani, R., Tominaga, T., Watanabe, S., Iijima, Y., Aoki, K., Shibata, D., Ashihara, H., Matsukura, C., *et al.* 2008. Biochemical mechanism on GABA accumulation during fruit development in tomato. *Plant Cell Physiol 49*, 1378-1389.

Astegno, A., Capitani, G., and Dominici, P. 2015. Functional roles of the hexamer organization of plant glutamate decarboxylase. *BBA - Proteins Proteome 1854*, 1229-1237.

Balzergue, C., Dartevelle, T., Godon, C., Laugier, E., Meisrimler, C., Teulon, J.-M., Creff, A., Bissler, M., Brouchoud, C., Hagège, A., *et al.* 2017. Low phosphate activates STOP1-ALMT1 to rapidly inhibit root cell elongation. *Nat Comm 8*, 15300.

Bender, K.W., Rosenbaum, D.M., Vanderbeld, B., Ubaid, M., and Snedden, W.A. 2013. The Arabidopsis calmodulin-like protein, CML 39, functions during early seedling establishment. *Plant J 76*, 634-647.

Benidickson, K. (2022). What is the role of the glutamate decarboxylase isozyme AtGAD1 during acclimation of *Arabidopsis thaliana* to phosphate starvation? BIOL537 Thesis, Dept. of Biology, Queen's University.

Bouché, N., Fait, A., Zik, M., and Fromm, H. 2004. The root-specific glutamate decarboxylase (GAD1) is essential for sustaining GABA levels in *Arabidopsis*. *Plant Mol Biol 55*, 315-325.

Bown, A.W., Hall, D.E., and MacGregor, K.B. 2002. Insect footsteps on leaves stimulate the accumulation of 4-aminobutyrate and can be visualized through increased chlorophyll fluorescence and superoxide production. *Plant Physiol 129*, 1430-1434.

Bown, A.W., and Shelp, B.J. 1997. The metabolism and functions of [gamma]-aminobutyric acid. *Plant Physiol 115*, 1-5.

Breitkreuz, K.E., and Shelp, B.J. 1995. Subcellular compartmentation of the 4-aminobutyrate shunt in protoplasts from developing soybean cotyledons. *Plant Physiol 108*, 99-103.

Breitkreuz, K.E., Shelp, B.J., Fischer, W.N., Schwacke, R., and Rentsch, D. 1999. Identification and characterization of GABA, proline and quaternary ammonium compound transporters from Arabidopsis thaliana. *FEBS letters 450*, 280-284.

Capitani, G., De Biase, D., Aurizi, C., Gut, H., Bossa, F., and Grütter, M.G. 2003. Crystal structure and functional analysis of Escherichia coli glutamate decarboxylase. *EMBO J 22*, 4027-4037.

Carvalhais, L.C., Dennis, P.G., Fedoseyenko, D., Hajirezaei, M.R., Borriss, R., and von Wirén, N. 2011. Root exudation of sugars, amino acids, and organic acids by maize as affected by nitrogen, phosphorus, potassium, and iron deficiency. *J Plant Nutr Soil Sci 174*, 3-11.

Castanie-Cornet, M.-P., Penfound, T.A., Smith, D., Elliott, J.F., and Foster, J.W. 1999. Control of acid resistance in Escherichia coli. *J Bacteriol 181*, 3525-3535.

Che-Othman, M.H., Jacoby, R.P., Millar, A.H., and Taylor, N.L. 2020. Wheat mitochondrial respiration shifts from the tricarboxylic acid cycle to the GABA shunt under salt stress. *New Phytol 225*, 1166-1180.

Chen, S., O'Reilly, L.P., Smithgall, T.E., and Engen, J.R. 2008. Tyrosine phosphorylation in the SH3 domain disrupts negative regulatory interactions within the c-Abl kinase core. *J Mol Biol 383*, 414-423.

Chevrot, R., Rosen, R., Haudecoeur, E., Cirou, A., Shelp, B.J., Ron, E., and Faure, D. 2006. GABA controls the level of quorum-sensing signal in *Agrobacterium tumefaciens*. *Proc Nat Acad Sci 103*, 7460-7464.

Chou, C.-C., Modi, J.P., Wang, C.-Y., Hsu, P.-C., Lee, Y.-H., Huang, K.-F., Wang, A.H.J., Nan, C., Huang, X., Prentice, H., *et al.* 2017. Activation of brain L-glutamate decarboxylase 65 isoform (GAD65) by phosphorylation at threonine 95 (T95). *Mol Neurobiol 54*, 866-873.

Crawford, L.A., Bown, A.W., Breitkreuz, K.E., and Guinel, F.C. 1994. The synthesis of [gamma]-aminobutyric acid in response to treatments reducing cytosolic pH. *Plant Physiol 104*, 865-871.

Dissanayaka, D.M.S.B., Ghahremani, M., Siebers, M., Wasaki, J., and Plaxton, W.C. 2021. Recent insights into the metabolic adaptations of phosphorus-deprived plants. *J Exp Bot 72*, 199-223.

Ezawa, T., and Saito, K. 2018. How do arbuscular mycorrhizal fungi handle phosphate? New insight into fine-tuning of phosphate metabolism. *New Phytol 220*, 1116-1121.

Fait, A., Fromm, H., Walter, D., Galili, G., and Fernie, A.R. 2008. Highway or byway: the metabolic role of the GABA shunt in plants. *Trends Plant Sci 13*, 14-19.

Fan, S., Meng, Y., Song, M., Pang, C., Wei, H., Liu, J., Zhan, X., Lan, J., Feng, C., and Zhang, S. 2014. Quantitative phosphoproteomics analysis of nitric oxide–responsive phosphoproteins in cotton leaf. *PLoS One 9*, e94261.

Fedosejevs, E.T., Ying, S., Park, J., Anderson, E.M., Mullen, R.T., She, Y.-M., and Plaxton, W.C. 2014. Biochemical and molecular characterization of RcSUS1, a cytosolic sucrose synthase phosphorylated *in vivo* at serine11 in developing castor oil seeds. *J Biol Chem 289*, 33412-33424.

Förster, S., Schmidt, L.K., Kopic, E., Anschütz, U., Huang, S., Schlücking, K., Köster, P., Waadt, R., Larrieu, A., Batistič, O., *et al.* 2019. Wounding-induced stomatal closure requires jasmonate-mediated activation of GORK K^+ channels by a Ca2+ sensor-kinase CBL1-CIPK5 complex. *Devel Cell 48*, 87-99.e86.

Gellatly, K.S., Moorhead, G.B., Duff, S.M., Lefebvre, D.D., and Plaxton, W.C. 1994. Purification and characterization of a potato tuber acid phosphatase having significant phosphotyrosine phosphatase activity. *Plant Physiol 106*, 223-232.

Gilliham, M., and Tyerman, S.D. 2016. Linking metabolism to membrane signaling: the GABA–malate connection. *Trends Plant Sci 21*, 295-301.

Greenblatt, H.K., and Greenblatt, D.J. (2018). Gabapentin and pregabalin for the treatment of anxiety disorders. Clinical Pharmacology in Drug Development, pp. 228-232.

Gut, H., Dominici, P., Pilati, S., Astegno, A., Petoukhov, M.V., Svergun, D.I., Grutter, M.G., and Capitani, G. 2009. A common structural basis for pH- and calmodulin-mediated regulation in plant glutamate decarboxylase. *J Mol Biol 392*, 334-351.

Hernández, G., Ramírez, M., Valdés-López, O., Tesfaye, M., Graham, M.A., Czechowski, T., Schlereth, A., Wandrey, M., Erban, A., and Cheung, F. 2007. Phosphorus stress in common bean: root transcript and metabolic responses. *Plant Physiol 144*, 752-767.

Hoehenwarter, W., Thomas, M., Nukarinen, E., Egelhofer, V., Röhrig, H., Weckwerth, W., Conrath, U., and Beckers, G.J. 2013. Identification of novel *in vivo* MAP kinase

substrates in Arabidopsis thaliana through use of tandem metal oxide affinity chromatography. *Mol Cell Proteomics 12*, 369-380.
Hosy, E., Vavasseur, A., Mouline, K., Dreyer, I., Gaymard, F., Porée, F., Boucherez, J., Lebaudy, A., Bouchez, D., and Véry, A.-A. 2003. The Arabidopsis outward K+ channel GORK is involved in regulation of stomatal movements and plant transpiration. *Proc Nat Acad Sci 100*, 5549-5554.
Huang, C.Y., Roessner, U., Eickmeier, I., Genc, Y., Callahan, D.L., Shirley, N., Langridge, P., and Bacic, A. 2008. Metabolite profiling reveals distinct changes in carbon and nitrogen metabolism in phosphate-deficient barley plants (*Hordeum vulgare* L.). *Plant Cell Physiol 49*, 691-703.
Inatomi, K., and Slaughter, J.C. 1975. Glutamate decarboxylase from barley embryos and roots: general properties and the occurrence of three enzymatic forms. *Biochem J 147*, 479-484.
Ito, J., Batth, T.S., Petzold, C.J., Redding-Johanson, A.M., Mukhopadhyay, A., Verboom, R., Meyer, E.H., Millar, A.H., and Heazlewood, J.L. 2011. Analysis of the *Arabidopsis* cytosolic proteome highlights subcellular partitioning of central plant metabolism. *J Prot Res 10*, 1571-1582.
Joshi, J., Folz, J.S., Gregory, J.F., 3rd, McCarty, D.R., Fiehn, O., and Hanson, A.D. 2019. Rethinking the PDH bypass and GABA shunt as thiamin-deficiency workarounds. *Plant Physiol 181*, 389-393.
Kiep, V., Vadassery, J., Lattke, J., Maaß, J.-P., Boland, W., Peiter, E., and Mithöfer, A. 2015. Systemic cytosolic Ca^{2+} elevation is activated upon wounding and herbivory in Arabidopsis. *New Phytol 207*, 996-1004.
Kinnersley, A.M., and Turano, F.J. 2000. Gamma aminobutyric acid (GABA) and plant responses to stress. *Crit Reviews Plant Sci 19*, 479-509.
Kreuzwieser, J., Hauberg, J., Howell, K.A., Carroll, A., Rennenberg, H., Millar, A.H., and Whelan, J. 2009. Differential response of gray poplar leaves and roots underpins stress adaptation during hypoxia. *Plant Physiol 149*, 461-473.
Krnjević, K., and Schwartz, S. 1967. The action of γ-Aminobutyric acid on cortical neurones. *Exp Brain Res 3*, 320-336.
Kuffler, S.W., and Edwards, C. 1958. Mechanism of gamma aminobutyric acid (GABA) action and its relation to synaptic inhibition. *J Neurophysiol 21*, 589-610.
Lambers, H., Martinoia, E., and Renton, M. 2015. Plant adaptations to severely phosphorus-impoverished soils. *Curr Op Plant Biol 25*, 23-31.
Lambers, H., and Plaxton, W. 2015. Phosphorus: Back to the Roots. In: Phosphorus Metabolism in Plants (W.C. Plaxton & H. Lambers, Eds.). *Ann Plant Rev.* Vol. 48, Wiley; pp. 3-22
Lan, P., Li, W., Wen, T.N., and Schmidt, W. 2012. Quantitative phosphoproteome profiling of iron-deficient Arabidopsis roots. *Plant Physiol 159*, 403-417.
Li, K., and Xu, E. 2008. The role and the mechanism of gamma-aminobutyric acid during central nervous system development. *Neurosci Bull 24*, 195-200.
Li, M., Wang, F., Li, S., Yu, G., Wang, L., Li, Q., Zhu, X., Li, Z., Yuan, L., and Liu, P. 2020. Importers drive leaf-to-leaf jasmonic acid transmission in wound-induced systemic immunity. *Mol Plant 13*, 1485-1498.
Li, R., Li, R., Li, X., Fu, D., Zhu, B., Tian, H., Luo, Y., and Zhu, H. 2018. Multiplexed CRISPR/Cas9-mediated metabolic engineering of γ-aminobutyric acid levels in *Solanum lycopersicum*. *Plant Biotech J 16*, 415-427.

Li, Z., Yu, J., Peng, Y., and Huang, B. 2016. Metabolic pathways regulated by γ-aminobutyric acid (GABA) contributing to heat tolerance in creeping bentgrass (*Agrostis stolonifera*). *Sci Rep 6*, 30338.

Lin, L.-L., Hsu, C.-L., Hu, C.-W., Ko, S.-Y., Hsieh, H.-L., Huang, H.-C., and Juan, H.-F. 2015. Integrating phosphoproteomics and bioinformatics to study brassinosteroid-regulated phosphorylation dynamics in *Arabidopsis*. *BMC genomics 16*, 533.

Lingard, M.J., Gidda, S.K., Bingham, S., Rothstein, S.J., Mullen, R.T., and Trelease, R.N. 2008. Arabidopsis PEROXIN11c-e, FISSION1b, and DYNAMIN-RELATED PROTEIN3A cooperate in cell cycle–associated replication of peroxisomes. *Plant Cell 20*, 1567-1585.

Long, Y., Tyerman, S.D., and Gilliham, M. 2020. Cytosolic GABA inhibits anion transport by wheat ALMT1. *New Phytol 225*, 671-678.

Lund, P., Tramonti, A., and De Biase, D. 2014. Coping with low pH: molecular strategies in neutralophilic bacteria. *FEMS Microbiol Rev 38*, 1091-1125.

MacGregor, K.B., Shelp, B.J., Peiris, S., and Bown, A.W. 2003. Overexpression of glutamate decarboxylase in transgenic tobacco plants deters feeding by phytophagous insect larvae. *J Chem Ecol 29*, 2177-2182.

Matsumoto, T., Yamaura, I., and Funatsu, M. 1996. Improved purification and spectroscopic properties of squash glutamate decarboxylase. *Biosci Biotech & Biochem 60*, 889-890.

Mayank, P., Grossman, J., Wuest, S., Boisson-Dernier, A., Roschitzki, B., Nanni, P., Nühse, T., and Grossniklaus, U. 2012. Characterization of the phosphoproteome of mature Arabidopsis pollen. *Plant J 72*, 89-101.

McLean, M.D., Yevtushenko, D.P., Deschene, A., Van Cauwenberghe, O.R., Makhmoudova, A., Potter, J.W., Bown, A.W., and Shelp, B.J. 2003. Overexpression of glutamate decarboxylase in transgenic tobacco plants confers resistance to the northern root-knot nematode. *Mol Breed 11*, 277-285.

Mehta, D., Ghahremani, M., Pérez-Fernández, M., Tan, M., Schläpfer, P., Plaxton, W.C., and Uhrig, R.G. 2021. Phosphate and phosphite have a differential impact on the proteome and phosphoproteome of *Arabidopsis* suspension cell cultures. *Plant J 105*, 924-941.

Mei, X., Chen, Y., Zhang, L., Fu, X., Wei, Q., Grierson, D., Zhou, Y., Huang, Y., Dong, F., and Yang, Z. 2016. Dual mechanisms regulating glutamate decarboxylases and accumulation of gamma-aminobutyric acid in tea (*Camellia sinensis*) leaves exposed to multiple stresses. *Sci Rep 6*, 23685.

Mekonnen, D.W., Flügge, U.-I., and Ludewig, F. 2016. Gamma-aminobutyric acid depletion affects stomata closure and drought tolerance of *Arabidopsis thaliana*. *Plant Sci 245*, 25-34.

Menz, J., Li, Z., Schulze, W.X., and Ludewig, U. 2016. Early nitrogen-deprivation responses in Arabidopsis roots reveal distinct differences on transcriptome and (phospho-) proteome levels between nitrate and ammonium nutrition. *Plant J 88*, 717-734.

Michaeli, S., Fait, A., Lagor, K., Nunes-Nesi, A., Grillich, N., Yellin, A., Bar, D., Khan, M., Fernie, A.R., Turano, F.J., *et al.* 2011. A mitochondrial GABA permease connects the GABA shunt and the TCA cycle, and is essential for normal carbon metabolism. *Plant J 67*, 485-498.

Michaeli, S., and Fromm, H. 2015. Closing the loop on the GABA shunt in plants: are GABA metabolism and signaling entwined? *Front Plant Sci 6*, 419-419.

Miyashita, Y., and Good, A. 2008. Contribution of the GABA shunt to hypoxia-induced alanine accumulation in roots of *Arabidopsis thaliana*. *Plant Cell Physiol 49*, 92-102.

Nakagami, H., Sugiyama, N., Mochida, K., Daudi, A., Yoshida, Y., Toyoda, T., Tomita, M., Ishihama, Y., and Shirasu, K. 2010. Large-scale comparative phosphoproteomics identifies conserved phosphorylation sites in plants. *Plant Physiol 153*, 1161-1174.

Namchuk, M., Lindsay, L., Turck, C.W., Kanaani, J., and Baekkeskov, S. 1997. Phosphorylation of serine residues 3, 6, 10, and 13 distinguishes membrane anchored from soluble glutamic acid decarboxylase 65 and is restricted to glutamic acid decarboxylase 65a. *J Biol Chem 272*, 1548-1557.

Narayan, V.S., and Nair, P. 1986. The 4-aminobutyrate shunt in Solanum tuberosum. *Phytochemistry 25*, 997-1001.

Narayan, V.S., and Nair, P.M. 1990. Metabolism, enzymology and possible roles of 4-aminobutyrate in higher plants. *Phytochemistry 29*, 367-375.

Nguyen-Kim, H., San Clemente, H., Balliau, T., Zivy, M., Dunand, C., Albenne, C., and Jamet, E. 2016. Arabidopsis thaliana root cell wall proteomics: Increasing the proteome coverage using a combinatorial peptide ligand library and description of unexpected Hyp in peroxidase amino acid sequences. *Proteomics 16*, 491-503.

O'Leary, B.M., Neale, H.C., Geilfus, C.-M., Jackson, R.W., Arnold, D.L., and Preston, G.M. 2016. Early changes in apoplast composition associated with defence and disease in interactions between *Phaseolus vulgaris* and the halo blight pathogen *Pseudomonas syringae* Pv. phaseolicola. *Plant Cell Environ 39*, 2172-2184.

Obata, K. (1972). The inhibitory action of γ-aminobutyric acid, a probable synaptic transmitter. In International Review of Neurobiology, C.C. Pfeiffer, and J.R. Smythies, eds. (Academic Press), pp. 167-187.

Palacios, J.M., Wamsley, J.K., and Kuhar, M.J. 1981. High affinity GABA receptors: autoradiographic localization. *Brain Res 222*, 285-307.

Palanivelu, R., Brass, L., Edlund, A.F., and Preuss, D. 2003. Pollen tube growth and guidance is regulated by POP2, an *Arabidopsis* gene that controls GABA levels. *Cell 114*, 47-59.

Pant, B.-D., Pant, P., Erban, A., Huhman, D., Kopka, J., and Scheible, W.R. 2015. Identification of primary and secondary metabolites with phosphorus status-dependent abundance in *Arabidopsis*, and of the transcription factor PHR 1 as a major regulator of metabolic changes during phosphorus limitation. *Plant Cell Environ 38*, 172-187.

Park, D.H., Mirabella, R., Bronstein, P.A., Preston, G.M., Haring, M.A., Lim, C.K., Collmer, A., and Schuurink, R.C. 2010. Mutations in γ-aminobutyric acid (GABA) transaminase genes in plants or *Pseudomonas syringae* reduce bacterial virulence. *Plant J 64*, 318-330.

Planamente, S., Mondy, S., Hommais, F., Vigouroux, A., Moréra, S., and Faure, D. 2012. Structural basis for selective GABA binding in bacterial pathogens. *Mol Microbiol 86*, 1085-1099.

Plaxton, W.C., and Shane, M.W. (2015). The essential role of post-translational enzyme modifications in the metabolic adaptations of phosphorus-deprived plants. In: Phosphorous Metabolism in Plants (W.C. Plaxton and H. Lambers, Eds). *Ann Plant Rev*, pp. 99-123.

Qiu, J., Hou, Y., Wang, Y., Li, Z., Zhao, J., Tong, X., Lin, H., Wei, X., Ao, H., and Zhang, J. 2017. A comprehensive proteomic survey of ABA-induced protein phosphorylation in rice (*Oryza sativa* L.). *Int J Mol Sci 18*, 60.

Ramesh, S.A., Kamran, M., Sullivan, W., Chirkova, L., Okamoto, M., Degryse, F., McLaughlin, M., Gilliham, M., and Tyerman, S.D. 2018. Aluminum-activated malate transporters can facilitate GABA transport. *Plant Cell 30*, 1147-1164.

Ramesh, S.A., Tyerman, S.D., Gilliham, M., and Xu, B. 2017. γ-Aminobutyric acid (GABA) signalling in plants. *Cell Mol Life Sci 74*, 1577-1603.

Ramesh, S.A., Tyerman, S.D., Xu, B., Bose, J., Kaur, S., Conn, V., Domingos, P., Ullah, S., Wege, S., Shabala, S., *et al.* 2015. GABA signalling modulates plant growth by directly regulating the activity of plant-specific anion transporters. *Nat Comm 6*, 7879.

Ramputh, A.I., and Bown, A.W. 1996. Rapid [gamma]-aminobutyric acid synthesis and the inhibition of the growth and development of oblique-banded leaf-roller larvae. *Plant Physiol 111*, 1349-1352.

Rayapuram, N., Bigeard, J., Alhoraibi, H., Bonhomme, L., Hesse, A.-M., Vinh, J., Hirt, H., and Pflieger, D. 2018. Quantitative phosphoproteomic analysis reveals shared and specific targets of *Arabidopsis* mitogen-activated protein kinases (MAPKs) MPK3, MPK4, and MPK6. *Mol Cell Proteom 17*, 61-80.

Rayapuram, N., Bonhomme, L., Bigeard, J., Haddadou, K., Przybylski, C., Hirt, H., and Pflieger, D. 2014. Identification of novel PAMP-triggered phosphorylation and dephosphorylation events in Arabidopsis thaliana by quantitative phosphoproteomic analysis. *J Proteome Res 13*, 2137-2151.

Renault, H., El Amrani, A., Berger, A., Mouille, G., Soubigou-Taconnat, L., Bouchereau, A., and Deleu, C. 2013. γ-Aminobutyric acid transaminase deficiency impairs central carbon metabolism and leads to cell wall defects during salt stress in Arabidopsis roots. *Plant Cell Environ 36*, 1009-1018.

Renault, H., El Amrani, A., Palanivelu, R., Updegraff, E.P., Yu, A., Renou, J.-P., Preuss, D., Bouchereau, A., and Deleu, C. 2011. GABA accumulation causes cell elongation defects and a decrease in expression of genes encoding secreted and cell wall-related proteins in *Arabidopsis thaliana*. *Plant Cell Physiol 52*, 894-908.

Renault, H., Roussel, V., El Amrani, A., Arzel, M., Renault, D., Bouchereau, A., and Deleu, C. 2010. The Arabidopsis pop2-1 mutant reveals the involvement of GABA transaminase in salt stress tolerance. *BMC Plant Biol 10*, 20.

Roberts, E., and Frankel, S. 1950. γ-aminobutyric acid in brain: its formation from glutamic acid. *J Biol Chem 187*, 55-63.

Roberts, M.R. 2007. Does GABA act as a signal in plants?: hints from molecular studies. *Plant Signal Behav 2*, 408-409.

Rossignoli, G., Phillips, R.S., Astegno, A., Menegazzi, M., Voltattorni, C.B., and Bertoldi, M. 2018. Phosphorylation of pyridoxal 5′-phosphate enzymes: an intriguing and neglected topic. *Amino Acids 50*, 205-215.

Salah, A., Zhan, M., Cao, C., Han, Y., Ling, L., Liu, Z., Li, P., Ye, M., and Jiang, Y. 2019. γ-aminobutyric acid promotes chloroplast ultrastructure, antioxidant capacity, and growth of waterlogged maize seedlings. *Sci Rep 9*, 484.

Sasaki, T., Mori, I.C., Furuichi, T., Munemasa, S., Toyooka, K., Matsuoka, K., Murata, Y., and Yamamoto, Y. 2010. Closing plant stomata requires a homolog of an aluminum-activated malate transporter. *Plant Cell Physiol 51*, 354-365.

Satyanarayan, V., and Nair, P.M. 1985. Purification and characterization of glutamate decarboxylase from Solanum tuberosum. *Eur J Biochem 150*, 53-60.

Sawaki, Y., Iuchi, S., Kobayashi, Y., Kobayashi, Y., Ikka, T., Sakurai, N., Fujita, M., Shinozaki, K., Shibata, D., Kobayashi, M., *et al.* 2009. STOP1 regulates multiple genes that protect *Arabidopsis* from proton and aluminum toxicities. *Plant Physiol 150*, 281-294.

Scholz, S.S., Malabarba, J., Reichelt, M., Heyer, M., Ludewig, F., and Mithöfer, A. 2017. Evidence for GABA-induced systemic GABA accumulation in *Arabidopsis* upon wounding. *Front Plant Sci 8*, 388-388.

Scholz, S.S., Reichelt, M., Mekonnen, D.W., Ludewig, F., and Mithöfer, A. 2015. Insect herbivory-elicited GABA accumulation in plants is a wound-induced, direct, systemic, and jasmonate-independent defense response. *Front Plant Sci 6*, 1128-1128.

Schreiber, T.B., Mäusbacher, N., Soroka, J., Wandinger, S.K., Buchner, J., and Daub, H. 2012. Global analysis of phosphoproteome regulation by the Ser/Thr phosphatase Ppt1 in *Saccharomyces cerevisiae*. *J Proteome Res 11*, 2397-2408.

Seifi, H.S., Curvers, K., De Vleesschauwer, D., Delaere, I., Aziz, A., and Höfte, M. 2013. Concurrent overactivation of the cytosolic glutamine synthetase and the GABA shunt in the ABA-deficient sitiens mutant of tomato leads to resistance against *Botrytis cinerea*. *New Phytol 199*, 490-504.

Seifikalhor, M., Aliniaeifard, S., Hassani, B., Niknam, V., and Lastochkina, O. 2019. Diverse role of gamma-aminobutyric acid in dynamic plant cell responses. *Plant Cell Rep 38*, 847-867.

Shabala, S. 2017. Signalling by potassium: another second messenger to add to the list? *J Exp Bot 68*, 4003-4007.

Sharma, T., Dreyer, I., Kochian, L., and Piñeros, M.A. 2016. The ALMT family of organic acid transporters in plants and their involvement in detoxification and nutrient security. *Front Plant Sci 7*, 1488.

Shelp, B.J., Aghdam, M.S., and Flaherty, E.J. 2021. γ-aminobutyrate (GABA) regulated plant defense: mechanisms and opportunities. *Plants 10*, 1939.

Shelp, B.J., Bown, A.W., and Zarei, A. 2017. 4-Aminobutyrate (GABA): a metabolite and signal with practical significance. *Bot 95*, 1015-1032.

Shelp, B.J., Bozzo, G.G., Trobacher, C.P., Chiu, G., and Bajwa, V.S. 2012a. Strategies and tools for studying the metabolism and function of γ-aminobutyrate in plants. I. Pathway structure. *Bot 90*, 651-668.

Shelp, B.J., Bozzo, G.G., Zarei, A., Simpson, J.P., Trobacher, C.P., and Allan, W.L. 2012b. Strategies and tools for studying the metabolism and function of γ-aminobutyrate in plants. II. Integrated analysis. *Bot 90*, 781-793.

Snedden, W.A., Arazi, T., Fromm, H., and Shelp, B.J. 1995. Calcium/calmodulin activation of soybean glutamate decarboxylase. *Plant Physiol 108*, 543-549.

Snedden, W.A., Koutsia, N., Baum, G., and Fromm, H. 1996. Activation of a recombinant petunia glutamate decarboxylase by calcium/calmodulin or by a monoclonal antibody which recognizes the calmodulin binding domain. *J Biol Chem 271*, 4148-4153.

Solomon, P.S., and Oliver, R.P. 2001. The nitrogen content of the tomato leaf apoplast increases during infection by *Cladosporium fulvum*. *Planta 213*, 241-249.

Solomon, P.S., and Oliver, R.P. 2002. Evidence that γ-aminobutyric acid is a major nitrogen source during *Cladosporium fulvum* infection of tomato. *Planta 214*, 414-420.

Steward, F. 1949. γ-Aminobutyric acid: a constituent of the potato tuber? *Science 110*, 439-440.

Streeter, J.G., and Thompson, J.F. 1972. Anaerobic accumulation of γ-aminobutyric acid and alanine in radish leaves (*Raphanus sativus*, L.). *Plant Physiol 49*, 572-578.

Sung, J., Sonn, Y., Lee, Y., Kang, S., Ha, S., Krishnan, H.B., and Oh, T.K. 2015. Compositional changes of selected amino acids, organic acids, and soluble sugars in the xylem sap of N, P, or K-deficient tomato plants. *J Plant Nutr Soil Sci 178*, 792-797.

Takayama, M., Matsukura, C., Ariizumi, T., and Ezura, H. 2017. Activating glutamate decarboxylase activity by removing the autoinhibitory domain leads to hyper γ-aminobutyric acid (GABA) accumulation in tomato fruit. *Plant Cell Reports 36*, 103-116.

Toubiana, D., Sade, N., Liu, L., Rubio Wilhelmi, M.d.M., Brotman, Y., Luzarowska, U., Vogel, J.P., and Blumwald, E. 2020. Correlation-based network analysis combined with machine learning techniques highlight the role of the GABA shunt in *Brachypodium sylvaticum* freezing tolerance. *Sci Rep 10*, 4489.

Trobacher, C.P., Zarei, A., Liu, J., Clark, S.M., Bozzo, G.G., and Shelp, B.J. 2013. Calmodulin-dependent and calmodulin-independent glutamate decarboxylases in apple fruit. *BMC Plant Biol 13*, 144.

Turano, F.J., and Fang, T.K. 1998. Characterization of two glutamate decarboxylase cDNA clones from *Arabidopsis*. *Plant Physiol 117*, 1411-1421.

Uhrig, R.G., Schläpfer, P., Roschitzki, B., Hirsch-Hoffmann, M., and Gruissem, W. 2019. Diurnal changes in concerted plant protein phosphorylation and acetylation in Arabidopsis organs and seedlings. *Plant J 99*, 176-194.

Umezawa, T., Sugiyama, N., Takahashi, F., Anderson, J.C., Ishihama, Y., Peck, S.C., and Shinozaki, K. 2013. Genetics and phosphoproteomics reveal a protein phosphorylation network in the abscisic acid signaling pathway in *Arabidopsis thaliana*. *Sci Signaling 6*, rs8-rs8.

Valentinuzzi, F., Pii, Y., Vigani, G., Lehmann, M., Cesco, S., and Mimmo, T. 2015. Phosphorus and iron deficiencies induce a metabolic reprogramming and affect the exudation traits of the woody plant *Fragaria ananassa*. *J Exp Bot 66*, 6483-6495.

van Wijk, K.J., Friso, G., Walther, D., and Schulze, W.X. 2014. Meta-analysis of *Arabidopsis thaliana* phospho-proteomics data reveals compartmentalization of phosphorylation motifs. *Plant Cell 26*, 2367-2389.

Veljanovski, V., Vanderbeld, B., Knowles, V.L., Snedden, W.A., and Plaxton, W.C. 2006. Biochemical and molecular characterization of AtPAP26, a vacuolar purple acid phosphatase up-regulated in phosphate-deprived *Arabidopsis* suspension cells and seedlings. *Plant Physiol 142*, 1282-1293.

Wallace, W., Secor, J., and Schrader, L.E. 1984. Rapid accumulation of γ-aminobutyric acid and alanine in soybean leaves in response to an abrupt transfer to lower temperature, darkness, or mechanical manipulation. *Plant Physiol 75*, 170-175.

Waltz, E. 2021. GABA-enriched tomato is first CRISPR-edited food to enter market. *Nat Biotech. 40*, 9.

Wang, G., Kong, J., Cui, D., Zhao, H., Niu, Y., Xu, M., Jiang, G., Zhao, Y., and Wang, W. 2019. Resistance against *Ralstonia solanacearum* in tomato depends on the methionine cycle and the γ-aminobutyric acid metabolic pathway. *Plant J 97*, 1032-1047.

Wang, J., Grubb, L.E., Wang, J., Liang, X., Li, L., Gao, C., Ma, M., Feng, F., Li, M., and Li, L. 2018. A regulatory module controlling homeostasis of a plant immune kinase. *Mol Cell 69*, 493-504. e496.

Wang, J., Yu, X., Ding, Z.J., Zhang, X., Luo, Y., Xu, X., Xie, Y., Li, X., Yuan, T., Zheng, S.J., *et al.* 2021. Structural basis of ALMT1-mediated aluminum resistance in Arabidopsis. *Cell Res 32*, 89-98.

Wang, L., Xu, D.X., Lv, Y.G., and Zhang, H. 2010. Purification and biochemical characterisation of a novel glutamate decarboxylase from rice bran. *J Sci Food Agri 90*, 1027-1033.

Wang, Y., Gu, W., Meng, Y., Xie, T., Li, L., Li, J., and Wei, S. 2017. γ-aminobutyric acid imparts partial protection from salt stress injury to maize seedlings by improving photosynthesis and upregulating osmoprotectants and antioxidants. *Sci Rep 7*, 43609.

Wiśniewski, J.R., Nagaraj, N., Zougman, A., Gnad, F., and Mann, M. 2010. Brain phosphoproteome obtained by a FASP-based method reveals plasma membrane protein topology. *J Proteome Res 9*, 3280-3289.

Wu, X.N., Rodriguez, C.S., Pertl-Obermeyer, H., Obermeyer, G., and Schulze, W.X. 2013. Sucrose-induced receptor kinase SIRK1 regulates a plasma membrane aquaporin in *Arabidopsis*. *Mol Cell Prot 12*, 2856-2873.

Xi, L., Zhang, Z., Herold, S., Kassem, S., Wu, X.N., and Schulze, W.X. 2021. Phosphorylation site motifs in plant protein kinases and their substrates. In: Plant Phosphoproteomics (Wu X.N, Ed), *Methods Mol Biol, 2358*, 1-16.

Xu, B., Long, Y., Feng, X., Zhu, X., Sai, N., Chirkova, L., Betts, A., Herrmann, J., Edwards, E.J., Okamoto, M., *et al.* 2021. GABA signalling modulates stomatal opening to enhance plant water use efficiency and drought resilience. *Nat Comm 12*, 1952.

Yevtushenko, D.P., McLean, M.D., Peiris, S., Van Cauwenberghe, O.R., and Shelp, B.J. 2003. Calcium/calmodulin activation of two divergent glutamate decarboxylases from tobacco. *J Exp Bot 54*, 2001-2002.

Yin, Y.-G., Tominaga, T., Iijima, Y., Aoki, K., Shibata, D., Ashihara, H., Nishimura, S., Ezura, H., and Matsukura, C. 2010. Metabolic alterations in organic acids and γ-aminobutyric acid in developing tomato (*Solanum lycopersicum* L.) fruits. *Plant Cell Physiol 51*, 1300-1314.

Yu, G.-H., Zou, J., Feng, J., Peng, X.-B., Wu, J.-Y., Wu, Y.-L., Palanivelu, R., and Sun, M.-X. 2014. Exogenous γ-aminobutyric acid (GABA) affects pollen tube growth via modulating putative Ca^{2+}-permeable membrane channels and is coupled to negative regulation on glutamate decarboxylase. *J Exp Bot 65*, 3235-3248.

Yun, S.J., and Oh, S.-H. 1998. Cloning and characterization of a tobacco eDNA encoding calcium/calmodulin-dependent glutamate decarboxylase. *Mol & Cell 8*, 125-129.

Zarei, A., Chiu, G.Z., Yu, G.-H., Trobacher, C.P., and Shelp, B.J. 2017. Salinity-regulated expression of genes involved in GABA metabolism and signaling. *Bot 95*, 621-627.

Zhang, G., and Bown, A.W. 1997. The rapid determination of γ-aminobutyric acid. *Phytochemistry 44*, 1007-1009.

Zhang, H., Yao, H.-y., Chen, F., and Wang, X. 2007. Purification and characterization of glutamate decarboxylase from rice germ. *Food Chem 101*, 1670-1676.

Zhao, X., Bai, X., Jiang, C., and Li, Z. 2019. Phosphoproteomic analysis of two contrasting maize inbred lines provides insights into the mechanism of salt-stress tolerance. *Int J Mol Sci 20*, 1886.

Appendix A: Supplementary Information (Chapter 3)

Table A-1. Primers used to generate *mCherry-AtGAD1* and *AtGAD1-mCherry* constructs.

Primer Designation	*Sequence (5'-3')*	*Purpose*
C-term FL-FP	GCACCCGGGATGGTGCTCTCCCACGCCG	mCherry fused to C-terminus of AtGAD1
C-term FL-RP	GCAGCTAGCGCAGATACCACTCGTCTTCTTCC	mCherry fused to C-terminus of AtGAD1
N-term FL-FP	GCAGGATCCATGGTGCTCTCCCACGCCG	mCherry fused to N-terminus of AtGAD1
N-term FL-RP	GCATCTAGATTCGCAGATACCACTCGTCTTCTTCC	mCherry fused to N-terminus of AtGAD1

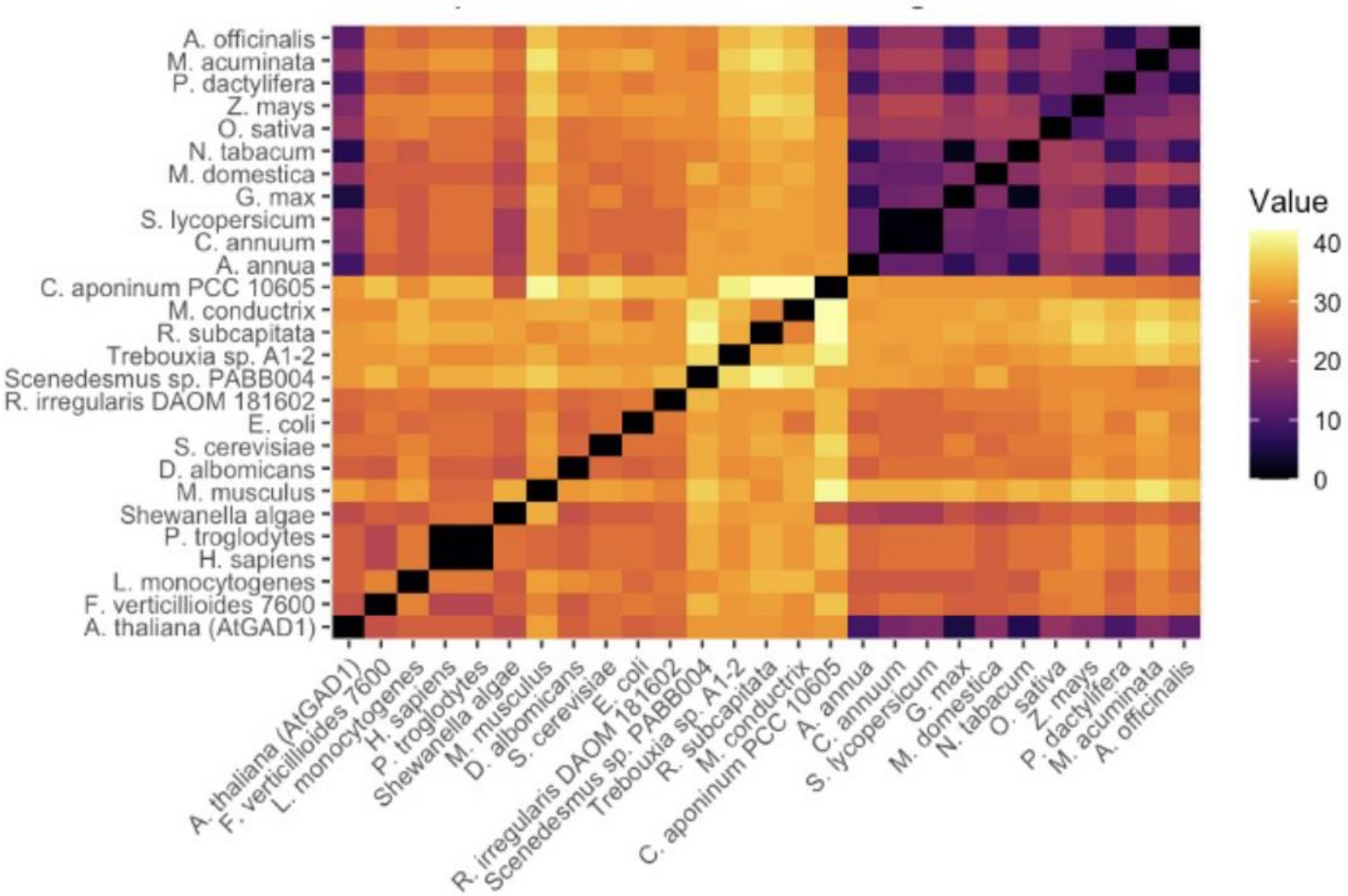

Fig. A-1. Distance matrix reflecting the Euclidian distance between the N-terminal sequences of various AtGAD1 orthologs. Higher values (lighter colors) denote greater dissimilarity between N-terminal sequences. Lower values (darker colors) denote highly similar N-terminal sequences.

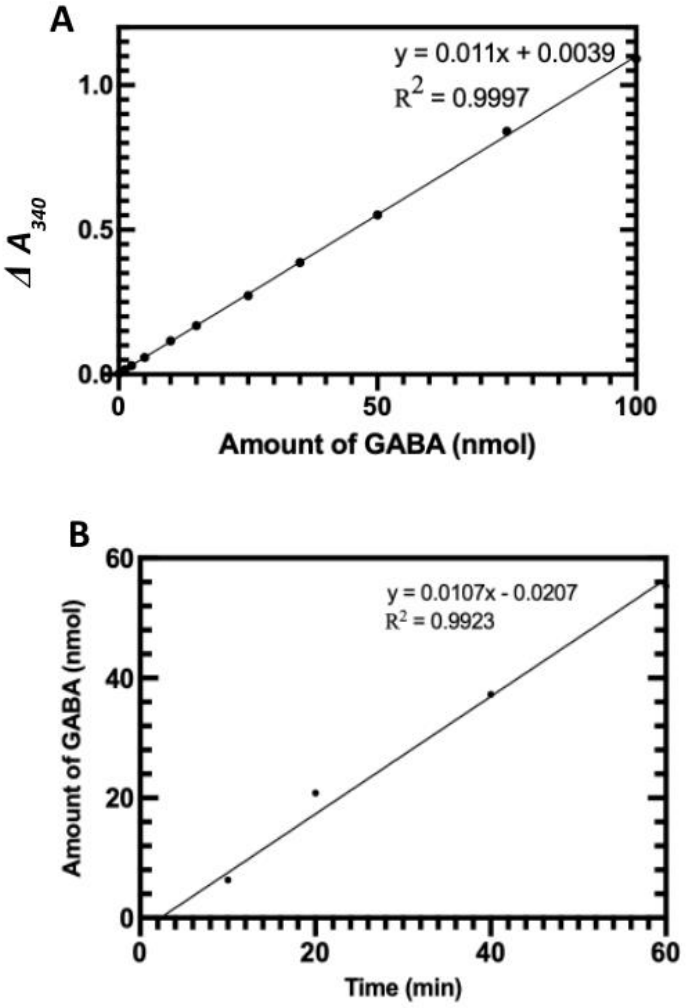

Fig. A-2. Validating the GAD-GABase linked enzyme activity assay. (A) A GABase calibration curve was generated using known amounts of GABA. **(B)** The linked assay was validated by showing that the amount of GABA produced by 20 μL of a clarified extract from –Pi Arabidopsis suspension cells was proportional to assay time. All values represent means ±SEM – which are too small to be discerned – of $n = 3$ separate assays, with linear regression values indicated for each graph

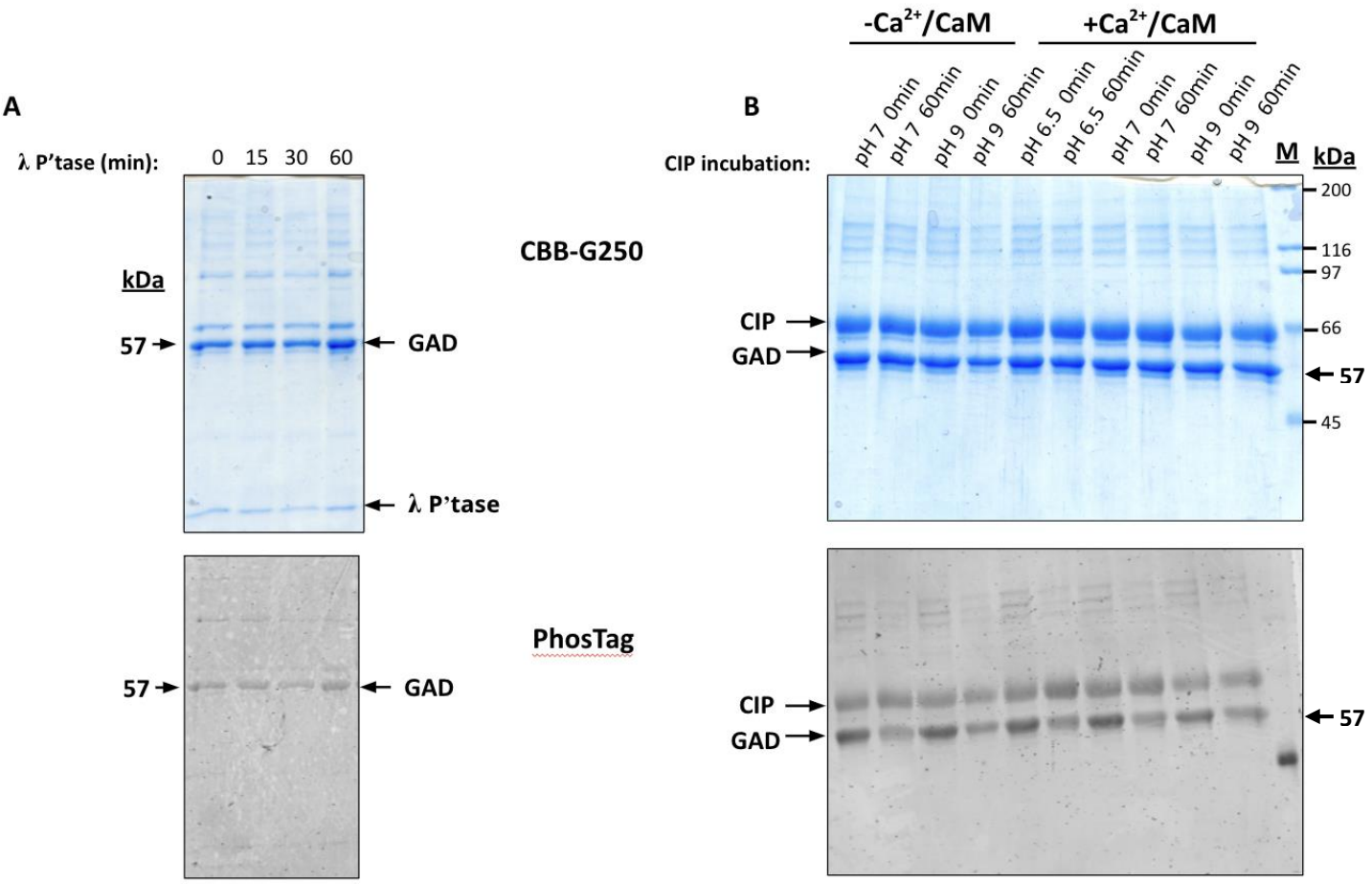

Fig. A-3. Attempted *in vitro* dephosphorylation of +P:GAD1 with exogenous phosphatases. The final preparation of +P:GAD1 was incubated with exogenous (**A**) λ phosphatase (λ P'tase) at 30◦C or (**B**) CIP for 1 h at 37 ºC as described in the Materials and Methods, and as indicated in the figure. (**B**) Dephosphorylation with CIP attempted at varying pH values (6.5, 7, 9) in the presence or absence of 1 mM Ca^{2+} with 1 μM CaM. Following SDS-PAGE, gels were multiplex stained first with Phos-Tag phosphoprotein stain (bottom panels), then with Coomassie brilliant blue G-250 (CBB-G250) for total protein staining (top panels). Each lane contained 1 μg of +P:GAD1; 'M' denotes various molecular weight standards that provide positive (45 kDa ovalbumin) and negative (other standards) controls for Phos-Tag phosphoprotein staining.

Appendix B: AtGAD1 Purification from *Arabidopsis* Cell Cultures and Kinetic Analysis

Table B-1. Purification of GAD from 500 g of +Pi *Arabidopsis* suspension cells.

Sample	*Volume (mL)*	*Activity (units)*	*Protein (mg)*	*Specific Activity (units/mg)*	*Purification (fold)*	*Yield (%)*
Clarified extract*	860	160	16,082	0.010	1	100
$(NH_4)_2SO_4$ fractionation	250	140	3,895	0.036	3.6	88
Butyl-Sepharose	24	88	1,764	0.05	5	55
Desalting Sephadex G-25	40	80	1,270	0.063	6.3	50
Fractogel DEAE-anion exchange	16	46	256	0.18	18	29
CaM-Sepharose	6	30	25	1.2	120	19
Gel-filtration	0.25	9.8	0.49	20	2,000	6

*Desalted extract to eliminate background (i.e. glutamate independent) 'NADP$^+$ reductase' activity.

Table B-2. Purification of GAD from 575 g of -Pi *Arabidopsis* suspension cells.

Sample	*Volume (mL)*	*Activity (units)*	*Protein (mg)*	*Specific Activity (units/mg)*	*Purification (fold)*	*Yield (%)*
Clarified extract*	1,525	463	7,510	0.062	1	100
$(NH_4)_2SO_4$ fractionation	230	300	2,500	0.12	1.9	65
Butyl-Sepharose	23	146	633	0.47	4.4	32
Desalting Sephadex G-25	33	145	501	0.22	4.7	31
Fractogel DEAE anion exchange	32	108.5	96	0.39	18.2	23
CaM-Sepharose	0.2	24	1.65	14.6	220	4.9
Gel-filtration	0.19	50	1.57	32	516	11

*Desalted extract to eliminate background (i.e. glutamate independent) 'NADP$^+$ reductase' activity.

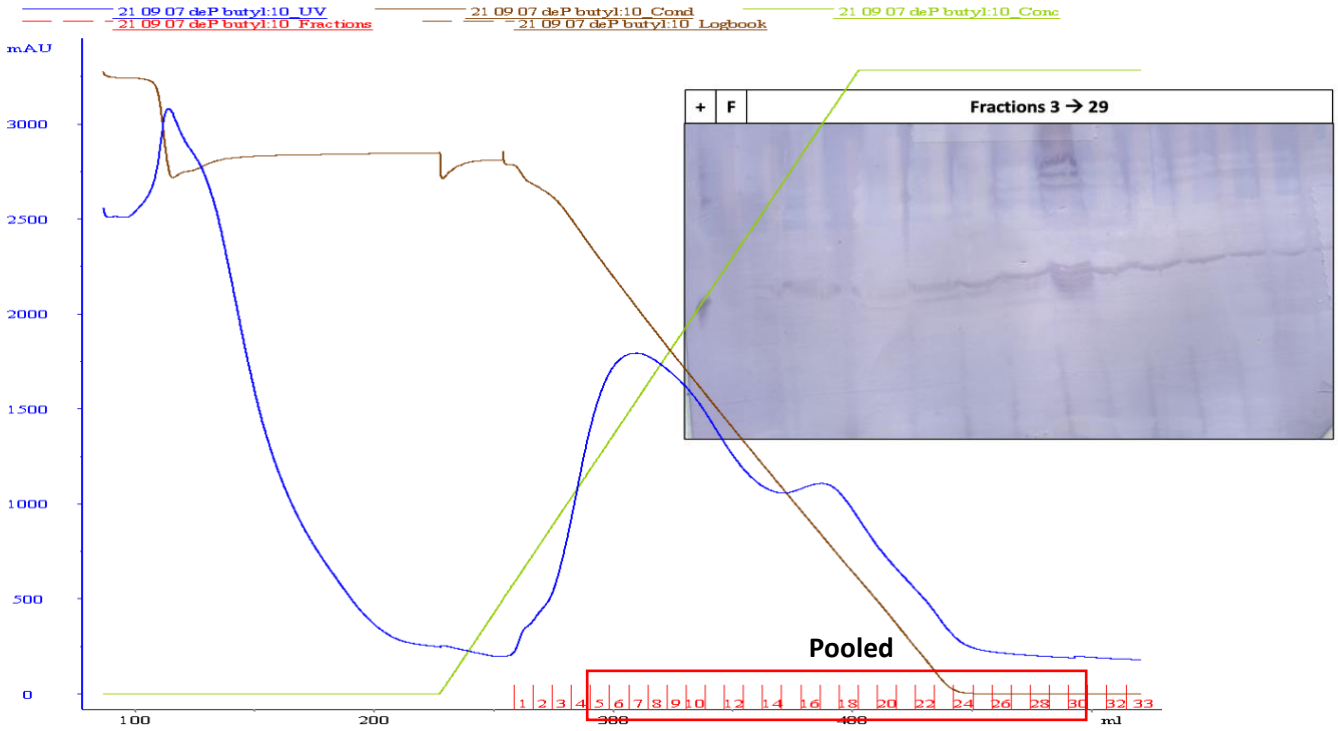

Fig. B-1. +P:GAD1 Butyl-Sepharose fast flow (hydrophobic interaction) FPLC. Elution profile was obtained during AtGAD1 purification using an ÄKTA Purifier FPLC system. An aliquot (10 µl) of every second fraction was subjected to SDS-PAGE and α-GAD immunoblotting alongside purified AtGAD1 (lane 1) and flow-through (F, lane 2) to identify the GAD-containing fractions to be pooled. The blue plot represents A_{280}, the brown plot is conductivity, and the green plot is (%buffer B).

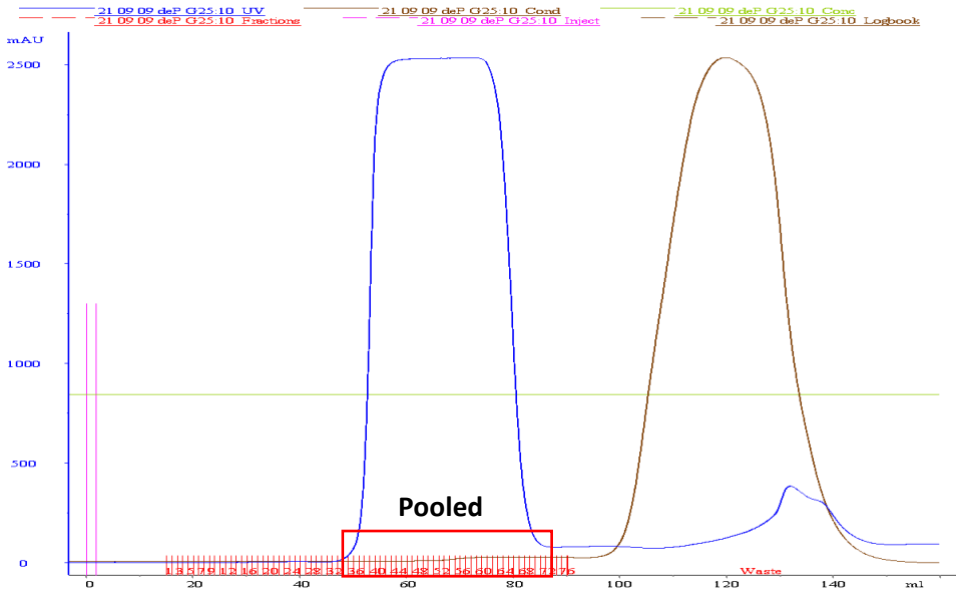

Fig. B-2. +P:GAD1 Sephadex-G-25 desalting FPLC. Elution profile was obtained during AtGAD1 purification using an ÄKTA Purifier FPLC system. The blue plot represents A_{280}, the brown plot is conductivity. All fractions contained in the A_{280} peak were pooled.

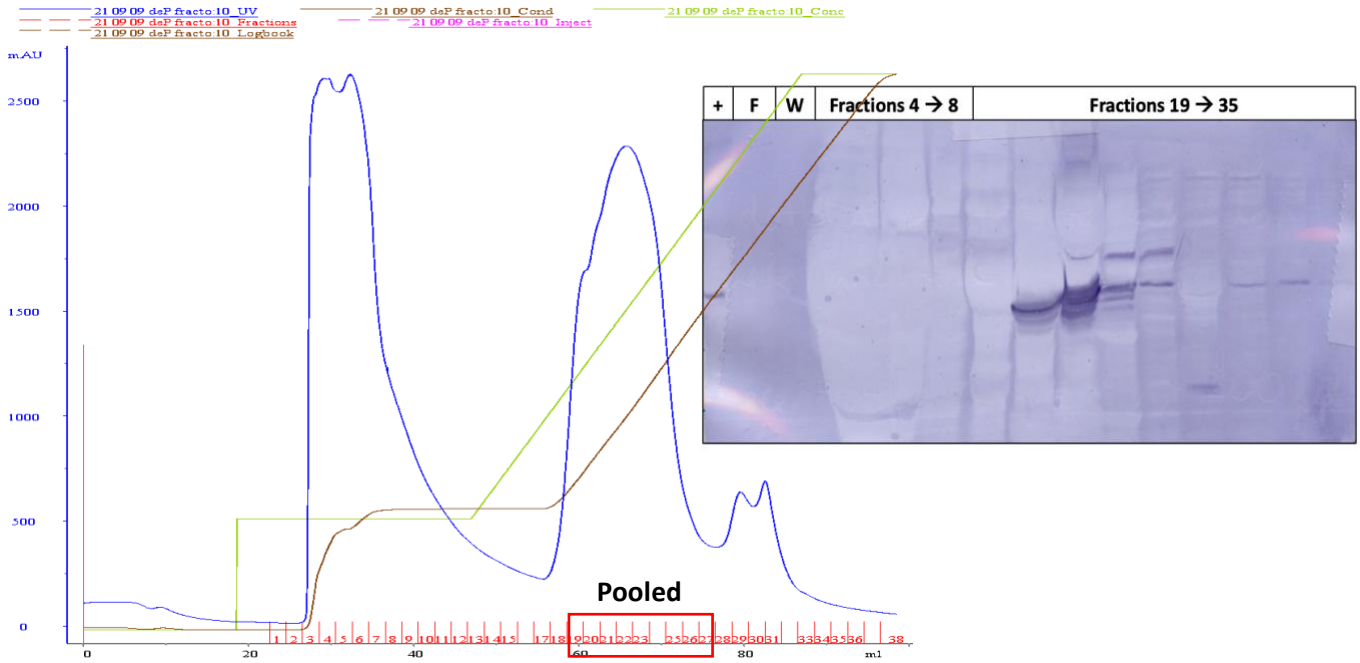

Fig. B-3. +P:GAD1 DEAE-Fractogel FPLC. Elution profile was obtained during AtGAD1 purification using AKTA FPLC. An aliquot (10 µl) of every second fraction was subjected to SDS-PAGE and α-GAD immunoblotting alongside purified AtGAD1 (lane 1), flow-through (F, lane 2), and wash fractions (W, lane 3) to identify GAD-containing fractions to be pooled. The blue plot represents A_{280}, the brown plot is conductivity, and the green plot is (%buffer B).

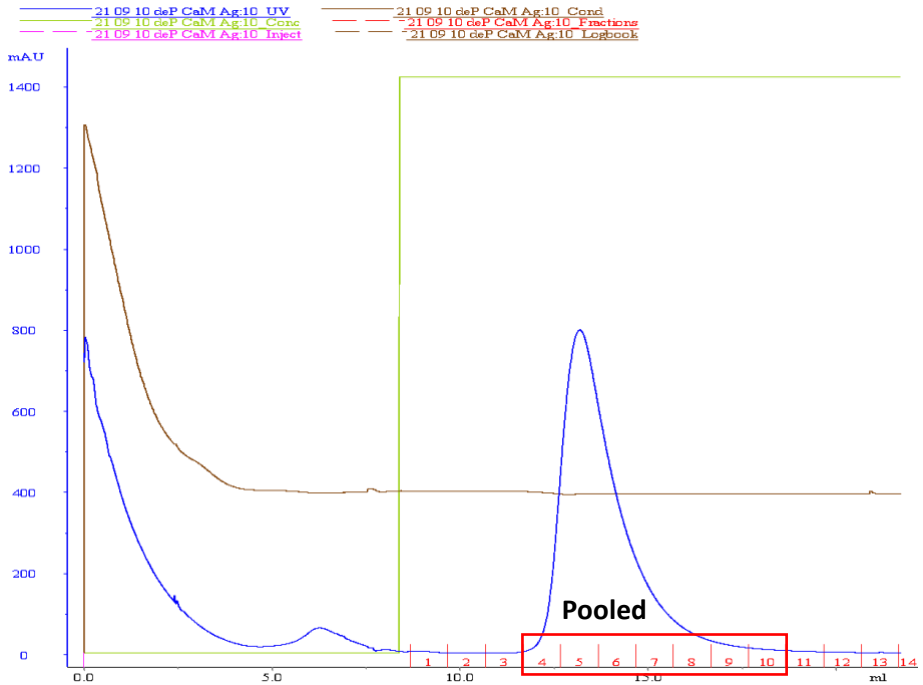

Fig. B-4. +P:GAD1 CaM-Sepharose affinity chromatography. Elution profile was obtained during AtGAD1 purification using the ÄKTA FPLC. The blue plot represents A_{280}, the brown plot is conductivity, and the green plot is (%buffer B). All fractions contained in the A_{280} peak were pooled.

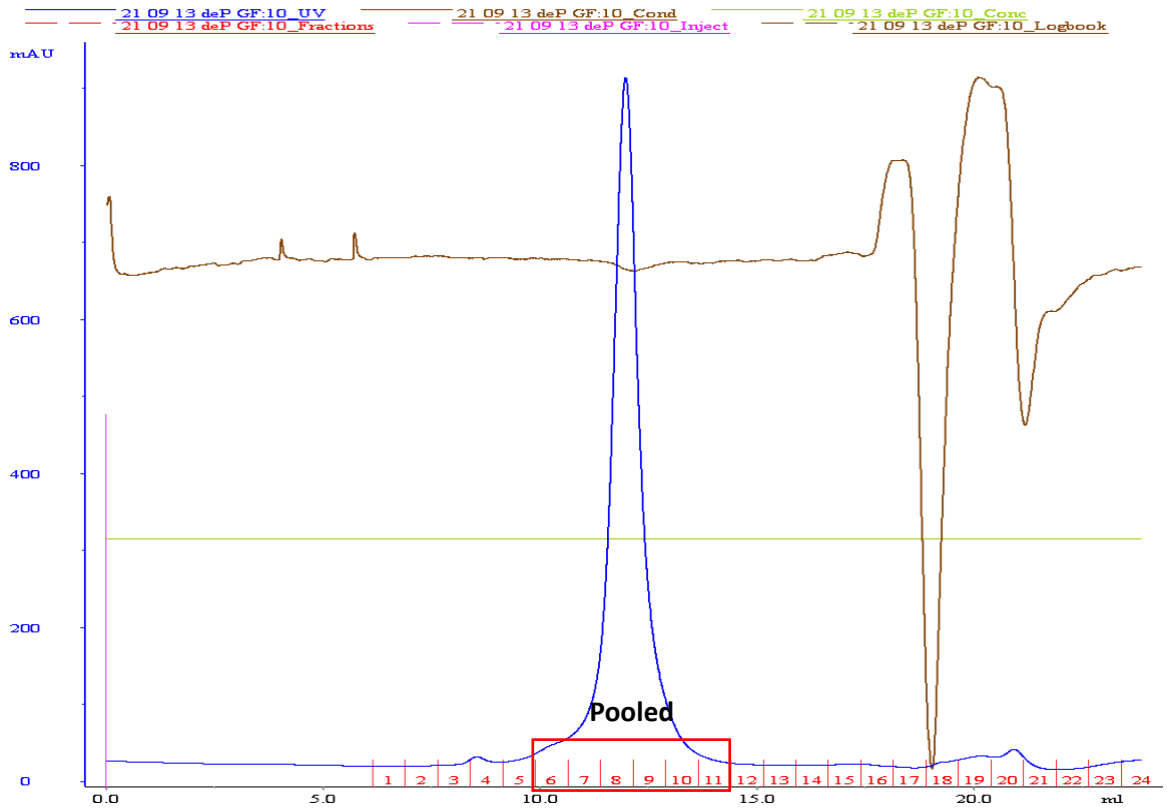

Fig. B-5. +P:GAD1 Superdex 200 Increase 10/300 gel filtration. Elution profile was obtained during AtGAD1 purification using the ÄKTA FPLC. The blue plot represents A_{280} and the brown plot is conductivity. All fractions contained in the A_{280} peak were pooled.

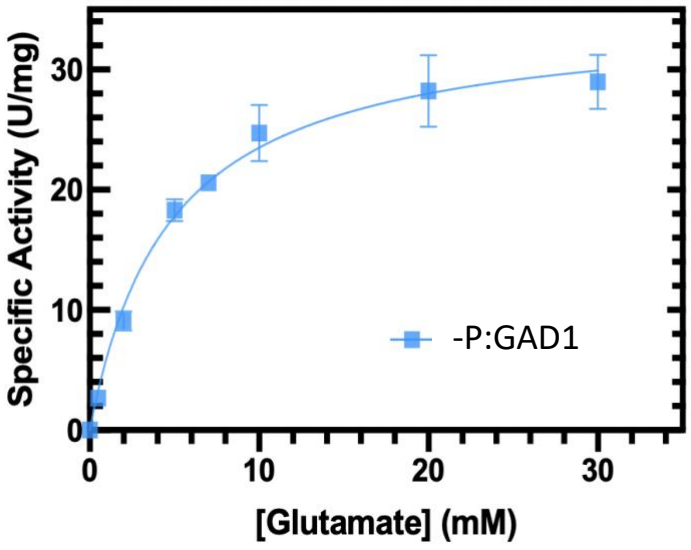

Fig. B-6. Glutamate saturation curve generated using purified -P:GAD1. All assays were conducted at pH 5.8 using 200 ng of –P:GAD1. All values represent mean ±SEM of n = 3 separate assays. GraphPad Prism 9.3.1 was used to calculate the following kinetic parameters: V_{max} = 33.0 ±2.2 units/mg, K_m = 3.9 ±0.66 mM.